الجمهورية الجزائرية الديمقراطية الشعبية

PEOPLE'S DEMOCRATIC REPUBLIC OF ALGERIA

وزارة التعليم العالي و البحث العلمي

Ministry of Higher Education and Scientific Research

جامعة أبي بكر بلقايد – تلمسان –

University of Abou Bekr Belkaid – Tlemcen –
Faculty of Technology

THESIS

Presented to obtain of the degree of **Doctorate**, **3rd Cycle**

In: Mechanical engineering

Specialty: Energetics

By: KHERRAFI Mohammed Abdelbassit

Subject

Numerical and experimental analysis of the thermo-energetic performance of ventilation in a solar drying chamber

Publicly defended on 07 January 2025, in front of the jury composed of:

M. KORTI Abdel Illah Nabil	Pr.	Univ. Tlemcen	President
M. SAIM Rachid	Pr.	Univ. Tlemcen	Thesis director
M. BENSEDDIK Abdelouahab	Pr.	URAER Ghardaia	Thesis co-director
M. ABDELGHANI Boubekri	Pr.	Univ. Ouargla	Examiner
M. SARI HASSOUNE Zakaria	Dr.	Univ. Tlemcen	Examiner
M. BENZENINE Hamidou	Pr.	Univ. Ain Témouchent	Guest

Academic year: 2024 - 2025

Dedication

First of all, I would like to thank God for giving me the strength to complete this work.

I would also like to show my gratitude to those who, from far and near, have supported me both materially and morally. I therefore dedicate this work:

To my dearest parents, may God protect them and keep them for me.

To my sister Fatima Zohra, who has always been at my side.

To all my friends.

Mohammed Abdelbassit

Acknowledgments

First and foremost, I wish to express my infinite gratitude to God Almighty, the source of strength, wisdom, and perseverance, who has guided me throughout this work.

I extend my heartfelt thanks to my thesis supervisors, **Professor Rachid SAIM** and **Professor Abdelouahab BENSEDDIK**, for their guidance, patience, and invaluable advice. Their expertise and unwavering support were instrumental in the successful completion of this research.

I am also deeply grateful to the members of the examination committee, **Professor Abdel Ilah Nabil KORTI**, **Professor Abdelghani BOUBEKRI**, **Dr. Zakaria SARI HASSOUNE**, and **Professor Hamidou BENZENINE**, for their time, effort, and thorough evaluation of my work. Their constructive feedback has significantly enriched this thesis.

A special thank you to my parents and my sister for their unconditional love, unwavering support, and constant encouragement. To my family and friends, thank you for your understanding and comforting presence during challenging times.

This work was carried out at the Applied Energy and Thermal Laboratory (ETAP) at the University of Tlemcen and the Applied Research Unit in Renewable Energies in Ghardaia. I am deeply appreciative of these institutions for providing the technical and scientific resources as well as a stimulating research environment.

To everyone who, in one way or another, contributed to this achievement, I extend my sincerest gratitude.

Abstract

The rising demand for energy, coupled with environmental concerns and the depletion of fossil fuels, has heightened the need for renewable energy solutions. Solar energy, characterized by its abundance and sustainability, plays a critical role in addressing these challenges. Among its many applications, solar drying has emerged as an efficient and eco-friendly method for preserving agricultural and food products. By leveraging solar energy, drying technologies reduce dependency on conventional energy sources while improving product quality and reducing waste. This thesis investigates the optimization of solar drying systems, focusing on the drying chamber's ventilation and the enhancement of solar collectors. A combination of experimental and numerical analyses was conducted to evaluate the impact of design modifications and material choices on drying performance. Experimental setups at the Applied Research Unit for Renewable Energies in Ghardaia explored various configurations, including the integration of obstacles, ribs, and inserts in both direct and indirect solar dryers. Numerical simulations using ANSYS Fluent provided insights into airflow patterns and heat transfer dynamics, validating experimental findings and guiding design improvements. The results demonstrate that integrating obstacles and other structural enhancements significantly improves heat transfer, airflow distribution, and drying efficiency, reducing drying time and energy consumption. Additionally, the study emphasizes the importance of sustainable materials and advanced monitoring systems to optimize operational parameters and minimize environmental impact. This work contributes to bridging gaps in solar drying research by focusing on internal chamber enhancements and integrating advanced design features. The findings support the development of cost-effective and environmentally friendly solar drying systems, offering practical solutions for food preservation and energy efficiency in agricultural and industrial applications.

Keywords: Solar drying, drying chamber, ventilation, solar collectors, heat transfer, energy efficiency, obstacles, ANSYS Fluent, experimental analysis, numerical simulation, food preservation, renewable energy.

ملخص

إن الطلب المتزايد على الطاقة، إلى جانب المخاوف البيئية واستنزاف الوقود الأحفوري، قد زاد من الحاجة إلى حلول الطاقة المتجددة. وتلعب الطاقة الشمسية، التي تتميز بوفرتها واستدامتها، دورًا حاسمًا في مواجهة هذه التحديات. ومن بين تطبيقاتها المتعددة، برز التجفيف الشمسي كوسيلة فعالة وصديقة للبيئة لحفظ المنتجات الزراعية والغذائية. ومن خلال استغلال الطاقة الشمسية، تقلل تقنيات التجفيف من الاعتماد على مصادر الطاقة التقليدية مع تحسين جودة المنتجات وتقليل الهدر. يتناول هذا البحث تحسين أنظمة التجفيف الشمسي، مع التركيز على التهوية داخل حجرة التجفيف وتعزيز أداء المجمعات الشمسية. وقد تم إجراء مجموعة من التحليلات التجريبية والعددية لتقييم تأثير تعديلات التصميم وخيارات المواد على كفاءة عملية التجفيف. وشملت التجارب التي أجريت في وحدة البحث التطبيقي للطاقات المتجددة بغرداية دراسة تكوينات متعددة، بما في ذلك دمج العوائق والضلوع والإضافات في كل من المجففات الشمسية المباشرة وغير المباشرة. كما وفرت المحاكاة العددية باستخدام برنامج ANSYS Fluent رؤى حول أنماط تدفق الهواء وديناميكيات انتقال الحرارة، مما ساهم في تأكيد النتائج التجريبية وتوجيه تحسينات التصميم. أظهرت النتائج أن دمج العوائق والتحسينات الهيكلية الأخرى يؤدي بشكل كبير إلى تحسين انتقال الحرارة وتوزيع تدفق الهواء وكفاءة التجفيف، مما يقلل من وقت التجفيف واستهلاك الطاقة. بالإضافة إلى ذلك، يبرز البحث أهمية استخدام المواد المستدامة وأنظمة المراقبة المتقدمة لتحسين معايير التشغيل وتقليل التأثير البيئي. يساهم هذا العمل في سد الفجوات في أبحاث التجفيف الشمسي من خلال التركيز على تحسينات داخلية لحجرة التجفيف ودمج ميزات تصميم متقدمة. تدعم النتائج تطوير أنظمة تجفيف شمسية منخفضة التكلفة وصديقة للبيئة، مما يوفر حلولًا عملية لحفظ الأغذية وتحسين كفاءة الطاقة في التطبيقات الزراعية والصناعية.

الكلمات المفتاحية: التجفيف الشمسي، حجرة التجفيف، التهوية، المجمعات الشمسية، انتقال الحرارة، كفاءة الطاقة، العوائق، ANSYS Fluent، التحليل التجريبي، المحاكاة العددية، حفظ الأغذية، الطاقة المتجددة.

Résumé

La demande croissante en énergie, combinée aux préoccupations environnementales et à l'épuisement des combustibles fossiles, accentue le besoin de solutions énergétiques renouvelables. L'énergie solaire, grâce à son abondance et sa durabilité, joue un rôle clé dans la réponse à ces défis. Parmi ses multiples applications, le séchage solaire se distingue comme une méthode efficace et respectueuse de l'environnement pour la conservation des produits agricoles et alimentaires. En exploitant l'énergie solaire, les technologies de séchage réduisent la dépendance aux sources d'énergie conventionnelles tout en améliorant la qualité des produits et en limitant le gaspillage. Ce travail de recherche se concentre sur l'amélioration des systèmes de séchage solaire, avec une attention particulière portée à la ventilation dans la chambre de séchage et à l'optimisation des performances des collecteurs solaires. Une série d'analyses expérimentales et numériques a été réalisée afin d'évaluer l'impact des modifications de conception et des choix de matériaux sur l'efficacité du processus de séchage. Les expériences, menées au sein de l’Unité de Recherche Appliquée en Énergies Renouvelables de Ghardaïa, ont examiné diverses configurations, notamment l'intégration d'obstacles, de nervures et d'inserts dans les séchoirs solaires directs et indirects. Les simulations numériques, effectuées à l'aide du logiciel ANSYS Fluent, ont fourni des informations détaillées sur les dynamiques de transfert de chaleur et de flux d'air, validant ainsi les résultats expérimentaux et guidant les améliorations du design. Les résultats ont montré que l'intégration d'obstacles et d'autres améliorations structurelles améliore significativement le transfert de chaleur, la distribution du flux d'air et l'efficacité du séchage, réduisant ainsi le temps de séchage et la consommation d'énergie. Par ailleurs, cette recherche met en avant l'importance de l'utilisation de matériaux durables et de systèmes de contrôle avancés pour optimiser les paramètres opérationnels et réduire l'impact environnemental. Cette étude comble les lacunes dans les recherches sur le séchage solaire en mettant l'accent sur les améliorations internes de la chambre de séchage et en intégrant des éléments de conception avancés. Les résultats soutiennent le développement de systèmes de séchage solaire à faible coût et respectueux de l’environnement, offrant des solutions pratiques pour la conservation des aliments et l’amélioration de l’efficacité énergétique dans les applications agricoles et industrielles.

Mots-clés : Séchage solaire, chambre de séchage, ventilation, collecteurs solaires, transfert de chaleur, efficacité énergétique, obstacles, ANSYS Fluent, analyse expérimentale, simulation numérique, conservation des aliments, énergie renouvelable.

Table of Contents

Chapter I: Literature review

Chapter II: Experimental study

Chapter III: Numerical study

Chapter IV: Results and discussions

List of tables

List of figures

Nomenclature

ABC	Air bottoming cycle
ANFIS	Adaptive neuro-fuzzy system
ANN	Artificial neural network
CFD	Computational fluid dynamics
CPC	Compound parabolic concentrator
DSD	Direct solar dryer
EJ	Exa joule
ETC	Evacuated tube collector
FPSC	Flat plate solar collector
GD	Greenhouse dryer
GW	Giga watt
HFC	Heliostat field collector
ITSD	Indirect type solar dryer
LHS	Latent heat storage
LPG	Liquefied petroleum gas
OSD	Open sun drying
PCM	Phase change material
PTC	Parabolic trough collector
PV	Photovoltaic
PV/T	Photovoltaic/thermal
RPH	Round per hour
SAH	Solar air heater
SC	Solar collector
SHS	Sensible heat storage
SP	Spray
SPETC	Single-pass evacuated tubular
SWH	Solar water heater
TES	Thermal energy storage
UV	Ultraviolet
WR	Instrument uncertainty

Mc	Moisture content (kg water⁄ kg wet basis)
M_0	Initial moisture content
M_f	Final moisture content
MR	Moisture ratio [-]
M_t	Moisture content at a certain time point
M_e	Equilibrium moisture content
DR	Drying rate (kg water/ kg dry basis min)
Q_o	Total heat output (kJ/s)
$\dot{m}$	Mass flow rate (kg/s)
C_p	Specific heat (J/kg K)
T	Temperature (°C)
Q_i	Total heat input (kJ/s)
I	Solar irradiation (W/m^2)
A_c	Apparent area of the dryer (m^2)
η_c	Efficiency
EPBT	Energy payback time
E_{aout}	Annual thermal Energy output
L	Lifetime
CO_2	Carbon dioxide

Subscripts

d.b.	Dry basis
w.b.	Wet basis
μ	Dynamic viscosity (kg/m s)
u, v, w	Velocity components in x, y, z directions (m/s)

General introduction

General introduction

Context

Global energy consumption has been steadily rising due to rapid industrialization, population growth, and increased urbanization [1, 2]. This surge in demand has placed immense pressure on conventional energy sources, which are not only finite but also contribute significantly to environmental pollution and climate change. Fossil fuels, which currently dominate the global energy mix, are unable to sustainably meet the burgeoning energy requirements of modern society. Consequently, there is an urgent need to transition to renewable energy sources that can provide a sustainable and environmentally friendly solution. Among the various renewable energy options, solar energy stands out due to its abundance, accessibility, and versatility. Harnessing the power of the sun can significantly reduce our reliance on depleting fossil fuels, mitigate greenhouse gas emissions, and ensure a more resilient and secure energy future. Solar energy, with its capability to be deployed at both large and small scales, offers a promising path towards addressing the escalating energy demands while promoting environmental sustainability [3].

Solar energy has found extensive applications in drying technologies, particularly in the agricultural and food processing sectors [1]. Utilizing solar energy for drying offers a sustainable and cost-effective alternative to traditional drying methods that rely on electricity or fossil fuels. Solar dryers harness the sun's radiant energy to remove moisture from a variety of products, including fruits, vegetables, grains, and medicinal plants. Solar drying not only reduces energy costs and dependency on non-renewable resources but also improves the quality of dried products by providing a controlled and uniform drying environment. Additionally, solar drying technologies can be adapted to different scales, making them suitable for both smallholder farmers and large-scale industrial operations [4].

Food preservation through drying is a critical process that extends the shelf life of agricultural products by removing moisture, thereby inhibiting the growth of bacteria, yeast, and molds [5]. This method not only prevents spoilage but also retains the nutritional value and flavor of the food. Drying provides a practical solution for reducing food waste and ensuring food security. By preserving food through drying, communities can enjoy a stable supply of nutritious produce year-round, supporting both local economies and sustainable agricultural practices.

Current drying chambers face significant challenges related to energy efficiency, which hamper their overall performance and sustainability. A major issue is the inconsistent distribution of heat within the chamber, often caused by inadequate design and poor insulation, leading to uneven drying and increased energy consumption [6]. Additionally, many drying systems rely on outdated technologies that fail to optimize heat transfer, resulting in substantial energy losses. The materials used in the construction of these chambers can also impact their efficiency; for instance, low-quality and inappropriate materials do not retain heat effectively [7]. Furthermore, the lack of integration with modern control systems means that many drying chambers cannot adjust to varying environmental conditions, further reducing their efficiency. Addressing these inefficiencies is crucial to improving the energy performance of drying chambers, reducing operational costs, and minimizing environmental impact.

From the literature reviewed, it is evident that most studies aimed at improving solar dryers have predominantly concentrated on the complete exterior redesign of the drying chamber and the enhancement of the solar air collector. Research efforts often focus on overhauling the chamber's design to optimize heat distribution and minimize energy losses, involving changes in chamber shape and size to achieve a more uniform drying environment. Concurrently, enhancements in the solar air collector are explored to improve its efficiency in capturing and converting solar energy, with investigations into advanced materials and innovative designs. While these areas have seen significant advancements, there remains a gap in integrating improvements across both the drying chamber and collector in a cohesive system. Additionally, addressing other factors such as ventilation, energy efficiency, and material sustainability is crucial for developing a more effective and comprehensive solar drying solution.

In the existing literature, there is a noticeable gap regarding the direct enhancement of heat transfer within the drying chamber through the integration of external shapes, such as fins or other geometric modifications aimed at improving heat distribution. While numerous studies have focused on redesigning the drying chamber's external configuration or improving the solar air collector's efficiency, the potential of incorporating external structural features to optimize thermal dynamics have not been explored. The use of fins, baffles, or other heat-enhancing structures could potentially address issues related to uneven heat distribution and inefficient heat transfer within the chamber, yet this aspect remains underexplored. As a result, the potential benefits of such integrations for enhancing the overall performance of solar dryers have not been fully realized or documented in current research, highlighting an important area for further investigation.

Study objectives

The objective of this thesis is to conduct a comprehensive analysis of ventilation in a solar dryer, focusing primarily on the drying chamber, to assess its impact on drying duration. The study will employ both experimental and numerical investigations to analyze the dynamic and thermal behavior within the chamber, exploring how different configurations affect the efficiency of the drying process. Specifically, the research will evaluate how design modifications and materials influence heat distribution and retention, with the goal of enhancing the uniformity and effectiveness of the drying process.

In addition to the drying chamber, the study also involves enhancements to the solar collector for drying applications, using various inserts. These collector modifications aim to improve heat absorption, contributing to an overall increase in drying performance. Furthermore, the study integrates advanced monitoring and control technologies to fine-tune operational parameters, ensuring optimal drying conditions.

This thesis also emphasizes developing a low-cost, environmentally friendly solar dryer by selecting sustainable materials and optimizing the design to minimize energy losses and maximize thermal efficiency.

Methodology

The methodology of this thesis is organized into distinct chapters, each addressing specific aspects of the research work. The overall approach includes experimental testing, numerical simulations, and comparative analysis to improve the efficiency of solar dryers, focusing on both the drying chamber and the solar collector. Below is an outline of the methodology employed in each chapter:

In chapter I, a thorough review of existing literature on solar drying technologies is conducted. The goal is to explore previous studies and identify gaps in knowledge regarding solar dryers' performance, particularly with respect to drying chambers and solar collectors. The chapter classifies solar dryers and discusses advancements in solar air collectors, drying chamber enhancements, and the integration of obstacles or inserts to improve heat transfer and airflow dynamics. This foundational understanding will inform the subsequent experimental and numerical work.

Chapter II presents the experimental setup, where all tests were carried out at the Applied Research Unit for Renewable Energies in Ghardaia. The experimental work focuses on enhancing solar dryers in four key areas:

- Solar Collector Enhancement: Modifications using different inserts (such as fins and rocks) to evaluate their impact on temperature performance.
- Drying Chamber Enhancement: Using different materials and integrating ribs to improve heat transfer and airflow distribution.
- Direct Solar Dryer Enhancement: Investigating the effect of obstacle integration to improve drying efficiency.
- Indirect Solar Dryer Enhancement: Adding ribs to optimize the drying process.

The experimental procedure includes measuring temperature, humidity, and airflow velocity, as well as monitoring drying rates and moisture content. The drying performance of the modified solar dryers is compared under similar meteorological conditions.

In chapter III, numerical simulations are performed using ANSYS Fluent software to model the airflow and heat transfer within the solar dryer configurations. The finite volume method is employed to solve the governing equations of heat and mass transfer. The following steps are included:

- Modeling and Boundary Conditions: The drying chamber and solar collector are modeled in 3D, and appropriate boundary conditions are applied to replicate the experimental setup.
- Simulation of Airflow and Heat Transfer: The numerical study investigates the influence of different inserts (such as obstacles) on the airflow patterns and heat transfer efficiency. The simulation results are validated against experimental data.
- Analysis of Results: Numerical outputs, such as temperature distribution and velocity profiles, are analyzed to gain insights into the internal dynamics of the solar dryers.

Chapter IV discusses the results obtained from both the experimental and numerical investigations. Key performance indicators, such as drying time, moisture reduction, energy efficiency, and temperature distribution, are compared between the different configurations. The chapter emphasizes the improvements achieved through the integration of obstacles, ribs, and solar collector enhancements, providing a comprehensive analysis of the effectiveness of the proposed modifications. Additionally, the chapter compares the drying rates and thermal efficiency of different solar dryer setups.

This structured methodology, combining experimental work, numerical modeling, and a comprehensive analysis, provides a holistic approach to optimizing solar dryer performance while addressing the key challenges in solar drying applications.

Chapter I: Literature review

I.1. Introduction

In the first chapter of this thesis, recent studies relevant to the scope of the research will be examined to provide a comprehensive overview of solar dryer technologies. The chapter will begin with a general classification of solar dryers, setting the stage for a deeper exploration of the subject. The primary focus will be on advancements in solar air collectors and their role in enhancing solar drying applications, highlighting various improvements and innovations in collector design that have contributed to increased efficiency and effectiveness. Additionally, the chapter will delve into the specific enhancements made to drying chambers, discussing different approaches and contributions aimed at optimizing heat transfer and distribution within the drying environment. This dual focus will offer a well-rounded understanding of current developments in solar drying technology and identify areas for further research and improvement. By reviewing these aspects, the chapter will provide a comprehensive overview of existing technologies and also highlight key areas where further research is needed, setting the stage for the subsequent work in the thesis.

I.2. Basic concepts and theoretical principles

I.2.1. Fundamentals of solar energy

I.2.1.1. Solar radiation

Solar radiation is the energy emitted by the sun, which reaches the Earth in the form of electromagnetic waves. Watts per square meter (W/m^2) is the unit of measurement for the amount of solar radiation received on Earth's surface, referred to as solar irradiance. Infrared (IR), visible light, and ultraviolet (UV) radiation make up the majority of the solar spectrum, which spans a variety of wavelengths. Each of these elements makes a distinct contribution to the thermal energy used in solar drying processes.

I.2.1.2. Solar geometry

Understanding solar geometry is crucial for optimizing the orientation and design of solar dryers. Three important angles to take into account are the angle of incidence (the angle between the sun's rays and a perpendicular to the surface), the angle of zenith (the angle between the sun and the vertical), and the angle of azimuth (the compass direction from which the sunlight is coming). These angles vary throughout the day and year, influenced by the Earth’s rotation and orbit, impacting the amount of solar energy received at a given location.

I.2.1.3. Solar energy conversion

Solar collectors are used to convert solar radiation into thermal energy, making it usable. These devices are designed to capture sunlight and transform it into heat. Various types of solar collectors, including flat-plate collectors, evacuated tube collectors, and parabolic trough collectors, are employed depending on their efficiency and specific applications. For instance, flat-plate collectors are simple and widely used, while evacuated tube collectors offer higher efficiency due to reduced heat loss.

I.2.2. Principles of drying processes

I.2.2.1. Moisture content

Defined as the proportion of a material's water content to its dry weight. It is usually expressed as a percentage. To guarantee the stability and quality of dried goods, precise moisture content control is essential.

I.2.2.2. Drying rate

Drying rate curve, which comprises the constant rate phase and the decreasing rate period, is commonly used to describe the drying process. Under the constant rate period, the material's surface loses moisture at a relatively constant rate that is influenced by external conditions like temperature and airflow. As surface moisture depletes, the process enters the falling rate period, where the drying rate decreases due to the migration of moisture from the interior to the surface.

I.2.2.3. Drying mechanisms

The primary mechanisms of moisture removal in drying processes are evaporation and diffusion. Evaporation involves the transformation of liquid water into vapor, which is then carried away by airflow. The term "diffusion" describes the flow of water molecules through a substance from higher concentration areas to lower concentration areas, eventually reaching the surface and evaporating.

I.2.2.4. Factors affecting drying

Various factors affect the drying process efficiency, including temperature, humidity, airflow, and the characteristics of the material being dried. Elevated temperatures accelerate evaporation, while reduced humidity promotes faster drying by creating a greater moisture gradient. Adequate airflow aids in the removal of moisture from the drying environment, and the material’s physical and chemical traits, such as porosity and hygroscopicity, are also crucial.

I.2.3. Heat transfer mechanisms in solar dryers

I.2.3.1. Conduction

In solar dryers, conduction occurs through the walls and materials of the drying chamber. The efficiency of heat conduction depends on the thermal conductivity of materials used in the construction of the dryer.

I.2.3.2. Convection

In the context of solar dryers, convection can be natural or forced. Natural convection occurs due to temperature-induced density differences, causing warm air to rise and cooler air to sink. Forced convection involves the use of fans or blowers to enhance airflow.

I.2.3.3. Radiation

Solar collectors in dryers absorb solar radiation and convert it into thermal energy, which is then radiated to the drying chamber. Radiant heat transfer is crucial for maintaining high temperatures in the drying environment, especially when direct sunlight is not consistently available.

I.2.3.4. Combined heat transfer

In practical applications, heat transfer in solar dryers involves a combination of conduction, convection, and radiation. Understanding the interplay of these mechanisms is essential for optimizing the design and operation of solar dryers. Efficient design ensures that heat is uniformly distributed within the drying chamber, minimizing energy losses and maximizing drying performance.

I.2.4. Design and operation of solar dryers

I.2.4.1. Types of solar dryers

Solar dryers can be divided into three primary categories: direct, indirect, and mixed-mode dryers. In direct solar dryers, the product is placed in direct contact with sunlight, which may cause uneven drying and potential quality loss due to UV exposure. Indirect solar dryers, on the other hand, utilize a solar collector to heat air, which is then circulated through the drying chamber, resulting in more consistent drying while shielding the product from direct sunlight. Using both direct solar radiation and heated air from a solar collector, mixed-mode dryers combine the benefits of direct and indirect systems.

I.2.4.2. Components of solar dryers

The drying chamber, solar collector, and auxiliary system are a solar dryer's key elements. The solar collector's role is to absorb and transform solar energy into heat. The drying chamber contains the items to be dried, ensuring uniform heat and airflow distribution. An auxiliary system in solar dryers is an additional component that supports the primary solar drying system to improve its efficiency.

I.2.4.3. Operational principles

The operation of solar dryers involves managing the flow of heat and air through the system. The air is heated by the collector, which is heated by solar radiation. The products' moisture is absorbed by the hot air as it circulates through the drying chamber. To guarantee effective and consistent drying, precise control over temperature, humidity, and airflow is necessary for optimal functioning. Monitoring and adjusting these parameters can significantly improve the performance and energy efficiency of the solar dryer.

I.2.4.4. Thermal properties of materials

For effective heat transfer, the thermal characteristics of the materials used to build solar dryers—such as thermal conductivity, specific heat, and emissivity— play a vital role. Materials with high thermal conductivity facilitate better heat distribution, while those with appropriate specific heat values can store and release heat effectively.

I.2.4.5. Environmental factors

The performance of solar dryers is influenced by environmental factors, including ambient temperature, solar insolation, and wind speed. Variations in these factors can affect the efficiency of solar energy capture and the drying process. Understanding and mitigating the impact of environmental fluctuations is essential for reliable dryer operation.

I.2.4.6. Energy efficiency

Energy efficiency in solar drying involves maximizing the use of solar energy while minimizing energy losses. Strategies to improve energy efficiency include optimizing the design of the drying chamber and solar collector, using advanced materials, and incorporating control systems to regulate airflow and temperature. In addition to reducing operating costs, efficient energy use improves the drying process's sustainability.

I.3. State of the art

I.3.1. Classification of solar dryers

There are several methods to categorize solar dryers based on their application or design. Historically, humans have relied on the sun to dry food, either by placing them directly under sunlight or in the shade, a method known as open sun drying. However, in recent years, various solar dryer models have been developed to protect the products from pests, such as insects and rodents. Current solar dryers generally fall into 3 categories, as shown in Figure I. 1: (a) air-circulating dryers; (b) solar-ray dryers; and (c) hybrid dryers.

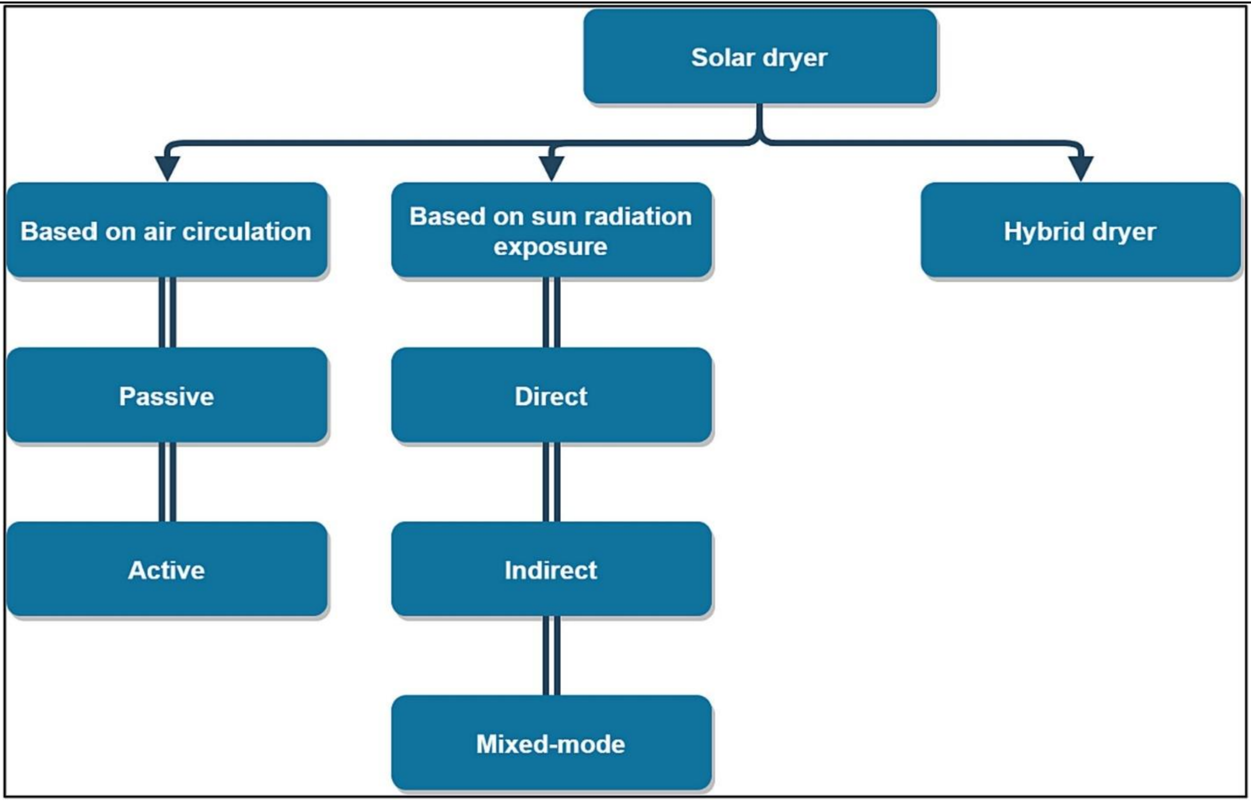

Figure I. 1. Classification of solar dryers [1]

I.3.1.1. Based on air circulation

These solar dryers are divided into passive and active dryers according on how air is circulated inside of them.

I.3.1.1.1. Passive solar dryers

Passive solar dryers depend on the natural movement of air, driven by buoyancy, shifts in wind pressure, or a combination of both (Figure I. 2). Referred to as natural convection solar dryers, they are typically employed for drying small quantities of products at temperatures up to 50°C [8]. These dryers are often used for small-scale applications, such as drying fruits and vegetables at home, and are usually constructed from inexpensive materials.

A passive indirect solar dryer was built by Tedesco et al [9] to dry apples, the process took two days in the sun, resulting in an 89% reduction in the initial mass and an approximate 24-month payback period.

Also, Gilago et al. [10] dried ivy gourd using an indirect solar dryer, achieving a collector efficiency of 62.56% and more than 6% in drying efficiency, with a payback period of 1.04 years.

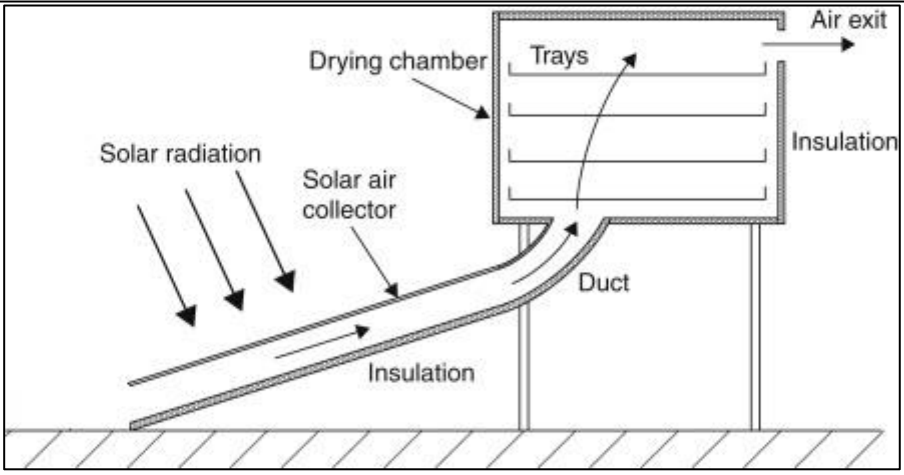

Figure I. 2. Schematic representation of a passive solar dryer [1]

I.3.1.1.2. Active solar dryers

These consist of systems in which heated air is transported from the solar collector to the drying cabinet with the use of a fan (Figure I. 3). As the air passes through the solar air collector, it gets heated and is then directed by the fan to facilitate the drying of the intended product within the drying chamber [11]. Fans regulate air movement at a specific speed, which varies based on the dryer's size or the product being dried, and they also require electricity for operation. Active drying systems have a higher drying rate than passive drying systems, which results in shorter drying times. However, this improved functionality comes with an increased consumption of energy that is linked to the fan that is necessary for airflow.

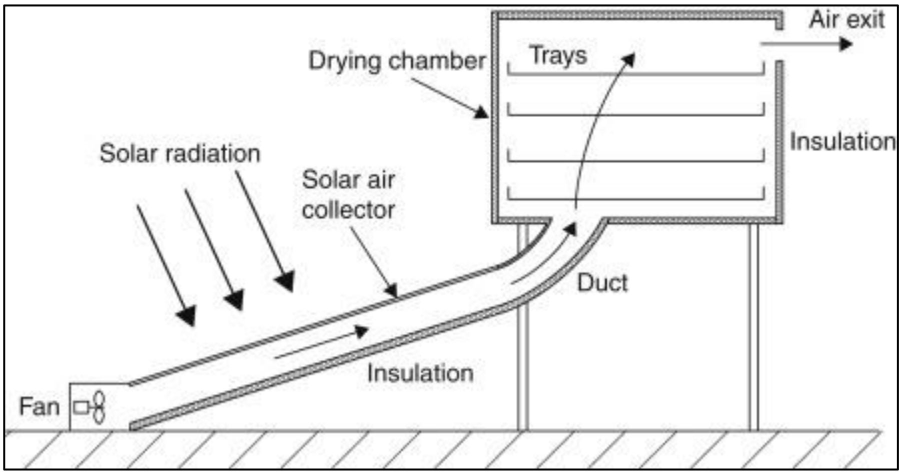

Figure I. 3. Schematic representation of active solar dryer [1]

I.3.1.2. Based on sun radiation exposure

I.3.1.2.1. Direct solar dryers

These dryers consist of a drying chamber as the entire drying system, with a transparent enclosure made of glass or plastic covering the top, where the item is subjected to direct sunlight, which eliminates moisture from the product (Figure I. 4). Experimentally, Castillo Téllez et al. [12] used forced and natural convection to dehydrate stevia plants within DSD. The results of the experiments demonstrated the technical viability of sun drying and the affordability and ease of use of direct drying. However, this method has limited monitoring over operational conditions, such as temperature, and does not offer insulation from exposure to solar radiation.

The effectiveness of a direct solar dryer is primarily influenced by climatic factors, particularly the level of direct solar radiation it receives, leading to a comparatively lower drying rate.

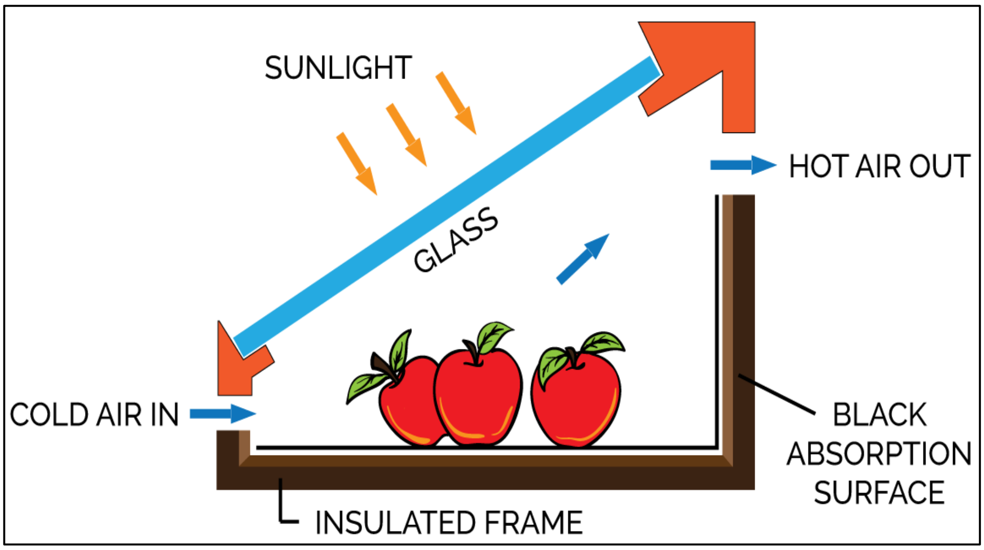

Figure I. 4. Schematic representation of direct solar dryer [1]

I.3.1.2.2. Indirect solar dryers

The items stored in these dryers are shielded from direct solar radiation. One component of the system is a solar collector that transfers heat from the sun to the chamber. Through the output, humid air leaves the chamber after being heated by the SC and removing moisture from the crops (Figure I. 5).

Singh et al. [13] developed an innovative indirect solar. After ten days of testing, an average thermal efficiency of 34.1% was achieved. El-Sebaii et al. [14] conducted an experiment drying thyme using an ITSD in forced mode, achieving a cabinet temperature of 54 °C. The process required 5 hours to attain an acceptable level of moisture content. While indirect solar dryers are highly efficient and generate more heat than direct dryers with minimal energy loss through exhaust, they are more expensive than their direct counterparts.

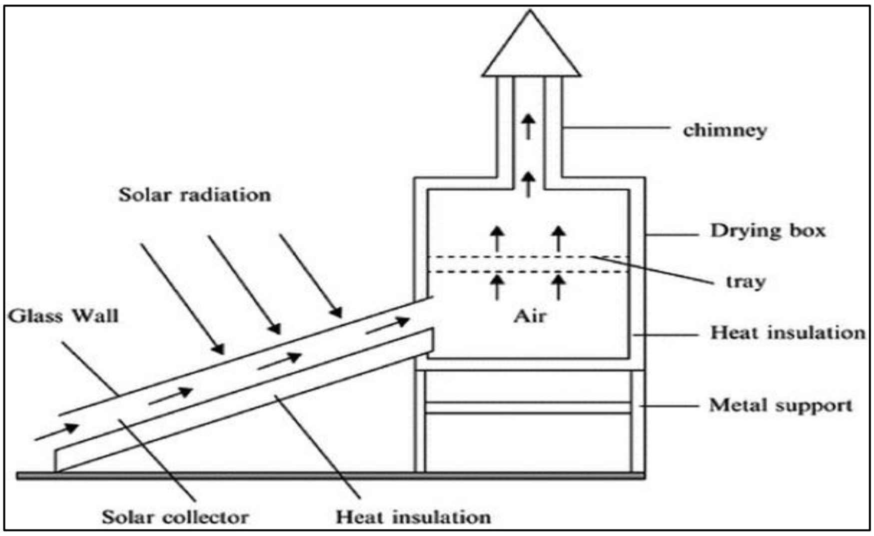

Figure I. 5. Schematic representation of indirect solar dryer [15]

I.3.1.2.3. Mixed-mode solar dryers

Both direct and indirect solar drying techniques are incorporated into these systems. Similar to an indirect type solar dryer (ITSD), they have a drying chamber and a solar air heater, but because the chamber's ceiling is transparent—made of glass or plastic, for example—solar radiation can enter both the drying chamber and the solar collector (Figure I. 6). The results of Lakshmi et al. [16] showed that drying stevia leaves required 330 minutes in a mixed-mode solar dryer to attain the required moisture content, and 870 minutes in open sun drying, with a total thermal efficiency of 33.5%.

By using more solar energy from the drying cabinet and collector to accelerate the evaporation of water, these dryers can reduce drying periods. Prolonged contact to sunlight, however, could be harmful to certain items.

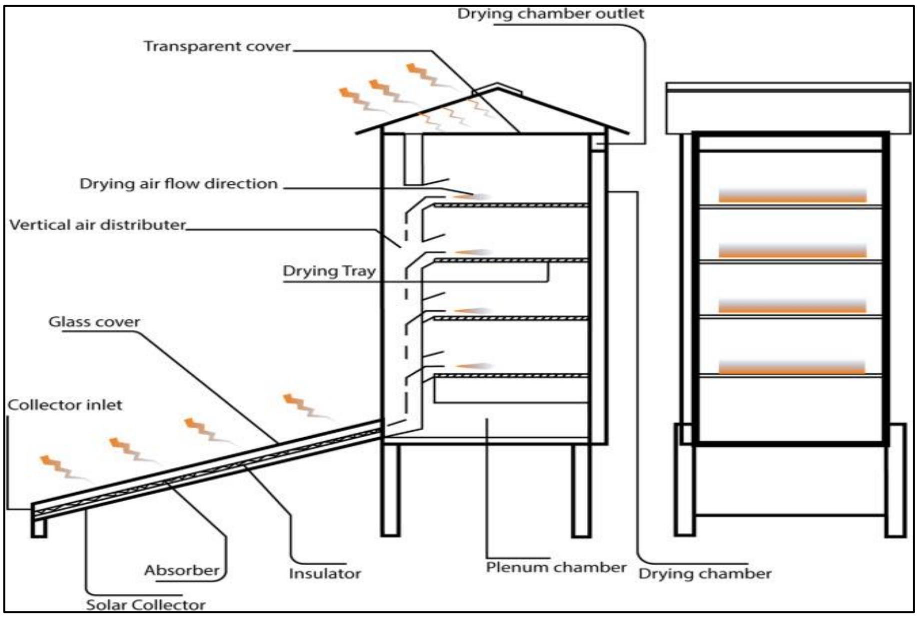

Figure I. 6. Schematic representation of mixed-mode solar dryer [17]

I.3.1.3. Hybrid dryer

Hybrid dryers refer to systems that utilize both solar radiation and additional energy sources, such as electricity, biomass, or fuel, allowing them to function even when sunlight is insufficient. These external sources, known as auxiliary systems, enable the dryer to operate independently of solar energy (Figure I. 7). While hybrid dryers consume more energy compared to other types, they offer improved efficiency by maintaining operation during low solar radiation. As a result, they are versatile across various climates. However, the need for complex control mechanisms and reliance on alternative energy sources makes these dryers more costly.

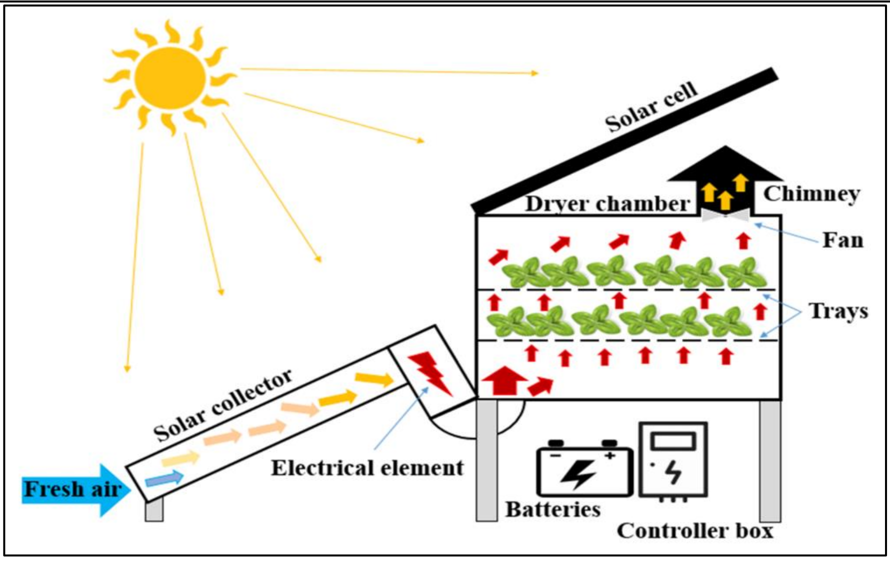

Figure I. 7. Schematic representation of hybrid solar dryer [18]

I.3.2. Advances in solar air collectors

Solar air collectors are essential for optimizing the efficiency and performance of solar drying systems. Their primary function is to absorb solar energy and convert it into heat, which is then used to warm the air circulated within the drying chamber. Notable progress has been achieved in improving the design, materials, and technologies of these collectors to boost their effectiveness and efficiency.

Solar collector is the element that transforms radiation into heat. In water-based solar collectors, heat is transferred between water and air. For air-based collectors used in drying processes, the air is heated within the collector before being directed to the drying chamber. Solar collectors come in various types. Typically, a specific material is used to gather and concentrate solar energy to heat the air. The simplest design employs black materials due to their high efficiency in absorbing solar radiation. Solar air collectors are the most commonly used type, largely because they are efficient at capturing both direct and diffuse solar radiation. Figure I. 8 illustrates different types of solar collectors.

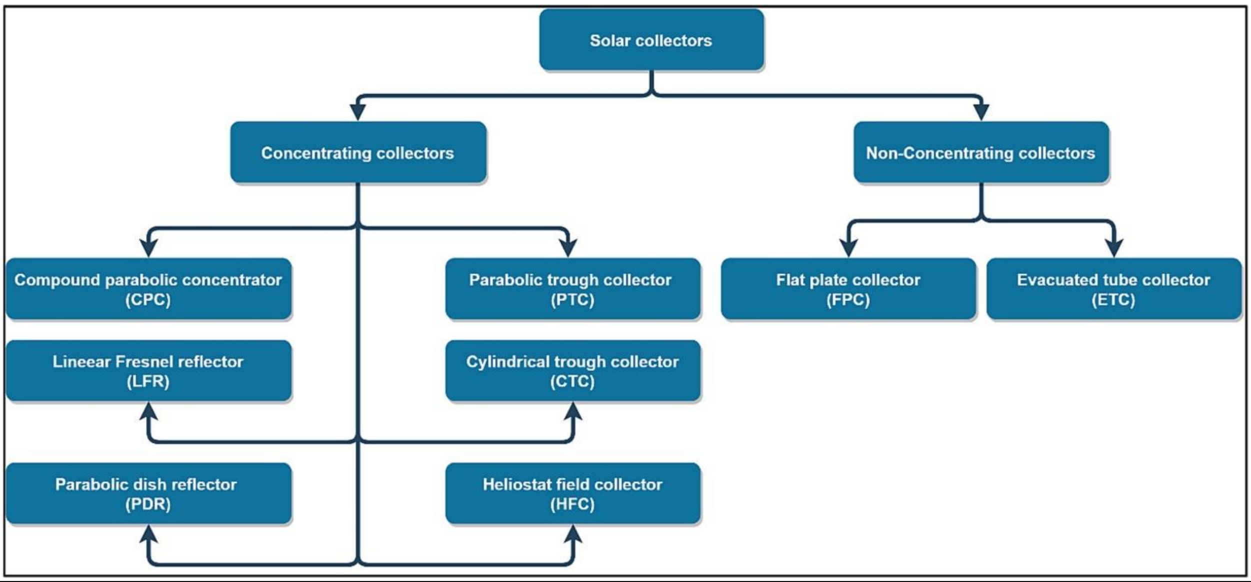

Figure I. 8. Different types of solar air heaters (SC) [1]

In order to attain high thermal performance, Khanlari et al. [19] built a novel parallel pass solar collector with double baffles. It was found that the designed collector's average efficiency was in the range of 71–75%.

In a different research, Gong et al. [20] developed a parabolic trough receiver. They discovered that their new configuration raised the total heat transfer by up to 12% and the average Nusselt number by up to 9%.

Rajendran et al. [21] delved into an experimental investigation on solar air heaters with perforated V-shaped inserts and discovered that the SAH with baffles produced a maximum thermal efficiency of 89.3%.

In a separate study conducted by Rani and Tripathy [22], which explored the thermal performance of a solar collector equipped with semicircular loop fins, the average temperature increase in the solar collector was 22 °C greater compared to a standard flat plate solar collector.

Various types of concentrating and non-concentrating collectors are illustrated in Figures I. 10 and I. 11, respectively. In their review, Tian et al. [23] focused on compound parabolic concentrators, which have garnered increasing attention from both researchers and commercial manufacturers due to their superior efficiency in harnessing solar energy. Temperature and irradiance distribution are the two most crucial factors to take into account while building CPC for many typical applications, such as PV systems.

In order to assess thermal performance and offer more information on the recommended design for other solar heat process applications, the system depicted in Figure I. 9 is a symmetrical CPC with a single-pass evacuated tubular collector.

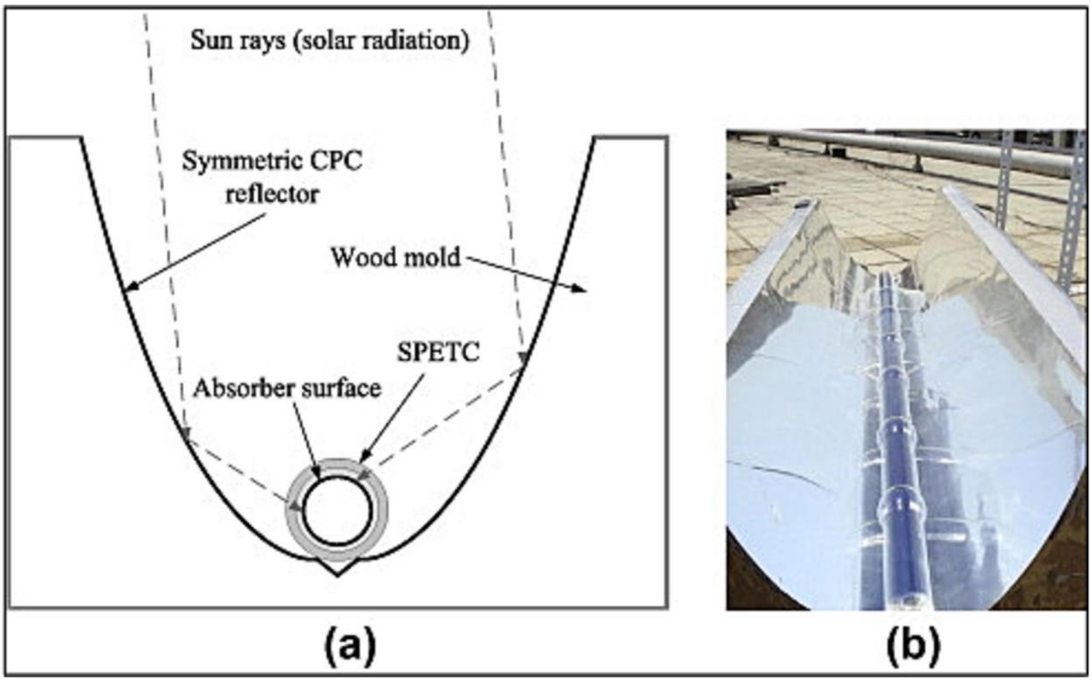

Figure I. 9. Compound parabolic concentrator with SPETC [24]

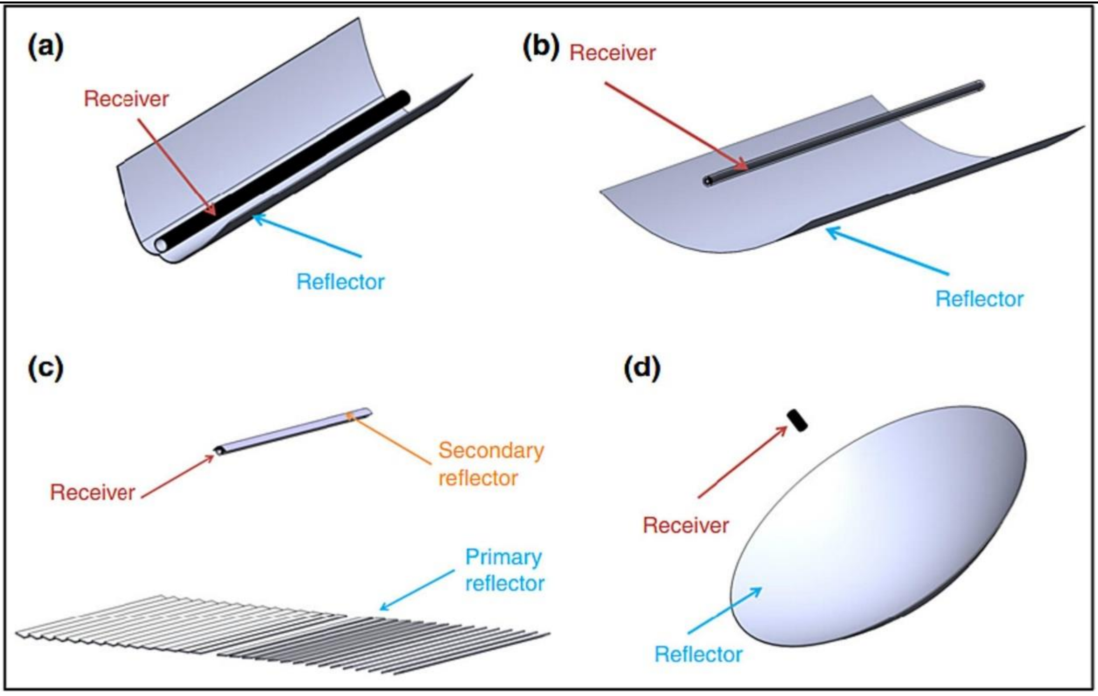

Figure I. 10. Schematic representation of concentrating collectors [25]

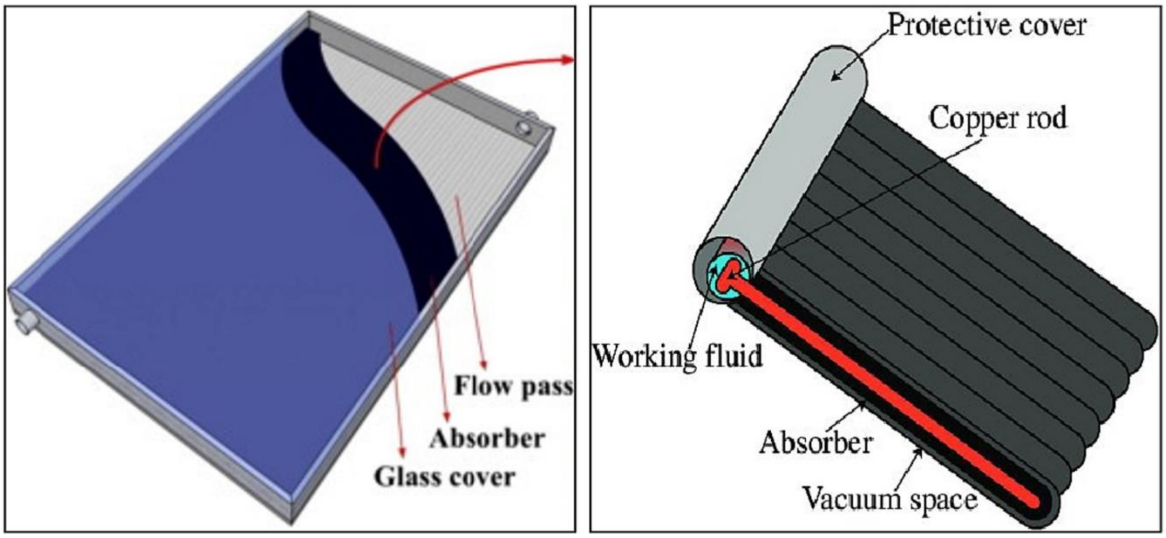

Figure I. 11. Non-concentrating solar collectors [26, 27]

Flat plate solar collectors [28] are commonly used for storing solar thermal energy for drying purposes, as well as for space and water heating.

Bhowmik and Amin [29] attempted to enhance the performance of a flat plate solar collector by adding a solar reflector to its sides, aiming to boost radiation by directing both diffuse and direct sunlight into the collector.

Rezaei et al. [30] analyzed the performance of a dryer equipped with a flat absorber, both with and without phase change material (PCM). The results showed that the collector effectiveness reached more than 70% with PCM and more than 60% without PCM, while the collector outlet temperature was approximately 3°C higher when PCM was used.

Using air as a heat-transfer medium, the traditional solar air heater is used for drying and heating applications. This results in a lightweight, reasonably priced collector and lowers the possibility of corrosion and freezing in solar collectors. However, the reduced specific heat and air density result in considerable pressure losses, requiring high volumetric flow rates [31, 32]. Furthermore, a considerable temperature difference between the heated plate and the airflow and increased heat-transfer resistance are caused by the air's reduced thermal conductivity [33-35].

A novel version of SAH with a spiral spoiler design was proposed by Jia et al. [36]. The effectiveness of this SAH concept was investigated through experiments. This innovative idea had a better heat collecting compared to classic designs, achieving more than 60%.

Also, Hassan et al. [37] conducted experiments on a tubular solar air heater (SAH), designing both a tubular and a flat plate SAH to compare their performance across different airflow rates. The proposed tubular SAH demonstrated superior efficiency compared to earlier designs, reaching an efficiency of 83.6% at 0.075 kg/s. Additionally, the tubular solar collector produced the maximal outlet air temperature increase of 13.2 °C, surpassing the performance of the flat plate SAH.

Dong et al. [38] explored the heat transfer and airflow characteristics of a solar air heater featuring innovative inclined grooved ripple surfaces. They examined the influence of factors such as gap size, penetration angle, and the number of arrays. The inclined grooves on the rippled surface induced a transverse spiral motion in the SAH channel, enhancing air mixing and heat transfer. The proposed design demonstrated an improvement of 50 to 94% compared to conventional solar air heaters. S-shaped blades with holes were used in the creation of a more effective SAH by Wang D. et al. [39]. In comparison to a flat plate, the thermal efficiency of a SAH with additional roughness was found to be improved by 13% to 48% under various circumstances.

In a single pass, Chabane et al. [40] assessed the thermal performance of a five-fin SAH. Underneath the absorber, longitudinal fins were used to enhance heat exchange and fluid flow homogeneity in the channel. Table I. 1 shows design based solar air heaters

Table I. 1. Different designs used for solar air heaters [1]

Insert type	SAH design	Highlights	Ref.
Perforated glass SAH	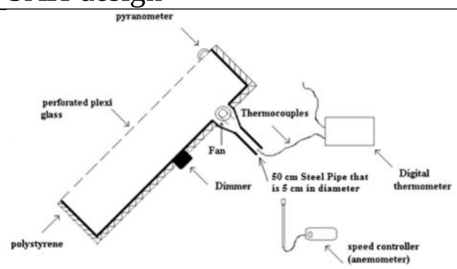	The efficiency of the SAH is significantly increased when plexi glass SAH is used. Promoting higher mass flow rates improves the efficiency while reducing the temperature gradient.	[41]
Helical flow path	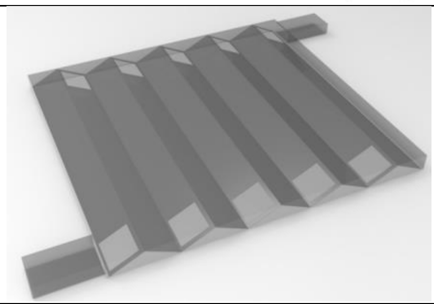	The estimated thermal efficiency of a double-pass SAH with helix channeling is 8.6% higher than that of a double-pass finned SAH and 14.7% higher than that of a regular conduit.	[42]

Curved SAH with semi-down turbulators	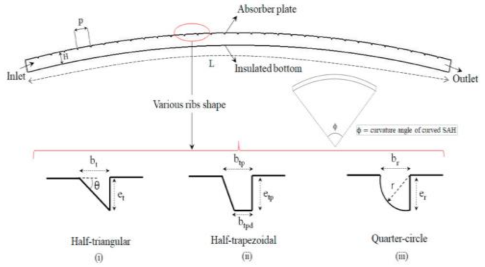	A curved SAH design performs better than a flat one. Half-trapezoidal and quarter-circular ribs have a 17% and 16% improvement in thermal performance, respectively.	[43]
Circular jet impingement	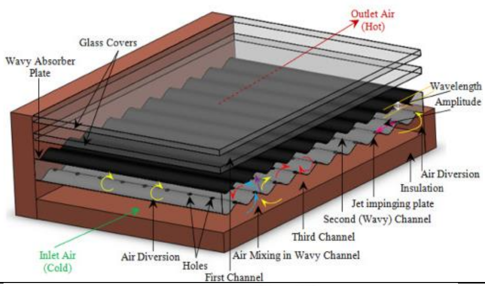	Achieving significant thermal efficiency with a thermohydraulic effectiveness of 94%.	[44]
Reverse L-shaped ribs	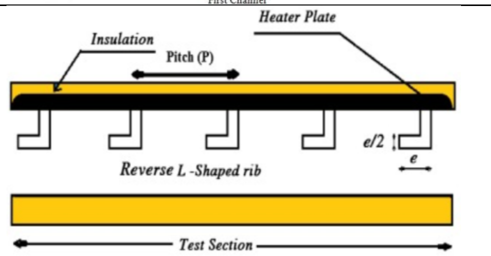	The coefficient of friction and heat transfer characteristics are greatly impacted by the presence of an opposing L-shaped groove.	[45]
Wavy finned SAH	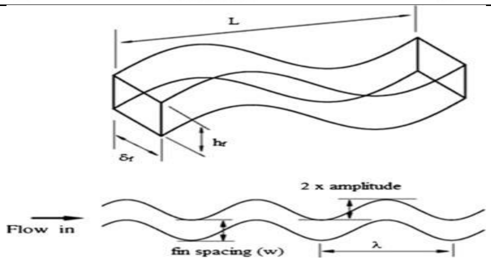	In comparison to conventional flat plate collectors operating in identical circumstances, solar air heaters with wavy finned absorbers demonstrate superior thermal efficiency and temperature, achieving improvements between 29.39% and 62.53%. The highest enhancement in thermohydraulic efficiency occurs in wavy-fin solar air heaters with the smallest fin spacing.	[46]
V-down discrete ribs	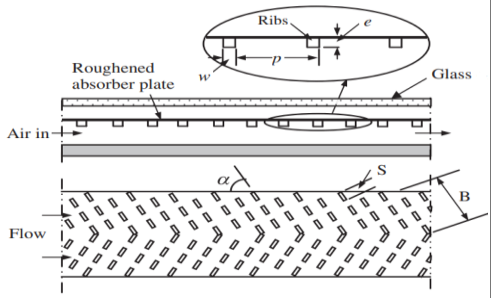	The roughened absorber plate improves thermal efficiency by up to 20%, depending on airflow rate. It operates at lower temperatures and shows greater thermal performance due to reduced energy losses associated with the roughened solar air heater (SAH), resulting in a smaller temperature difference compared to the smooth duct.	[47]

Porous baffles		An airflow of 0.025 kg/s with a collector thickness of 0.6 cm yield the best temperature rise and efficiency in solar air heater. The barriers provide turbulence, encourage sufficient airflow above and below the absorber, and reduce stagnant spots in the SAH.	[48]
C shape roughness	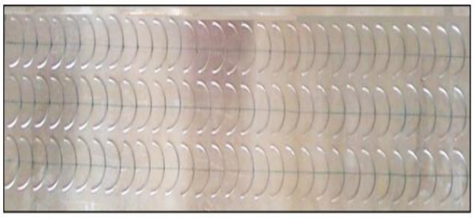	The double-flow solar air heater (SAH) demonstrates superior performance compared to the single-flow design. Multiple C-shaped configurations on either side of the absorber are more efficient than evenly spaced C-shaped roughness in facilitating heat transfer.	[49]
Conical surface		Significant increases in thermal efficiency of 6.0%, 9.8%, and 10.6% were achieved at airflow rates of 0.04, 0.08, and 0.1 kg/s, respectively, due to the conical surface design. The design enables efficient air circulation, increases surface area, minimizes shadowing, and reduces stagnant zones within the duct.	[50]
Arcs with gap	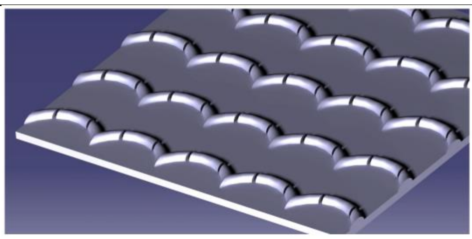	With a maximum augmentation of 5.85, there is a significant improvement in the Nusselt number when employing the suggested roughness configuration.	[51]
Offset strip fins		There was a diminution of almost 43% in drying time. A 33% enhancement to economic efficiency. The drying rate is higher in comparison to traditional solar air heaters (SAH).	[52]

I.3.3. Innovations in drying chambers

A solar dryer's overall efficiency and effectiveness are largely dependent on the design and arrangement of its drying chambers. In order to improve drying performance and energy economy, recent improvements try to optimize heat distribution, ventilation, and moisture removal. This section covers the most current breakthroughs in drying chamber technologies and designs.

Design is very important, and even a small change may make a big difference in total efficiency. To achieve maximum performance and efficiency, it is important to take into account many parameters, in addition to the climate in which the solar dryer runs.

In order to increase drying efficiency, Tuncer et al. [53] investigated the dryer's efficiency under various conditions. The dryer is designed with a novel conical-type solar absorber integrated into the drying cabinet (Figure I. 12). Due to the recommended design's increased internal temperature and air circulation, the drying time was lowered by up to 35%. The convex-type cabinet also had a 51% increase in energy efficiency over the conventional model. Table I. 2 shows design based solar dryers

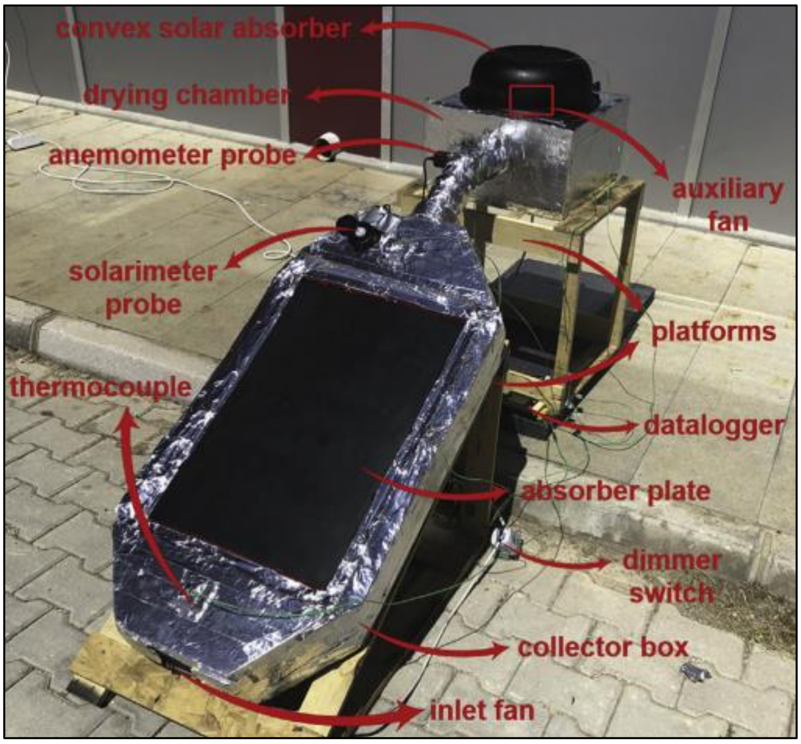

Figure I. 12. Convex-type solar dryer [53]

Krabch et al. [54] developed a natural convection indirect solar thermal dryer (ITSD) featuring a single compartment specifically for drying pears (Figure I. 13). This design functions similarly to a drying cabinet, with walls that absorb radiation and block UV rays. They found that the temperature in the drying chamber could reach 50 °C, with the potential to rise to 60 °C, while maintaining a low humidity level of around 10%.

M.K. John et al. [55] designed the porous mesh-integrated plate SC [48]. When compared to a standard collector, the innovative structure employed maximizes heat transmission and enhances drying efficiency, reducing the drying time by more than 45%.

Figure I. 13. Single compartment ITSD [54]

Singh Parihar et al. [56] introduced an innovative box solar dryer utilizing a UV cover as a substitute for a glass cover, chosen for its cost-effectiveness (Figure I. 14). Their experimental results showed that in a forced convection mode, the final moisture content dropped to 13.75% (w.b.) after 16 hours of drying, while natural convection yielded a moisture content of 17.5% (w.b.) over the same period. The internal temperature of the dryer ranged from 55.2 to 59.2 °C across various trays.

The most widely used TES systems for sun drying have been classified by L. Bennamoun [57]. They concluded that the popular substance used for energy storage is packed-bed storage. They also examined the optimal design parameters for the dryers. The study concluded that incorporating TES enhances the efficiency of solar dryers.

Figure I. 14. UV sheet drying chamber [56]

In order to produce milk powder, Camci [58] developed a hybrid system that included PV panels as an auxiliary system and a spray drier with an integrated SC and PTC. The study aimed to assess the feasibility of utilizing sustainable solar energy for milk powder production. Results indicated that the integration of PTC-SP into the system significantly enhances solar energy utilization, achieving an energy efficiency of more than 75%, and potential improvements in efficiency ranging from 50% to 89% based on the concentration.

Singh et al. [59] developed a solar hybrid greenhouse dryer featuring an evacuated tube collector (ETC) to enhance drying efficiency. The testing included both active and passive modes. Over three non-consecutive days, ginger was dried from an initial moisture content of 79.8% to 9.82% in 13 hours for the active mode and 23 hours for the passive mode. The maximum efficiency of the dryer reached 28.53%, with average efficiencies of 4.81% for active and 3.39% for passive modes. A slow drying process might result in the degradation of high-moisture crops.

A solar conduction dryer (SCD) was created and examined by Jain et al. [60]. The SCD (Figure I. 15) proved to be more effective than other kinds of solar dryers with a drying efficiency of 59.4%, especially those that depended on convection mode, and a payback period of 12 months in terms of thermal efficiency, drying time, and drying rate.

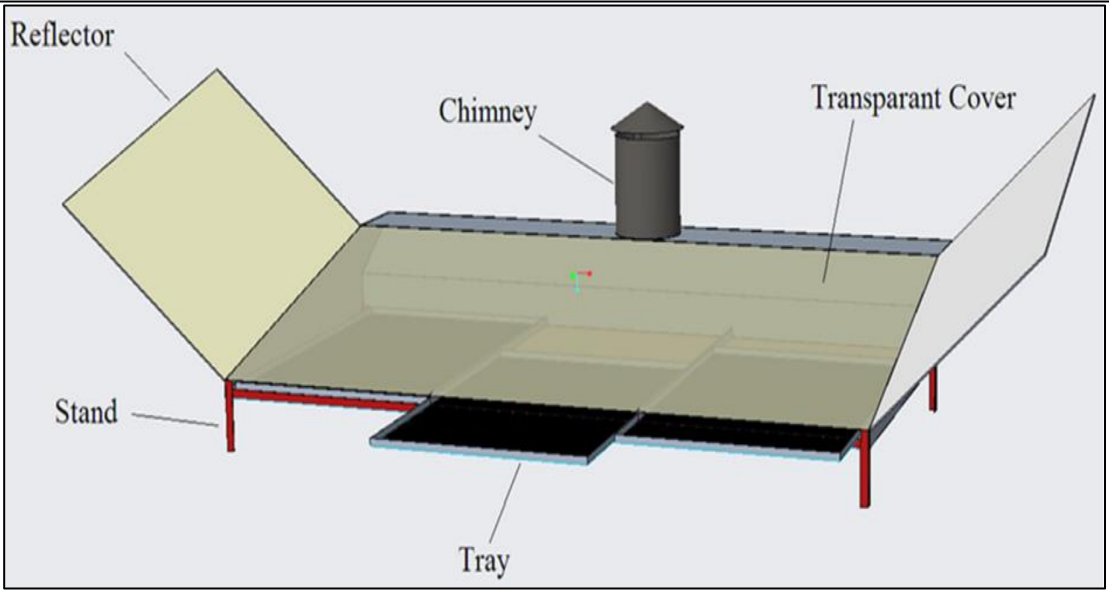

Figure I. 15. Illustration of solar conduction dryer [60]

In order to examine the effectiveness of SAH, Kansara et al. [61] evaluated an FPSC integrating fins with porous medium. According to CFD projections, adding fins raises the temperature by 8.19%, while adding porous medium raises the temperature by 16.17% more than leaving the channel empty.

Verma et al. [62] studied a mixed-mode tent house dryer designed with UV sheets for drying potato slices (Figure I. 16). The drying process relied on natural convection, with temperatures ranging from 33.6 to 59.7 °C. The highest dryer efficiency, 26.62%, was obtained when the potato slices had a thickness of 2.5 mm.

Figure I. 16. Tent house solar dryer [62]

Table I. 2. Different designs used for solar dryers [1]

Dryer type	Design	Discussion	Ref.
Mixed-mode	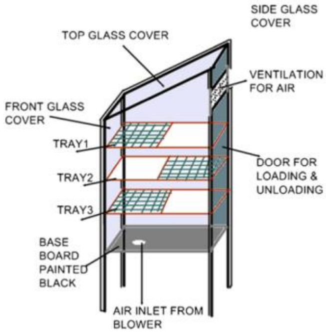	The temperature inside the drying chamber increased by 22°C, reaching 64.5% during most of the daylight hours. The dryer demonstrated its ability to produce outstanding dry goods and quickly and efficiently dry food products to a suitable moisture content.	[63]
Indirect solar dryer		47.15 to 50.68 °C are the average drying temperatures. It takes 18 hours to dry green chilies and 9 hours to dry okra.	[64]
PV-driven quadruple-flow solar dryer		The average exergy efficiency of the drying chamber varied from 44.16% to 58.38%, although the collector's total efficiency varied from 73.27% to 78.19%.	[65]
Indirect solar dryer		In addition to making the dried goods impervious to rain and insects, this innovative drier was found to significantly reduce the amount of time needed for drying. 1.37 years is the dryer's payback time.	[66]
Indirect solar dryer	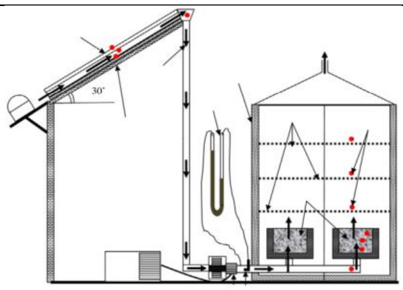	The use of PCM raised the air temperature by as much as 7.5 °C after sunset for a minimum of five hours. The innovative design sustained an optimal temperature for seven hours throughout the testing period.	[67]

Direct conical solar dryer		Operating continuously throughout the day, the conical-shaped solar drier demonstrated its efficiency in drying operations. In addition to providing heat energy for the drying process, using LEDs in the dryer allows the temperature to be maintained overnight.	[68]

I.3.4. Advances in numerical studies of solar dryers

The performance of sun drying systems is examined through numerical research by use of mathematical models and simulations, concentrating on the creation of precise models capable of predicting solar dryer performance in different circumstances. Improving solar dryer operation and design to maximize efficiency and minimize energy consumption is the ultimate objective of numerical research on sun drying. These studies are essential for creating drying methods that are both economical and sustainable for a wide range of agricultural goods.

I.3.4.1. Computational fluid dynamics (CFD)

In solar dryers, airflow and heat transport may be modeled and examined using computational fluid dynamics (CFD). By predicting temperature trends, air movement, and moisture levels under various operating settings, it aids in improving the design and effectiveness of solar dryers. Additionally, CFD is used to investigate how the architecture of the drying chamber, the geometry of the collector, and elements like the location of the air intakes and exits affect the dryer's overall performance.

Fterich et al. [69] conducted an experimental and theoretical study on a solar dryer with a PV/T air collector for drying agricultural food items. The study looked into how temperature and airflow were distributed. The best thermal efficiency for the PV/T was found to be 53% at 0,025 kg/s. Both the computer findings and the experimental results.

For the temperature-controlled fluidized bed solar dryer built by Gürel et al. [70], numerical investigation of the thermal behavior of SAC outfitted with zigzag and flat fins within was also conducted. The created drying method was deemed successful after conducting numerical, experimental, and modelling assessments.

S.A. Sadri et al. [71] conducted both numerical and experimental studies on the impact of incorporating an aluminum honeycomb structure as a latent heat storage (LHS) component in a solar collector (SC). Their findings revealed that the honeycomb core notably reduced the melting time by more than 35%. Additionally, the configuration improved heat transfer by 25% at a mass flow rate of 0.04 kg/s.

The performance of a cost-effective small solar dryer with and without baffles was determined by Afshari et al.'s [72] computational and experimental analysis of the flow and thermal behavior. The dryer with baffles had an edge over the other configuration in terms of performance (Figure I. 17); its average energy efficiency was 55.28% for the dryer with baffles and 44.91 for the dryer without.

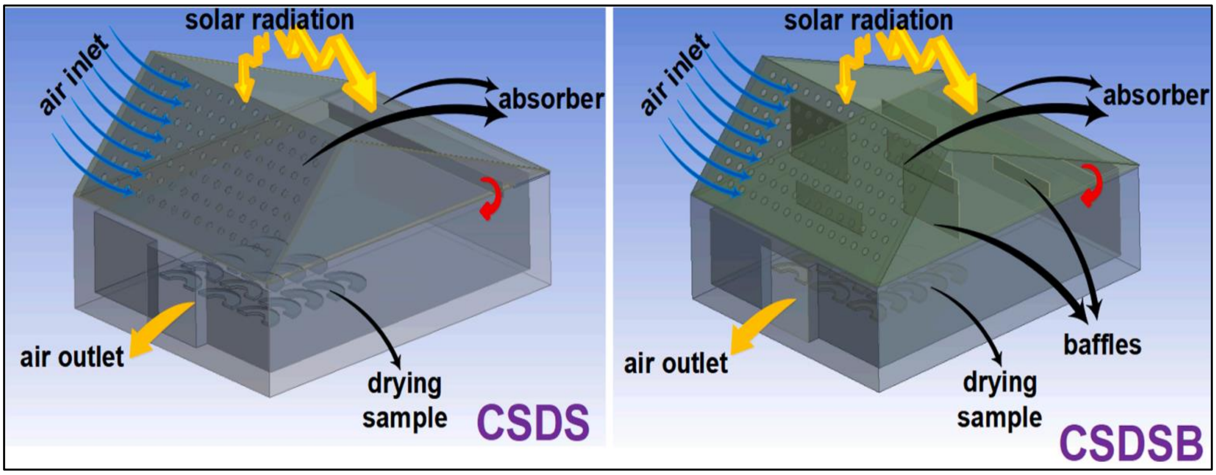

Figure I. 17. Geometry of compact solar dryers [72]

The effect of triangular corrugations on heat transmission inside a solar air collector (SAC) was investigated by Prajapati et al. [73] Ten SAC models with varied pitches were made, and their performance was assessed at various Reynolds numbers along with their flow properties. The results showed that the highest Nusselt number and thermo-hydraulic performance were obtained with a pitch of 135 mm. Moreover, the turbulent kinetic energy increased from 0.05146 to 0.0546 m^2/s^2 when the pitch was raised from 55 to 75 mm. Tuncer et al. [74] quantitatively examined four different PVT collecting configurations to create a special hybrid PVT dryer as shown in Figure I. 18. The outlet temperature of the PVT collector with round tabulators, obstacle configurations, and grooves was 15.77% higher than the collection without any alterations. The estimated payback period for the dryer was three to 3.5 years, and the thermal efficiency of the PVT collector was 77.49%.

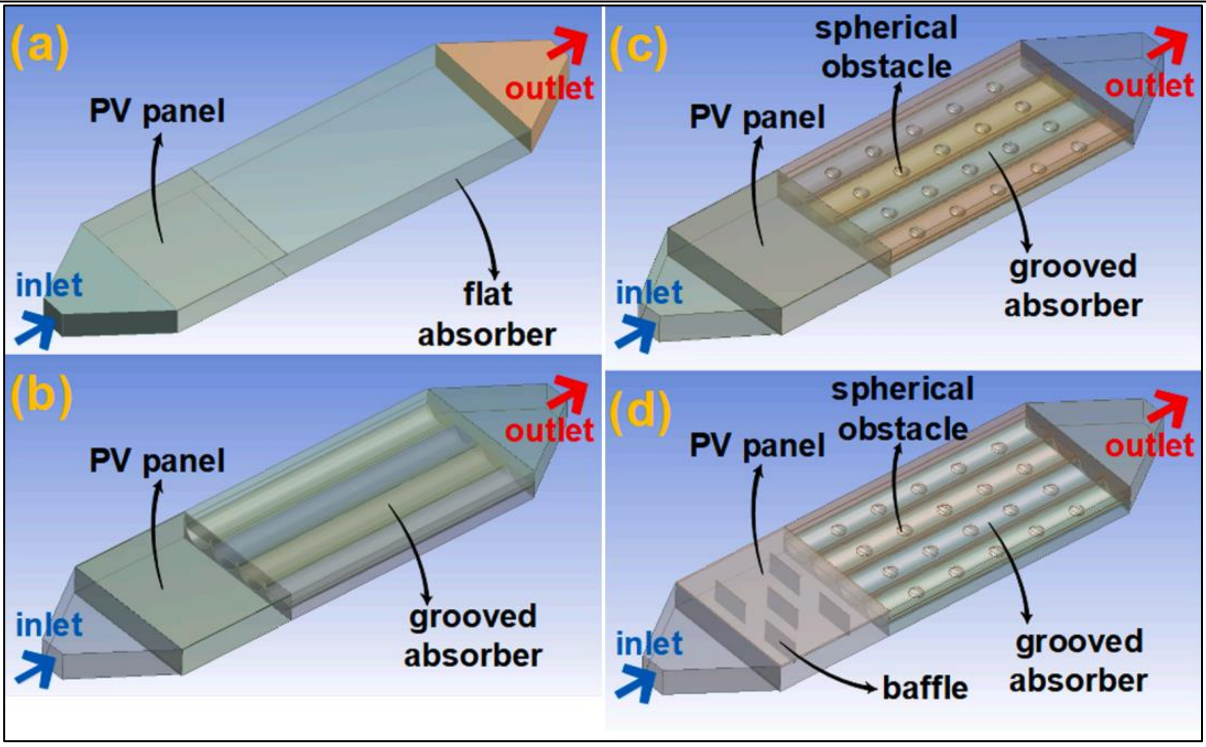

Figure I. 18. Geometries of PVT collectors [74]

A hybrid geothermal-PCM flat plate solar collector drier that is used to dry food was analyzed by Ananno et al. [75]. Their computational analysis showed that the hybrid system's efficiency was 20.5% higher than that of conventional flat plate solar collectors, resulting in a 20% decrease in energy consumption. The collector's highest temperature was 60.59 °C at the exit.

Abhay et al. [76] used 2D numerical simulations to study the airflow and heat transmission properties of an indirect-type solar dryer with a square-shaped rib above the absorber plate. When compared to a smooth duct, the roughened surface of the solar air collector can improve heat transmission by up to 112.85% and potentially reach a maximum heat gain of 106%.

Motahayyer et al. [77] aimed to increase solar collectors' thermal efficiency for sun-drying food. Three separate setups were used to conduct the investigation: a porous system, a porous system, and a porous and recycling system. The findings showed that the porosity and recycling system, with a drying efficiency of 54%, had the highest overall heat transfer increase of 21.19%. In order to evaluate the environmental impact of four absorber plate solar air collectors, Alic et al. [78] performed a numerical analysis using exergetic evaluation. The Z-type solar collector showed the maximum efficiency, reaching 78%, based on the numerical results.

Using CFD, Al-Kayiem et al. [79] modeled four distinct inlet designs. The air at the chimney had a larger mass flow and velocity than at the other three entrance types, indicating that the inlet with a vertical cross-section had the maximum efficiency. According to this CFD study, the upper area over the intake was where most of the airflow in the collector originated.

Sozen et al. [80] developed a single-pass heater with a tube-style absorber and incorporated it into a drying chamber, guided by numerical simulations. The experiments, conducted at two distinct airflow rates, revealed that incorporating aluminum wool inside the tubes led to a 24-40% increase in energy consumption while reducing drying time by 30%.

I.3.4.2. Thermodynamic analysis

A thermodynamic study of solar dryers involves assessing and evaluating the energy and heat transfer mechanisms within the system. This analysis utilizes the principles of thermodynamics to gain insights into various aspects of solar drying systems, including their performance, efficiency, and overall energy consumption.

A PV hybrid dryer was used by Silva et al. [81] to analyze the energy and exergy of drying corn. Control volumes in the thermodynamic study were used to assess the system's performance for the drying chamber, the drying chamber with SAH, and the entire system. With exergy ranging from 22 to 45%, it was discovered that control volume had an impact on efficiency.

Hassan et al. [82] conducted a thermodynamic analysis of a double-pass solar air heater (SAH) to improve its performance as shown in Figure I. 19. The thermodynamic model was validated using experimental data, and the results demonstrated strong alignment in terms of the outlet temperature, thermal efficiency, and exergy efficiency of the collector.

As part of the thermal analysis developed by Hatami et al. [83], the energy consumption and drying process efficiency are computed using a model to investigate energy and exergy based on multiple variables. The model and the experimental data demonstrated good agreement, with variances ranging from 1% to 4.8%.

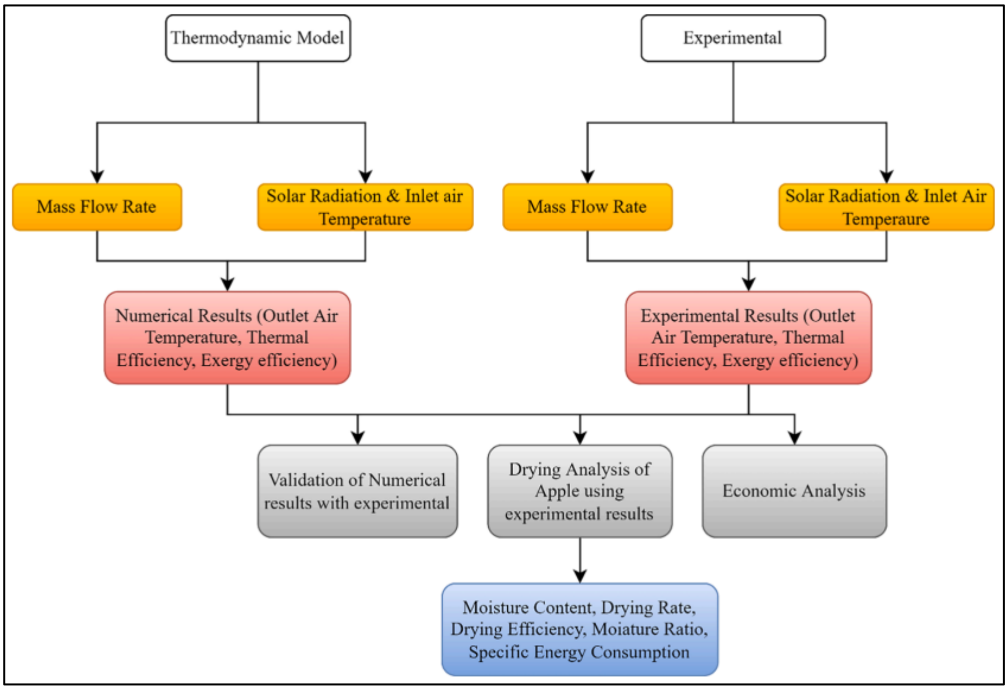

Figure I. 19. Tree structure of a thermodynamic model [82]

A thermodynamic analysis of a combined sun drier was conducted by Djebli et al. [84] in order to determine the drying curves, effective moisture diffusivity, and thermodynamic features of tomato drying. The model was validated against the model published in the literature, and it passed. The outcomes also showed that the drying process is spontaneous in accordance with Gibbs free energy values. Additionally, the exergy and energy performance of a passive solar dryer was investigated by Lingayat et al. [85]. After calculating the energy used by the solar air heater (SAH), they discovered that there were energy losses of between 7.4% and 45.32% during the drying process.

I.3.5. Identified research gaps and future directions

The motivation for this study is grounded in several key observations from the existing literature on solar drying technologies. Firstly, while solar air heaters have been extensively investigated for their efficiency and performance, there is a notable gap in research directly applying these advancements to drying applications. This presents an opportunity to bridge the gap between solar air heater innovations and their practical implementation in solar dryers, adding significant value to this study. Secondly, the current body of research on solar dryers often overlooks the consideration of environmentally friendly materials in their design and construction. With the increasing emphasis on sustainability and reducing the environmental impact of industrial processes, it is crucial to explore the use of eco-friendly materials in solar drying systems. Highlighting this aspect not only aligns with global sustainability goals but also promotes the development of more sustainable drying solutions. Moreover, the focus of most studies on solar dryers has been predominantly on improving the solar air collectors and the overall system design, with limited attention given to the drying chamber itself. Enhancing the efficiency of the drying chamber by optimizing heat transfer mechanisms within the chamber can lead to significant improvements in drying performance. Integrating external shapes such and other geometric modifications to enhance internal heat distribution is a relatively unexplored area that holds promise for further advancements. In summary, this study is motivated by the need to address these gaps in the literature: the direct application of advanced solar air heater technologies to drying applications, the use of environmentally friendly materials in solar dryers, and the improvement of heat transfer within the drying chamber. By focusing on these areas, this research aims to develop more efficient, sustainable, and effective solar drying systems, contributing to the broader adoption of renewable energy technologies and enhancing the sustainability of drying processes in various industries.

Chapter II: Experimental study

II.1. Introduction

In this chapter, we delve into the experimental study conducted at the Applied Research Unit for Renewable Energies in Ghardaia. The focus of this chapter is to provide a comprehensive overview of the various experimental setups and methodologies employed to enhance solar drying technologies. The chapter begins with a detailed description of four key experimental setups: the enhancement of solar collectors, the optimization of drying chambers through material considerations, the improvement of direct solar dryer via the integration of obstacles, and the improvement of indirect solar dryer through the addition of ribs. Following the setup descriptions, the chapter outlines the experimental procedures, measuring instruments used, and the specific drying experiments carried out. Additionally, the chapter covers energy evaluations, economic analyses, and environmental impact assessments, offering a thorough examination of the effectiveness and benefits of each enhancement in the context of renewable energy applications.

II.2. Experimental setup

In this section, we present the experimental setups employed to assess the performance and efficiency of various solar drying configurations. Four distinct setups were designed and tested, each incorporating unique design features and materials to evaluate their influence on the drying process. These setups include a baseline conventional indirect solar dryer enhanced with collector inserts, a dryer equipped with internal baffles, a dryer constructed with environmentally friendly materials, and a dryer featuring integrated heat transfer enhancements, such as fins. Each setup is detailed below to offer a comprehensive understanding of its design, construction, and operational principles.

The experiments were developed and conducted at the Applied Research Unit for Renewable Energies (URAER) in Algeria (32°36′N, 3°48′E).

II.2.1. Experiment 1: Solar air collector enhancements

The solar air collector consists of an absorber plate made from 0.8 mm thick aluminum, covered by a 5 mm thick glass panel. The collector's overall dimensions are 2000 mm in length, 1000 mm in width, and 150 mm in height. Figure II. 1 illustrates the solar collector with integrated fins, while Figure II. 2 depicts the collector containing rocks as a storage medium.

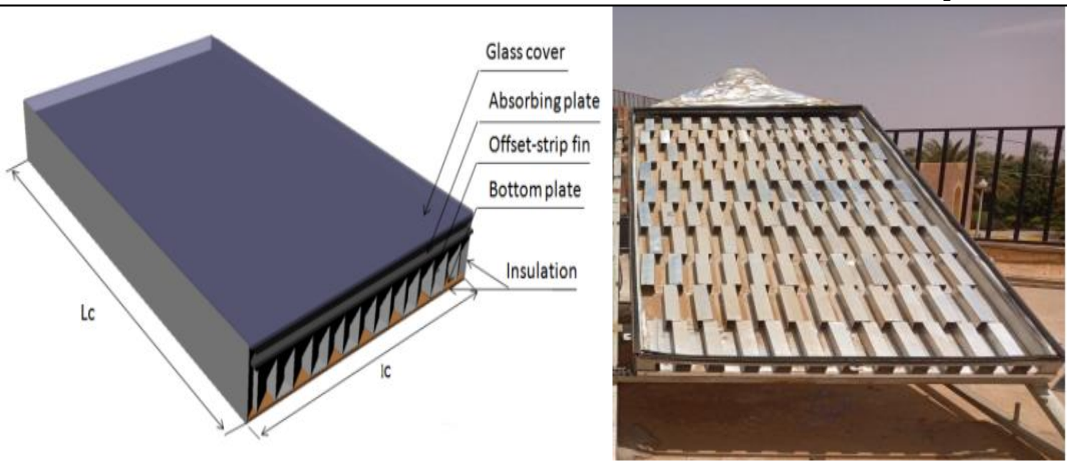

a) b)

Figure II. 1. Solar collector with fins, a) Schematic illustration; b) Photograph of the air collector

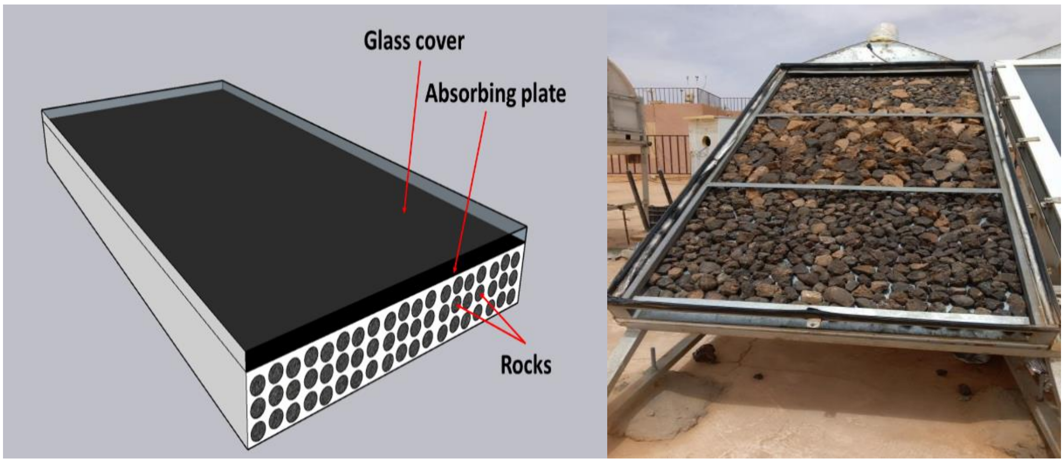

a) b)

Figure II. 2. Solar collector with rocks, a) Schematic illustration; b) Photograph of the air collector

II.2.2. Experiment 2: Material consideration

The direct solar dryer consists of a triangular-shaped enclosure made from a mixture of clay and hay with a 14 cm thickness, with dimensions shown in Figure II. 3. The front side is constructed with 6 mm thick polycarbonate sheets to permit sunlight to enter and is inclined at 32° with a surface area of 2.36 m^2. For the sides, one serves as the door, also made of polycarbonate, while the other functions as a wall with a fan positioned in the center to extract air from the chamber. Similarly, the indirect solar dryer is constructed in the same manner as the direct dryer. However, on the front side, a solar collector is positioned directly above the chamber, also inclined at 32°. The solar collector has a surface area of 2 m^2 and is covered with a 6 mm thick polycarbonate sheet. The absorber, painted in black, is 0.5 mm thick with a 5 cm gap in between for air to pass. The sides are constructed similarly to the direct dryer. Both dryers have four shelves each, with each shelf capable of holding up to five trays.

Figure II. 3. Image and illustration of the clay based direct solar dryer

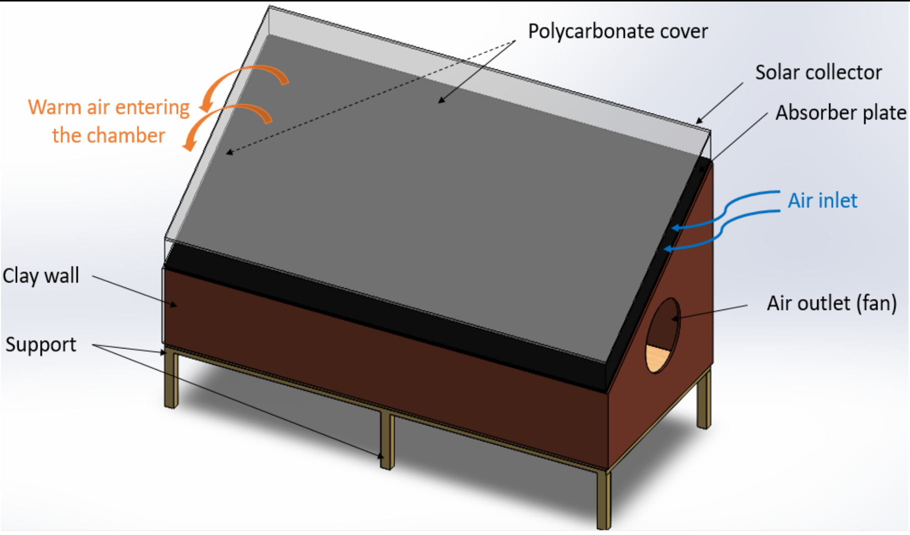

Figure II. 4. Image and illustration of the clay based indirect solar dryer

II.2.3. Experiment 3: Direct solar dryer enhancement

Two direct solar dryers in the shape of triangular boxes were designed and constructed using 40 mm thick sandwich panels for effective insulation. The front featured an inclined glass cover set at 32°, corresponding to the latitude, with an additional smaller glass cover below to maximize sunlight capture. Inside, a 1 mm thick aluminum sheet painted black was used to enhance heat absorption. Each dryer included an 80 mm inlet on one side at the bottom and a 150 mm outlet with a 50 W fan on the other side. Both dryers were oriented south to capture maximum solar energy. The two dryers were identical, with one incorporating UV sheets as obstacles to optimize airflow distribution. The two developed direct solar dryers are shown in Figure II. 5.

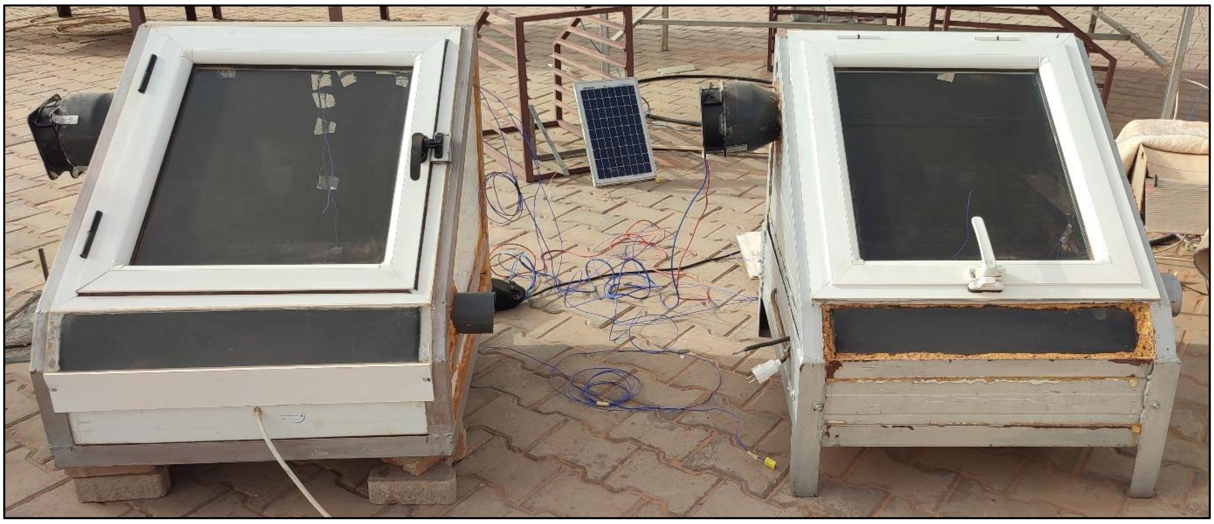

(a)

(b)

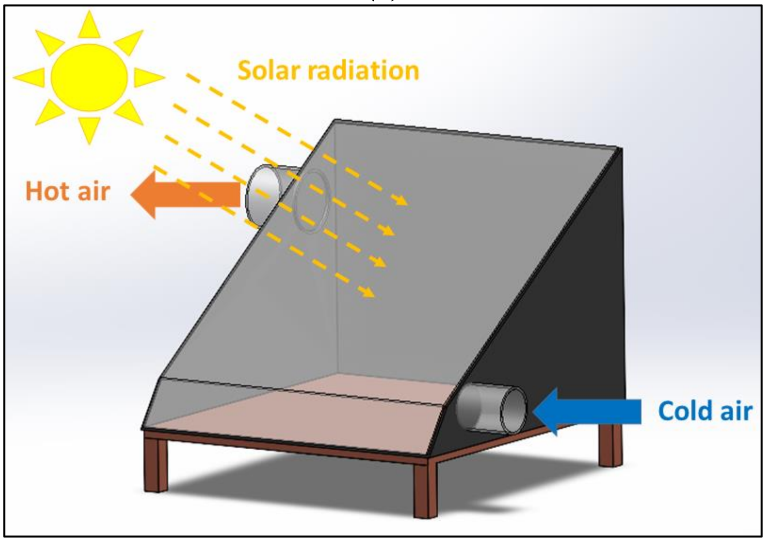

(c)

Figure II. 5. Photographic image and schematic representation of the experimental setup: (a) Solar dryers before modifications; (b) Solar dryers after modifications; (c) Boundary conditions

II.2.4. Experiment 4: Indirect solar dryer enhancement

The experimental setup is an indirect type solar dryer tailored for laboratory use. It features a solar collector measuring 1.5 meters by 0.6 meters, equipped with a 1500 W electrical heater situated in the airflow passage beneath the absorber plate to ensure consistent heat distribution. This heater is regulated by an Arduino board, which adjusts the temperature based on real-time signals to maintain optimal drying conditions. The drying chamber, measuring 1.2 meters by 0.4 meters by 0.4 meters, is horizontally placed and directly connected to the collector outlet. To ensure uniform airflow and enhance drying efficiency, a 50 W fan is positioned at the center of the chamber's outlet side.

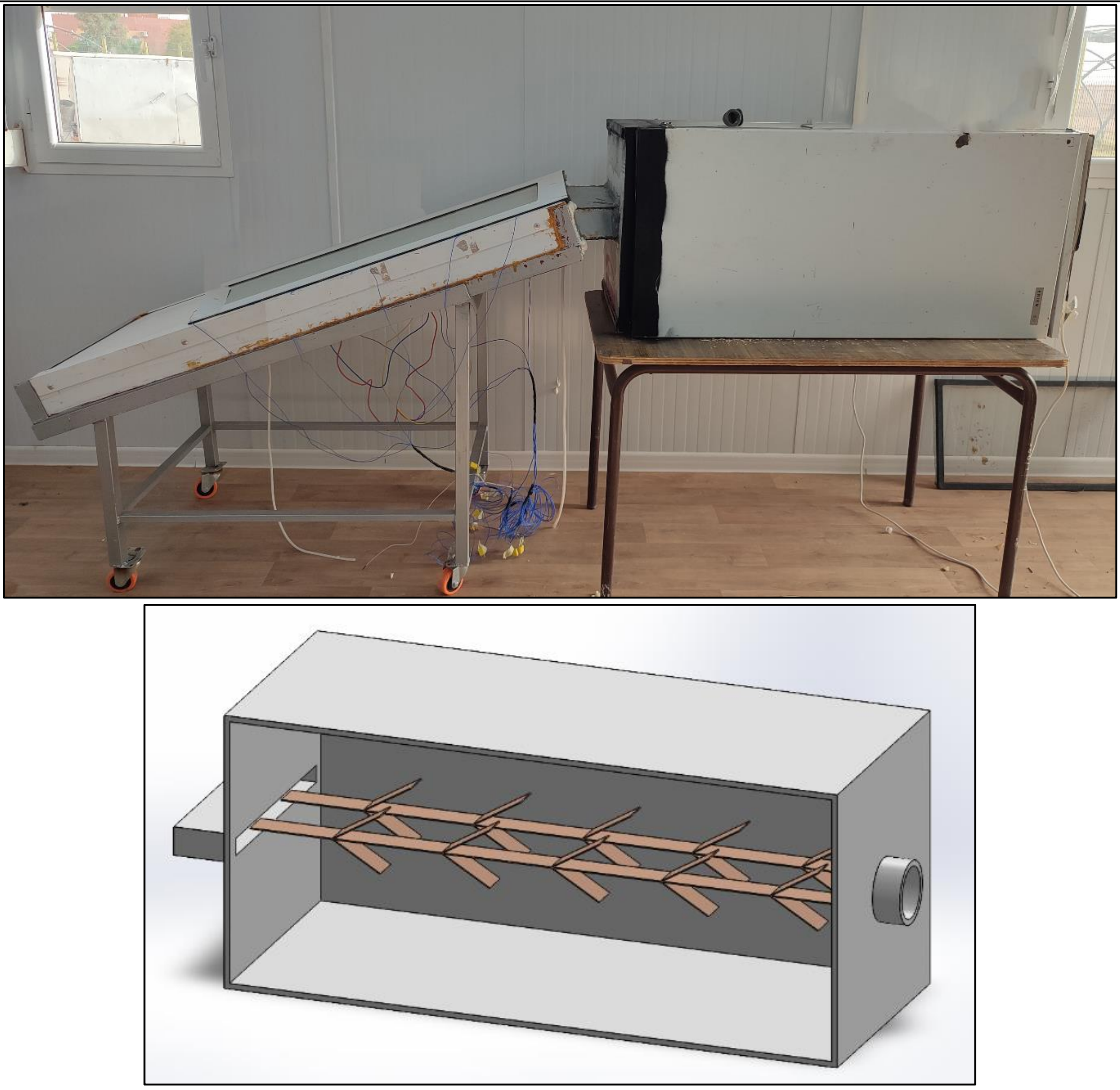

Figure II. 6. Photograph and schematic illustration of the indirect solar dryer

II.3. Experimental procedure

II.3.1. Samples preparation

Fresh products were obtained from a local market. To determine the dry mass, samples were sliced and placed in an oven at 105°C for 24 hours. For the drying process, the products were uniformly sliced into 5 mm thick pieces.

Figure II. 7. Moisture content determination process

II.3.2. Systems performance

All the constructed solar dryers and solar air collectors were tested under forced convection conditions. The testing process was divided into two phases. The first phase involved monitoring the thermal behavior of the systems without any products loaded. This baseline test aimed to assess the temperature distribution, airflow characteristics, and overall heat transfer efficiency of the dryers and air collectors. In the second phase, the trays were filled with fresh products, and their drying performance was observed. This test evaluated the systems' effectiveness in reducing moisture content, drying rates, and uniformity of drying across the products. By conducting these two phases of testing, a comprehensive understanding of both the thermal dynamics and practical drying capabilities of the solar drying systems was achieved.

II.4. Measuring instruments and uncertainty

A digital anemometer, thermo-hygrometer, thermocouples, and pyranometer were utilized sequentially to measure and automatically record air velocity, ambient temperature, inlet and outlet temperatures of the system, and solar radiation. An analytical balance was employed to measure the mass. Detailed specifications of the measuring instruments, along with their associated uncertainty values, are presented in Table II. 1.

(a) (b) (c) (d)

Figure II. 8. Measuring instruments used in the experiments: (a) Thermocouple; (b) Anemometer; (c) 12 Channel temperature data logger; (d) Pyranometer

Assessing uncertainty in empirical findings is essential for any experimental study, as it indicates the degree of accuracy and reliability of the results. Various methods have been proposed by researchers to address this issue. To ensure a thorough examination of the results within an acceptable range, we used a method in this study that assesses the uncertainty of any dependent factor relying on the uncertainty of independent variables.

Let $x_1,x_2,x_3,\ldots,x_n$ are the independent variables, and R is the dependent variable. Thus, the uncertainty of R dependent variable WR is [86]:

$$W_R = \left[\left(\frac{\partial R}{\partial x_1} w_1\right)^2 + \left(\frac{\partial R}{\partial x_2} w_2\right)^2 + \cdots + \left(\frac{\partial R}{\partial x_n} w_n\right)^2\right]^{1/2} \qquad \text{(II.1)}$$

The uncertainties of the results are computed using the mentioned equation. Table II. 1 presents the uncertainty values that were computed throughout the performance tests.

Table II. 1. Measuring instruments and uncertainties

Instrument and model name	Usage	Range	Uncertainty
Anemometer - EMC-9400SD	Air velocity	0.4 to 25 m/s	0.245
Type K thermocouples - Nickel-Chrome/Nickel-Aluminum	Temperature	−200 to 1350 °C	0.287
Balance - KERN ABT 220–4 M	Mass	20 to 220 g	0.224
Balance - KERN PCB 3500–2	Mass	0 to 3500 g	2.002
Pyranometer -	Solar radiation	0 to 2000 W/m²	0.51

II.5. Drying experiences

II.5.1. Moisture content

Water extraction procedure involved periodic weighing of the sweet pepper samples until no additional weight loss was detected. The moisture content that had been extracted out of the product was then calculated as:

$$Mc = \frac{M_0 - M_f}{M_0} \times 100 \tag{II.2}$$

In Equation (II.2), M_c stands for the initial moisture content of the product (w.b. %), M_0 represents the original weight of the product prior to drying, and M_f indicates the final weight of the product following the drying procedure.

The moisture ratio (MR) of the materials was assessed within the experimental context by using the next equation:

$$MR = \frac{M_t - M_e}{M_0 - M_e} \tag{II.3}$$

The moisture content (on a dry basis) at a given time (t), at equilibrium, and at the beginning time (t = 0) are represented by the variables (M_t), (M_e), and (M_0) in Equation (II.3), respectively. By taking into account the difference between the equilibrium moisture content and the moisture content at any given moment, normalized by the difference between the equilibrium moisture content and the initial moisture content, this equation calculates the moisture ratio.

The drying rate at which the product was dried during the tests is referred to as:

$$DR = \frac{d_M}{dt} = \frac{M_t - M_{t+\Delta t}}{\Delta t} \tag{II.4}$$

II.5.2. Modeling of drying kinetics

The moisture ratio (MR) of the samples was consistently calculated during the experiments using the following equation:

$$MR = \frac{Mt - Me}{M0 - Me} \tag{II.5}$$

Where Mt is the moisture content (d.b.) at time t, Me at the equilibrium, and M0 at t=0.

Table II. 2. Thin-layer drying models

Model	Equation	Reference
Newton	$MR = \exp(-kt)$	[87]
Page	$MR = \exp(-kt^n)$	[88]

Modified Page	$MR = \exp(-(kt)^n)$	[89]
Henderson and Pabis	$MR = a\exp(-kt)$	[90]
Logarithmic	$MR = a\exp(-kt) + b$	[91]
Midilli-Kucuk	$MR = a\exp(-kt^n) + bt$	[89]
Approximation of Diffusion	$MR = a\exp(-kt) + (1-a)\exp(-kbt)$	[92]
Modified Two-Term Exponential	$MR = a\exp(-k1t) + (1-a)\exp(-k2t)$	[93]
Two-Terms	$MR = a\exp(-k1t) + b\exp(-k2t)$	[94]
Two-Terms Exponential	$MR = a\exp(-kt) + (1-a)\exp(-kat)$	[95]

The dynamics of the drying process are represented by thin layer drying models. Ten distinct proposed models are compared in order to determine which is the most suitable. Finding the best model to describe the drying curves depends heavily on the coefficient of determination (R^2). To assess the goodness of fit, additional statistical measures are used in addition to R^2, such as root mean square error (RMSE) and reduced chi-square (X^2). Here is how these coefficients are computed [96]:

$$R^2 = 1 - \frac{\sum_{i=1}^{V}(MR_{exp,i} - MR_{pre,i})^2}{\sum_{i=1}^{V}(\overline{MR_{exp,i}} - MR_{pre,i})^2} \tag{II.6}$$

$$\chi^2 = \frac{\sum_{i=1}^{V}(MR_{exp,i} - MR_{pre,i})^2}{V - v} \tag{II.7}$$

$$RMSE = \sqrt{\frac{1}{N}\sum_{i=1}^{V}\left(MR_{pre,i} - MR_{exp,i}\right)^2} \tag{II.8}$$

With

$$\overline{MR_{exp,i}} = \frac{\sum_{i=1}^{V} MR_{exp,i}}{V} \tag{II.9}$$

Here, $MR_{exp,i}$ denotes the moisture content observed during the tests, and $MR_{pre,i}$ denotes the moisture content forecasted by the model. *V* represents the total number of observations, and *v* signifies the constants number.

II.5.3. Effective moisture diffusivity

Diffusion is the main factor that controls mass transfer throughout drying, which is affected by the moisture content of the material. To properly describe this mass transfer, it is crucial to determine the effective moisture diffusion. This coefficient is derived using Fick's equation, which provides a mathematical framework for understanding how moisture migrates through the material:

$$\frac{\partial MR}{\partial t} = D_{eff}\nabla^2 MR \tag{II.10}$$

Assuming the slab exhibits an infinitely rigid and undeformable geometry, Crank [97] formulated Fick's approach as follows:

$$MR = \frac{8}{\pi^2}\sum_{n=0}^{\infty}\frac{1}{(2n+1)^2}exp\left(-(2n+1)^2\pi^2 D_{eff} t/4L^2\right) \quad \text{(II.11)}$$

In this context, (D_{eff}) represents the effective diffusivity measured in (m^2/s). The variable (t) refers to time in (s), while (L) denotes the half-thickness of the material sample in (m). The parameter (n) is a positive integer that signifies the order of the diffusion process.

Equation (II.11) can be represented in logarithmic form:

$$ln(MR) = ln\left(\frac{8}{\pi^2}\right) - \frac{\pi^2 D_{eff} t}{4L^2} \quad \text{(II.12)}$$

The formula for effective moisture diffusivity is:

$$Slope(k) = \frac{\pi^2 D_{eff}}{4L^2} \quad \text{(II.13)}$$

II.6. Energy evaluation

The performance of a dryer is assessed by its drying efficiency, which measures the proportion of heat effectively used for drying relative to the total heat consumed. Mathematically, drying efficiency is defined as the ratio of the heat utilized for drying to the total heat input [98].

Total heat received and dispensed by the solar dryer can be calculated using:

$$Q_o = \dot{m}C_p(T_{out} - T_{in}) \quad \text{(II.14)}$$

With Q_o is the total heat output (kJ/s), $\dot{m}$ is the mass flow rate (kg/s), C_p is the specific heat (J/kg.K), T_{out} and T_{in} the temperature at the outlet and inlet of the dryer, respectively.

$$Q_i = IA_c \quad \text{(II.15)}$$

Here, Q_i is the total heat input (kJ/s), I is the solar irradiation (W/m^2), and A_c is the apparent area of the dryer (m^2).

With specific heat capacity expressed as a polynomial function of air temperature at the inlet [99]:

$$C_p = 1009.26 - 0.0040403 * T + 0.00061759 * T^2 - 0.0000004097 * T^3 \quad \text{(II.16)}$$

The efficiency of solar dryer is determined by:

$$\eta_c = \frac{Q_o}{Q_i} \times 100 \quad \text{(II.17)}$$

II.7. Economic study

Economic study is a critical stage in gaining public approval for a project. Annual cost, life cycle savings, and payback period. These are the three important aspects that should be addressed while analyzing a solar dryer project

II.7.1. Annualized cost

Annual cost considers the annual salvage value (S_a), the cost of the dryer's elements (C_{ac}), maintenance costs (C_m), and electrical energy costs (C_{el}).

As per [100] annualized cost is denoted by:

$$AC = C_{el} + C_{ac} + C_m - S_a \quad \text{(II.18)}$$

With C_{ac} and S_a are computed by:

$$C_{ac} = C_{cd} \times \frac{i(1+i)^n}{(1+i)^n - 1} \quad \text{(II.19)}$$

$$S_a = S \times \frac{i}{(1+i)^n - 1} \quad \text{(II.20)}$$

Here, C_{cd} denotes the cost of the direct and indirect dryers, amounting to $898 and $1031, respectively. Additionally, S denotes the salvage value in dollars, equivalent to 1/10 times C_{cd}. The annual cost of power (C_{el}) required to operate the setup is computed based on the electricity generated by the fan. The unit price of electricity in Algeria (C_{ee}) is $0.03:

$$C_{el} = C_{ee} \times W_p \times t \quad \text{(II.21)}$$

Annual cost split by the annual amount of dried product (M_{year}) yields the required amount to dry one kilogram (CD_{kg}). To compute CD_{kg}, equation below is used:

$$CD_{kg} = \frac{AC}{M_{year}} \quad \text{(II.22)}$$

II.7.2. Life cycle savings

The savings per day of drying is determined by dividing the cost of the initial product designated for dehydration by the kilograms of dried items yielded from the dryer:

$$C_{dry} = C_{fre} \times \frac{M_{fre}}{M_{dry}} \quad \text{(II.23)}$$

The cost per kilogram of dried plants (C_{drys}) produced by the solar dryer is calculated by adding the pre-drying cost of the raw material (C_{dry}) to the drying cost (CD_{kg}) incurred for each kilogram of the dried product.:

$$C_{drys} = C_{dry} + CD_{kg} \quad \text{(II.24)}$$

The following values pertain to the financial benefits achieved: savings per kilogram of dried material obtained (B_{kg}) for the reference year, savings per batch processed (B_b), and savings accrued per day of drying (B_d):

$$B_{kg} = C_{bdp} - C_{drys} \quad \text{(II.25)}$$

$$B_b = B_{kg} \times M_{dry} \quad \text{(II.26)}$$

$$B_d = \frac{B_b}{D_b} \quad \text{(II.27)}$$

The drying system's annual savings (B_j) over its full lifespan are represented as:

$$B_j = B_d \times D_{year} \times (1 + r)^{j-1} \quad \text{(II.28)}$$

II.7.3. Payback period

The period of time necessary to repay the original investment in a drying system. Moreover, as mentioned by:

$$P_b = \frac{\ln(1-\frac{C_{cd}}{B_1}(i-r))}{\ln(\frac{1+r}{1+i})} \quad (II.29)$$

II.8. Environmental analysis

During the building, operating, and disposal phases of its life cycle, any created facility uses a large quantity of energy. Operational energy and embodied energy make up the two parts of total energy consumption. The entire energy used in the extraction, shipping, production, building, usage, and disposal of raw materials is known as embodied energy [101]. The quantity of energy needed to power the equipment when it is in use or during operation is known as the operational energy. A system's operating energy makes up a sizable amount of its overall energy usage. However, embodied energy is contributing more and more to the overall lifetime energy consumption in the construction of energy-efficient structures.

In an effort to utilize less traditional energy resources, experts have concentrated on lowering the overall energy consumption of constructed structures in recent years. Solar dryers are among the energy-efficient buildings because they run on solar energy, a renewable energy source that is clean, free, and environmentally good. The system's overall energy consumption may be used to evaluate its energy efficiency, while indicators like embodied energy, energy payback period, and greenhouse gas emissions during the system's lifetime can be used to evaluate the system's environmental impact.

II.8.1. Energy payback time (EPBT)

The amount of time needed to recover the energy used in creating the first parts of the system is known as the energy payback time (EPBT). It is said as follows [102]:

$$EPBT = \frac{Embodied\ energy\ (kWh)}{Annual\ energy\ output\ (\frac{kWh}{yr})} \quad (II.30)$$

The thermal energy production of the dryer per year can be computed using:

$$Annual\ thermal\ Energy\ output\ (E_{aout}) = Daily\ thermal\ output \times N_d \quad (II.31)$$

Algeria experiences roughly 320 days of bright sunshine annually, where N_d is the total number of sunny days. The daily heat output of the dryer is indicated by:

$$Daily\ thermal\ output\ of\ dryer\ (kWh) = \frac{Moisture\ evaporated\ (kg)\ latent\ heat\ of\ evaporation\ J(kg)}{3.6 \times 10^6} \quad (II.32)$$

II.8.2. Carbon dioxide (CO_2) emission

The average carbon dioxide (CO_2) emission from coal-fired energy generation is roughly equal to 0.98 kg of CO_2/kWh. The CO_2 emissions per year are indicated by [103]:

$$CO_2\ emissions\ per\ year = \frac{Embodied\ energy \times 0.98}{Life\ time} \quad (II.33)$$

When transmission and domestic costs are taken into account in the computation, equation (II.33) becomes:

$$CO_2\ emissions\ per\ year = \frac{E_{in}}{L} \times \frac{1}{1-L_a} \times \frac{1}{1-L_t} \times 0.98\ kg \qquad (II.34)$$

In this case, E_{in} stands for embedded energy, L for dryer life, L_t for transmission costs, and L_a for home appliance costs. Equation (II.34) becomes if the losses resulting from outdated equipment are taken to be L_t = 40% and L_a = 20% [104]:

$$CO_2\ emissions\ per\ year = \frac{E_{in}}{L} \times 2.042\ kg \qquad (II.35)$$

II.8.3. CO_2 mitigation

CO_2 mitigation is calculated using:

$$Annual\ CO_2\ mitigation = (E_{aout} \times L - E_{in}) \times \frac{1}{1-L_a} \times \frac{1}{1-L_t} \times 0.98\ kg \qquad (II.36)$$

$$Annual\ CO_2\ mitigation = (E_{aout} \times L - E_{in}) \times 2.042\ kg \qquad (II.37)$$

Where E_{in} is the embedded energy, E_{aout} is the annual energy output, and L is the dryer's life span—in this case, 15 years.

II.8.4. Carbon credit earned

One ton of emission reduction is represented by one carbon credit, and the credit that a solar dryer earns is expressed as [104]:

$$Earned\ Carbon\ credit = net\ mitigation\ of\ CO_2\ in\ life\ time \times \text{Price per ton of } \mathrm{CO_2} \text{ mitigation} \qquad (II.38)$$

Chapter III: Numerical study

III.1. Introduction

This chapter presents the development and application of theoretical and numerical models. A three-dimensional stationary model has been created to evaluate the thermal performance of a direct solar dryer integrated with obstacles. This model analyzes enhancements in heat transfer and airflow distribution within the drying chamber, utilizing the Computational Fluid Dynamics (CFD) software package, ANSYS Fluent. The governing equations were discretized through the finite volume method, allowing for the transformation of these equations into a set of algebraic equations that can be solved numerically within Fluent. The following sections outline the setup of the CFD model, detailing aspects such as boundary conditions, mesh configuration, and the solution methodology employed to ensure accurate simulation outcomes.

III.2. Physical model

The numerical model developed for the direct solar dryer focuses on simulating and analyzing its thermal and fluid flow behavior, specifically incorporating the effects of obstacles integrated into the drying chamber. As shown in Figure III. 1.

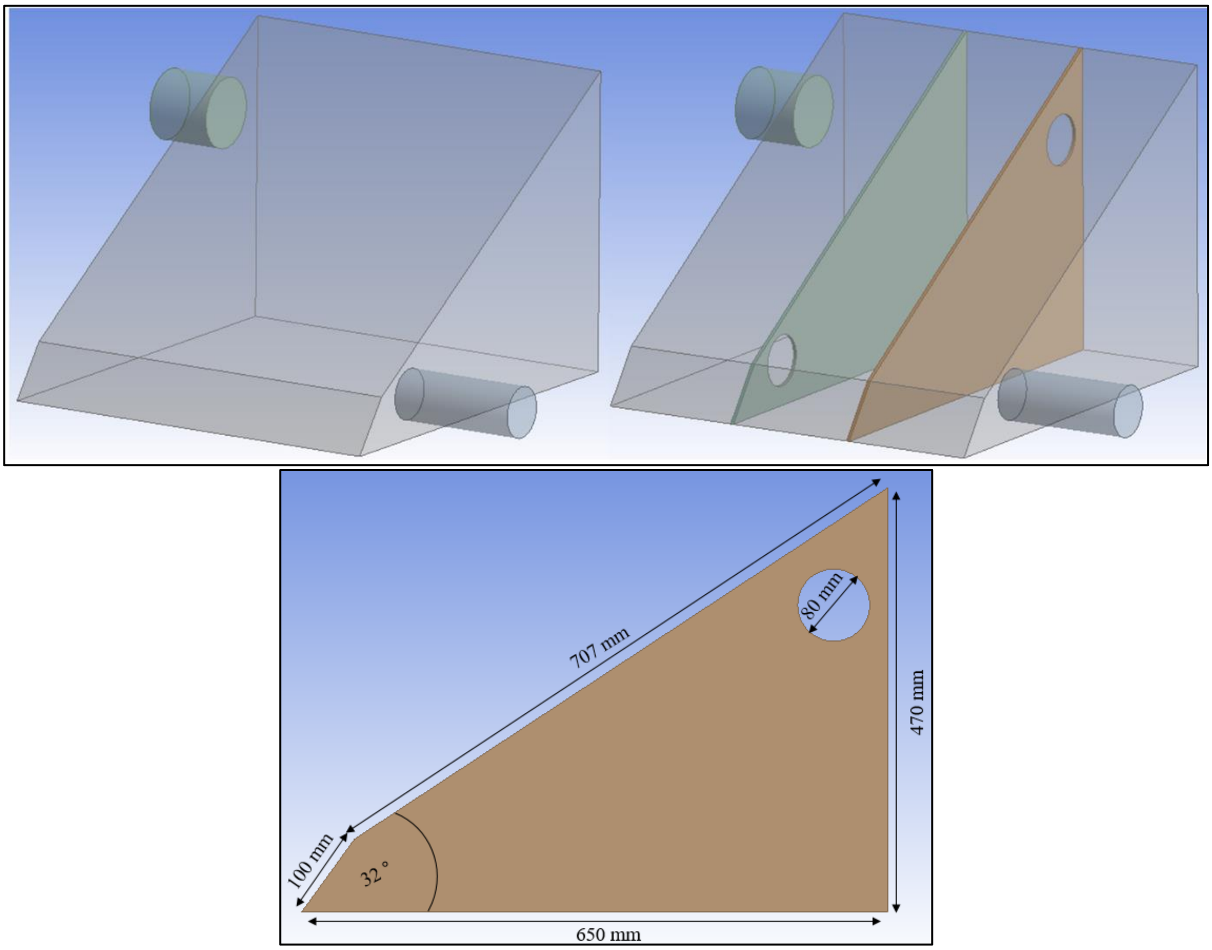

Figure III. 1. Numerical model of direct solar dryer with and without obstacles

III.3. Assumptions and governing equations

The following assumptions were made for the analysis: the flow is three-dimensional, incompressible, and steady-state. The thermophysical properties of air and the absorber are treated as independent of temperature. A no-slip condition is applied at the surfaces, and body forces are excluded from the analysis.

The governing equations for continuity, momentum, and energy are expressed as:

Continuity equation

$$\frac{\partial u}{\partial x}+\frac{\partial v}{\partial y}+\frac{\partial w}{\partial z}=0 \quad \text{(III.1)}$$

In the x-direction:

$$\frac{\partial u}{\partial x}\approx\frac{u_i-u_{i-1}}{\Delta_x}$$

In the y-direction:

$$\frac{\partial v}{\partial y}\approx\frac{v_j-v_{j-1}}{\Delta_y}$$

In the z-direction:

$$\frac{\partial w}{\partial z}\approx\frac{w_k-w_{k-1}}{\Delta_z}$$

Here u_i, v_j and w_k are the velocity components at the grid nodes in their respective directions, and i , j , k represent the indices of the grid points.

For a given control volume centered at (i, j, k), the discretized form of the continuity equation becomes:

$$\frac{u_i-u_{i-1}}{\Delta_x}+\frac{v_j-v_{j-1}}{\Delta_y}+\frac{w_k-w_{k-1}}{\Delta_z}=0$$

This equation must be solved for the velocity components at the nodes of the control volume.

Momentum equation

$$\rho(u\frac{\partial u}{\partial x}+v\frac{\partial u}{\partial x}+w\frac{\partial u}{\partial x})=-\frac{\partial p}{\partial x}+\mu(\frac{\partial^2 u}{\partial x^2}+\frac{\partial^2 u}{\partial y^2}+\frac{\partial^2 u}{\partial z^2}) \quad \text{(III.2)}$$

$$\rho(u\frac{\partial v}{\partial y}+v\frac{\partial v}{\partial y}+w\frac{\partial v}{\partial y})=-\frac{\partial p}{\partial y}+\mu(\frac{\partial^2 v}{\partial x^2}+\frac{\partial^2 v}{\partial y^2}+\frac{\partial^2 v}{\partial z^2}) \quad \text{(III.3)}$$

$$\rho\left(u\frac{\partial w}{\partial z}+v\frac{\partial w}{\partial z}+w\frac{\partial w}{\partial z}\right)=-\frac{\partial p}{\partial z}+\mu\left(\frac{\partial^2 w}{\partial x^2}+\frac{\partial^2 w}{\partial y^2}+\frac{\partial^2 w}{\partial z^2}\right) \quad \text{(III.4)}$$

Energy equation

$$(u\frac{\partial T}{\partial x}+v\frac{\partial T}{\partial y}+w\frac{\partial T}{\partial z})=\alpha(\frac{\partial^2 T}{\partial x^2}+\frac{\partial^2 T}{\partial y^2}+\frac{\partial^2 T}{\partial z^2}) \quad \text{(III.5)}$$

Standard k–ε turbulence equation

$$\frac{\partial}{\partial xi}(\rho k u_i)=\frac{\partial}{\partial xj}[(\mu+\frac{\mu t}{\sigma k})\frac{\partial k}{\partial xj})]+G_k+\ G_b-\rho\varepsilon-Y_M+S_k \quad \text{(III.6)}$$

Convective term

$$\frac{\partial}{\partial xi}(\rho k u_i)$$

For this term, upwind is typically used. The upwind scheme is more stable for convective terms.

The discretization would be:

$$\left[\frac{\partial}{\partial xi}(\rho k u_i)\right]_i = \frac{\rho_i k_i u_i}{V_i}$$

Where V_i is the volume of the control volume.

Diffusive term

$$\frac{\partial}{\partial xj}[(\mu + \frac{\mu t}{\sigma k})\frac{\partial k}{\partial xj})]$$

The diffusive term is discretized using the central differencing scheme

$$\left[\frac{\partial}{\partial xj}\left(\left(\mu + \frac{\mu t}{\sigma k}\right)\frac{\partial k}{\partial xj}\right)\right]_j = \frac{1}{V_i}\sum_j \left[\left(\left(\mu + \frac{\mu t}{\sigma k}\right)\left(\frac{\partial k}{\partial xj}\right)_{ij}\right]$$

Source terms

G_k Turbulent kinetic energy production

G_b

$\rho\varepsilon$ Turbulent dissipation

Y_M

S_k

$$\frac{\partial}{\partial xi}(\rho\varepsilon uj) = \frac{\partial}{\partial xj}[(\mu + \frac{\mu t}{\sigma\varepsilon})\frac{\partial \varepsilon}{\partial xj}] + C_1\varepsilon\frac{\varepsilon}{k}(G_k + C_3\varepsilon Gb) - C_2\varepsilon\rho\frac{\varepsilon^2}{k} + S\varepsilon \qquad \text{(III.7)}$$

The discretization steps are similar to the k-equation:

Convective term

$$\frac{\partial}{\partial xi}(\rho\varepsilon u_i)$$

Using an upwind scheme for the convective term:

$$\left[\frac{\partial}{\partial xi}(\rho\varepsilon u_i)\right]_i = \frac{\rho_i \varepsilon_i u_i}{V_i}$$

Diffusive term

$$\frac{\partial}{\partial xj}[(\mu + \frac{\mu t}{\sigma\varepsilon})\frac{\partial \varepsilon}{\partial xj})]$$

This term is also discretized using central differencing:

$$\left[\frac{\partial}{\partial xj}\left(\left(\mu+\frac{\mu t}{\sigma\varepsilon}\right)\frac{\partial\varepsilon}{\partial xj}\right)\right]_j=\frac{1}{V_i}\sum_j\left[\left(\left(\mu+\frac{\mu t}{\sigma\varepsilon}\right)\left(\frac{\partial\varepsilon}{\partial xj}\right)_{ij}\right]$$

With

$$\mu=\rho C_\mu\frac{k^2}{\varepsilon} \quad \text{(III.8)}$$

Solar Ray Tracing

In order to specify the intensity of solar radiation that represents the solar load, Solar Ray Tracing makes use of two illumination factors in addition to the location vector. The direction and intensity of sun radiation are provided by the solar calculator. For all solid materials, absorptivity and transmissivity have fixed values.

III.4. Meshing and numerical resolution

The numerical simulation domain was created using the meshing component of ANSYS software. Mesh generation is a critical process involving the creation of topological cells that subdivide a continuous structure into discrete geometry. The mesh configurations for different parts of the direct solar dryer are shown in Figure III. 2. As depicted in the figure, a tetrahedral mesh was applied to the main domain. To achieve accurate results, the size and number of mesh elements must be carefully analyzed.

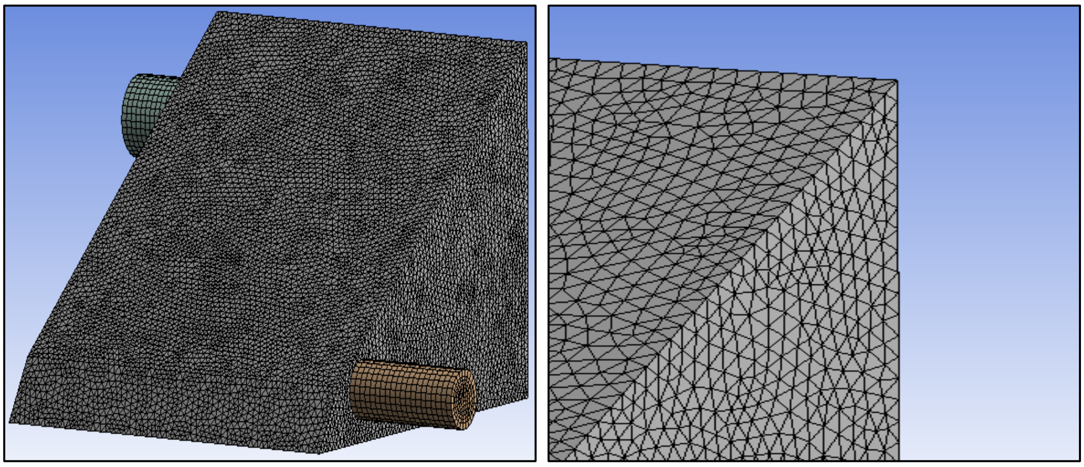

Figure III. 2. Mesh view of the direct solar dryer

For the connection of velocity and pressure, a SIMPLE algorithm is selected. The k-epsilon standard model is selected to solve the problem. In order to solve the governing equation, a double-precision solver is selected. For each transport equation, the second-order upwind discretization is selected. The continuity, x, and y velocity criteria in residual monitoring are set at 10^{-4}. To compute all zones, standard initialization is used.

III.5. Boundary conditions

The air inlet temperature was set to the ambient temperature of the surrounding environment, as recorded from experimental data. Solar radiation intensity was also based on experimental measurements. The inlet air velocity was fixed. A pressure outlet boundary condition was applied at the exit of the dryer as shown in Table III. 1. All other walls of the dryer were treated as adiabatic.

Table III. 1. Boundary conditions

Parameter	Condition	Value
Inlet	Velocity inlet	4.5 m/s
	Ambient temperature	Experimental data
Outlet	Pressure outlet	Pression atm
Solar radiation	Solar ray tracing	Experimental data
Glass	Transmissivity	0.85
	Absorptivity	0.1

III.6. Conclusion

In conclusion, this chapter has focused on developing and validating numerical models to simulate the solar drying systems. We covered both mathematical and physical modeling methods and confirmed their accuracy by comparing them with experimental data. This process has helped to understand how different configurations affect the system's performance. The insights gained from these models will be used in the next chapter to analyze and discuss the practical results and effectiveness of the solar drying technologies. This chapter has provided a clear foundation for understanding how various factors influence drying performance, setting up the analysis of real-world results to come.

Chapter IV: Results and discussions

IV.1. Introduction

In this chapter, we present and analyze the results obtained from the experimental and numerical studies conducted as part of this research. Building on the experimental setups and procedures detailed in previous chapters, this chapter provides a comprehensive discussion of the findings related to solar collector enhancements, drying chamber optimizations, and the improvements made to both direct and indirect solar dryers. In addition to the experimental results, we also incorporate insights from the numerical study, which was used to simulate and validate the performance of the various enhancements. The chapter is structured to first present the results of each experimental setup, followed by a detailed discussion of the performance metrics, including energy efficiency, drying rates, and overall system effectiveness. Additionally, we compare experimental findings with numerical predictions to assess the accuracy and reliability of the simulations

IV.2. Experiment 1: Solar air collector enhancements

IV.2.1. Effect of offset strip fins (OSF)

Hourly variations in the surrounding temperature and solar radiation were measured during the experiment under a clear sky. The changes in solar radiation and ambient temperature over time are depicted in Figure IV. 1. At 11:00, the radiation reached its peak of 942 W/m², while the average ambient temperature was above 31 °C.

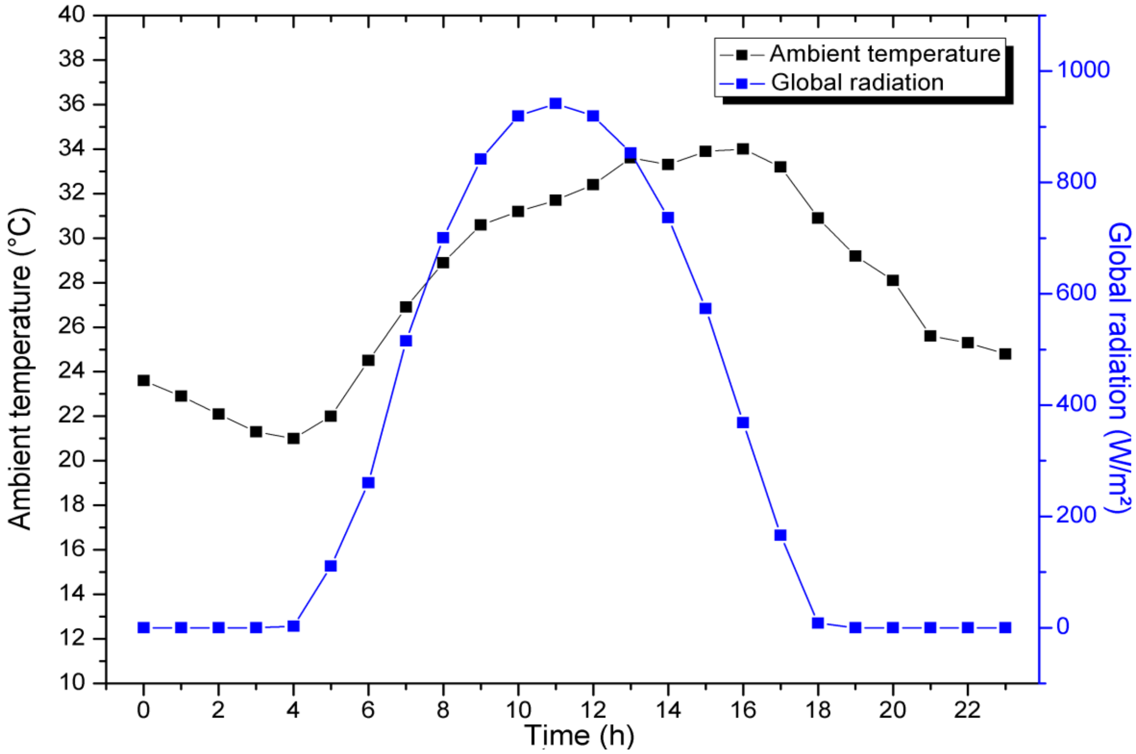

Figure IV. 1. Variations of ambient temperature and solar radiation with time for the 1st experiment

One important component that affects how the product dries is the air temperature. The outlet temperature variation of the solar air heater is depicted in Figure IV. 2 over time. For both setups, the temperature increases over time, peaking at 65.3 °C for the SAH with offset strip fins (OSF). The two collectors' measured temperature differences reached 11.3 °C at 11:00, with an average difference of 8 °C during the experiment. Fins were added to the solar air heater to improve its effectiveness. This is because adding fins to the air flow boosted convective exchange. Additionally, adding fins creates a turbulent flow that promotes heat exchange and speeds up the drying process because of the increased temperature gain. Excellent agreements with Youcef-Ali [105] because these fins enhance the drying kinetics by extending the heat transfer area and conducting heat to the rear of the air heater.

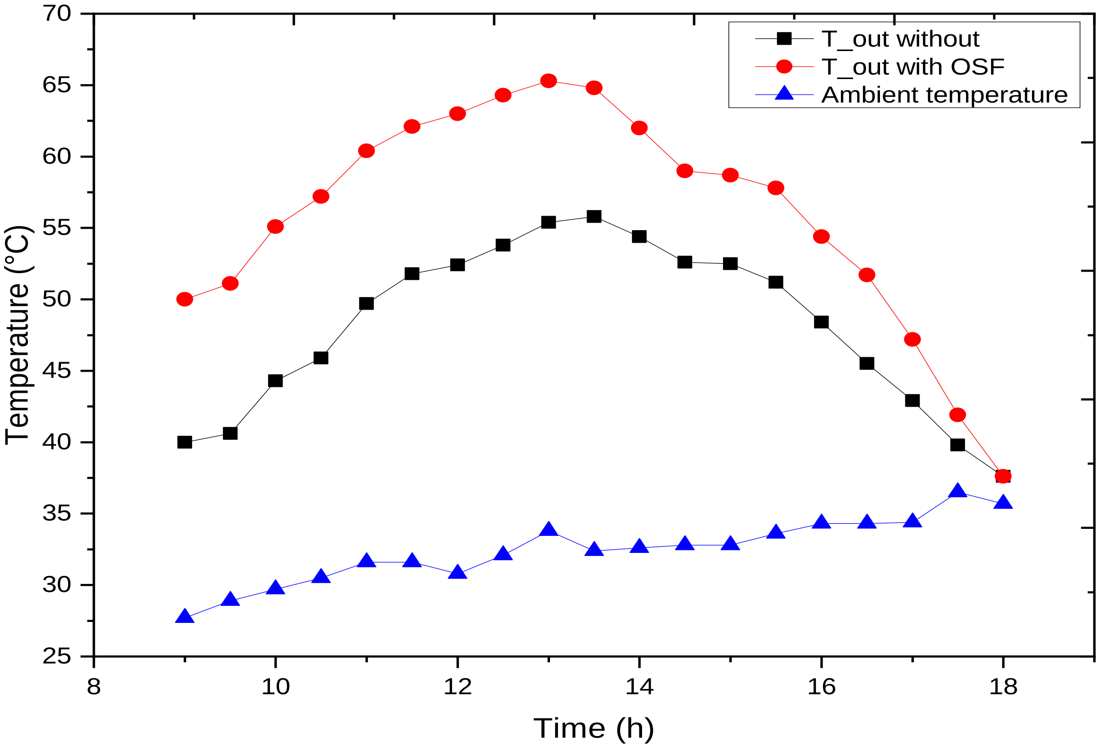

Figure IV. 2. Temperature at the outlet of the solar air collector with and without fins

IV.2.1.1. Drying characteristics

Drying curves

Figure IV. 3 displays the experimental moisture content data, which is then converted into a more accurate form of the moisture ratio (MR) and displayed in Figure IV. 4.

The pauses on the lines represent the time of night. The courgette, which had an initial moisture content of 26.29 (kg water/kg dry basis), was dried in 20 hours and 18 minutes in the solar drier with OSF, whereas it took 35 hours and 45 minutes to obtain the same value. The drying time was reduced by using OSF in the solar collector.

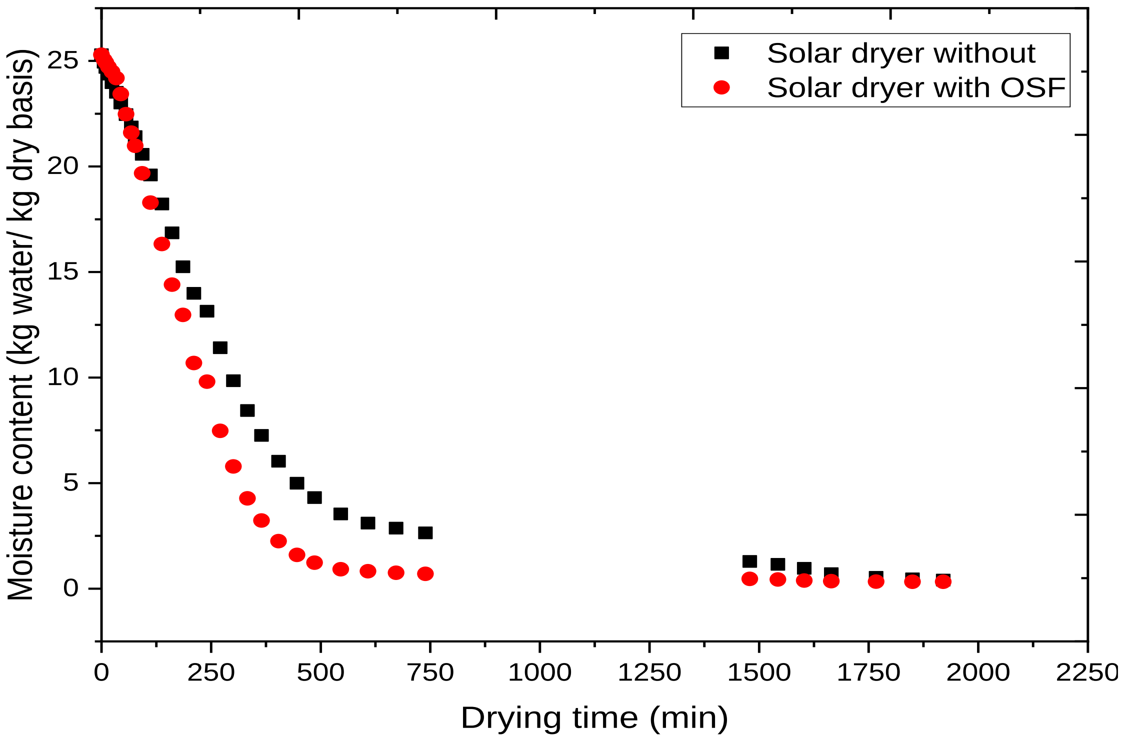

Figure IV. 3. Moisture content variation with drying time for the dryer equipped with solar air collector with and without OSF

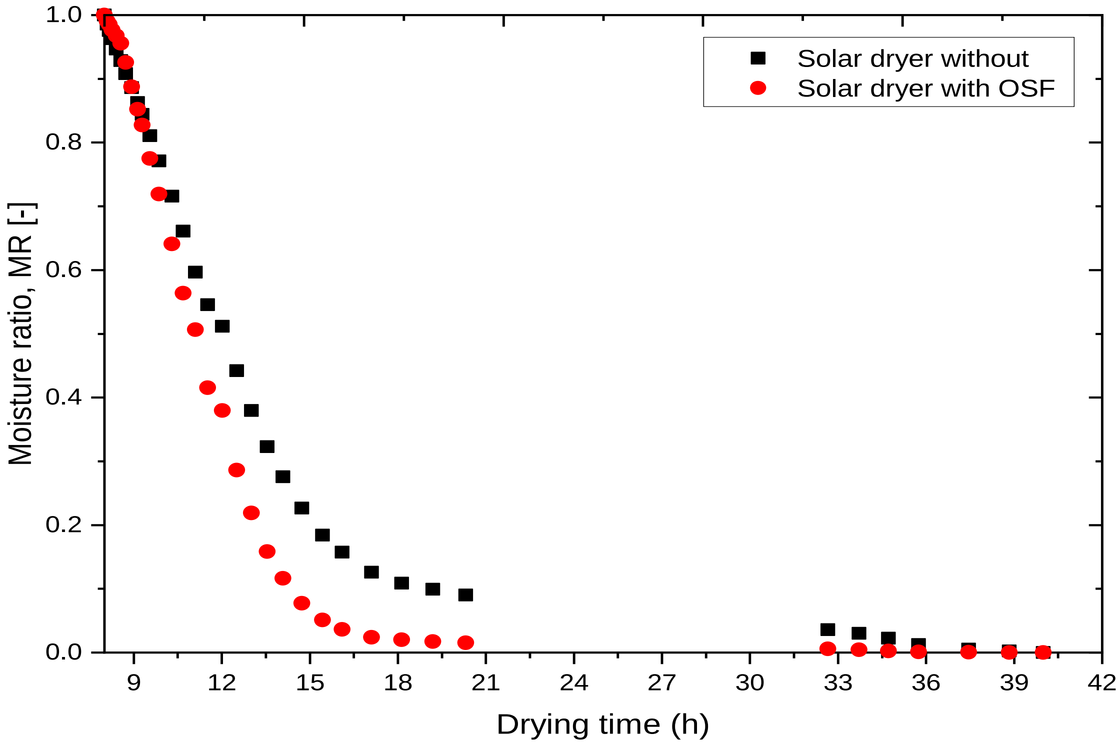

Figure IV. 4. Moisture ratio variation with drying time for the dryer equipped with solar air collector with and without OSF

The experimental moisture content data is shown in Figure IV. 3. It is subsequently transformed into a more precise version of the moisture ratio (MR) and shown in Figure IV. 4.

The hour of night is indicated by the breaks in the lines. The courgette was dried in 20 hours and 18 minutes in the solar drier with OSF, compared to 35 hours and 45 minutes to achieve the same value, with an initial moisture content of 26.29 (kg water/kg dry basis). By employing OSF in the solar collector, the drying time was decreased.

Figure IV. 5 shows drying rate variations with the level of moisture content, the process of drying consisted of two periods, where at a high moisture content the drying rate increases reaching 0.091 (kg water/kg d.b.)/s, and start to drop after the water start to evaporate reaching the lowest rate of 0.00051 (kg water/kg d.b.)/s. The indirect solar dryer with fins has higher drying rate reaching 0.091 (kg water/kg d.b.)/s compared to the other 0.064 (kg water/kg d.b.)/s, due to high temperature inside the drying chamber accelerating the water evaporation.

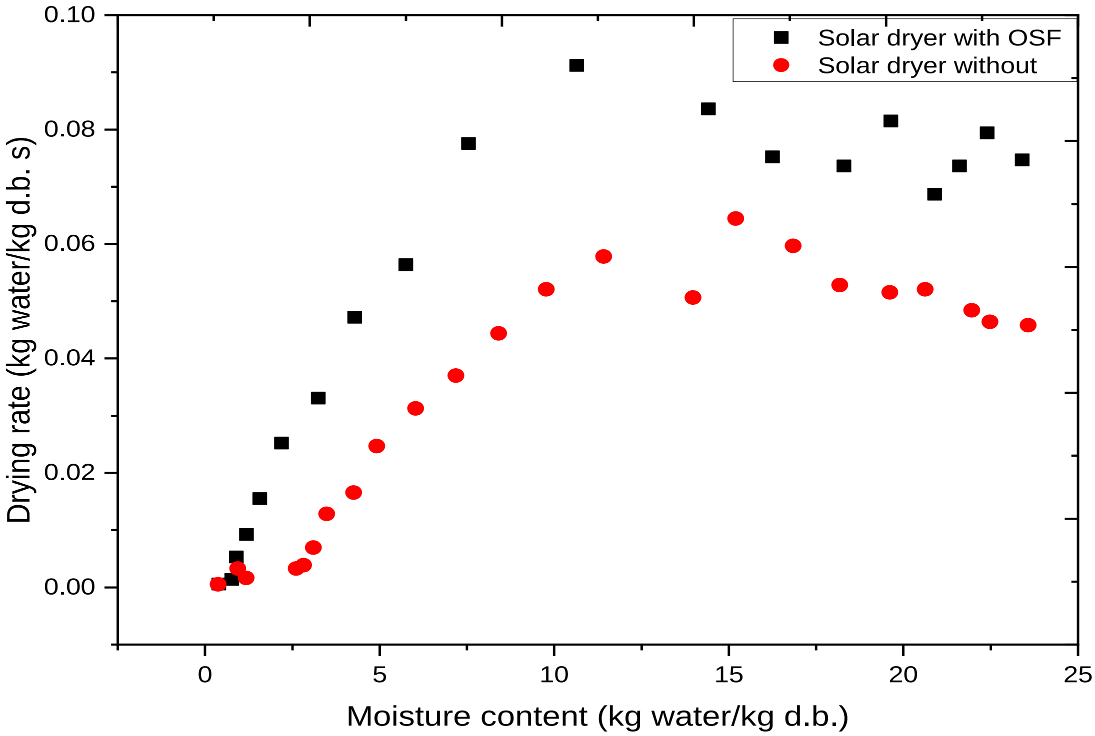

Figure IV. 5. Drying rate variation with moisture content for the dryer equipped with solar air collector with and without OSF

IV.2.1.2. Empirical models of thin layer drying process

To determine the moisture content ratio as a function of drying time, the experimental data were fitted to each of the seven different thin-layer drying models in Table II. 2. Table IV. 1 displayed the statistical analysis's findings. The most suited model is the one with the highest coefficient of determination (R^2), lowest reduced chi-square (χ^2), and lowest root mean square error (RMSE). As a result, the values for the models that are most appropriate are shown as bold numbers in Table IV. 1. When compared to other models, Midilli-Kucuk and Page both offered the best agreement between experimental and anticipated moisture ratios; the small variation can be attributable to measurement error.

Table IV. 1. Results of statistics derived from several drying models for courgette

Model	System	Constants	R^2	χ^2	RMSE
Newton	Without OSF	$k = 31 \times 10^{-4}$	0.9891	1.5×10^{-3}	0.0391

	With OSF	k = 42 x 10^{-4}	0.9727	4.4 x 10^{-3}	0.0664
Page	Without OSF	k = 0.7 x 10^{-3}; n = 1.3	0.998	3 x 10^{-4}	0.0169
	With OSF	k = 0.2 x 10^{-3}; n = 1.5	0.9994	1 x 10^{-4}	0.0101
Modified Page	Without OSF	k = 32 x 10^{-4}; n = 1.27	0.998	3 x 10^{-4}	0.0169
	With OSF	k = 43 x 10^{-4}; n = 1.55	0.9994	1 x 10^{-4}	0.0101
Henderson and Pabis	Without OSF	k = 33 x 10^{-4}; a = 1.05	0.9924	1.1 x 10^{-3}	0.0331
	With OSF	k = 47 x 10^{-4}; a = 1.1	0.9832	2.8 x 10^{-3}	0.0529
Logarithmic	Without OSF	k = 0.4 x 10^{-3}; a = 10.36; b = -10.3196	0.9577	0.1192	0.3452
	With OSF	k = 0.6 x 10^{-3}; a = 11; b = -10.9	0.9446	0.4004	0.6328
Midilli-Kucuk	**Without OSF**	**k = 0.5 x 10^{-3}; n = 1.3; a = 0.99; b = 0**	**0.9986**	**2 x 10^{-4}**	**0.0148**
	With OSF	**k = 0.2 x 10^{-3}; n = 1.58; a = 0.99; b = 0**	**0.9995**	**1 x 10^{-4}**	**0.0099**
Approximation of Diffusion	Without OSF	k = 21 x 10^{-4}; a = 51.6; b = 0.99	0.9909	1.4 x 10^{-3}	0.0367
	With OSF	k = 94 x 10^{-4}; a = -119.2; b = 0.99	0.9986	2 x 10^{-4}	0.0154

IV.2.1.3. Determination of the effective moisture diffusivity of courgette

We next calculated the effective diffusivity using Crank's analytical solution of Fick's second equation [97] in order to assess the drying kinetics. In comparison to other systems, a higher value of effective diffusivity is recorded due to the accelerated water evaporation from courgette slices caused by the high drying temperature produced by the OSF solar collector. Table IV. 2 presents the R^2, χ^2, and RMSE in addition to the effective moisture diffusivity.

Table IV. 2. Effective moisture diffusivity and statistical results for Courgette

Test	Average D_{eff} (m^2/s)	Statistical result		
		R^2	RMSE	χ^2
Without fins	1.18x10^{-09}	0,9722	0,1993	0,0397
With fins	1.8x10^{-09}	0,9600	0,4185	0,1752

Figure IV. 6 depicts the dried courgette slices in both configurations. It's interesting to see that the textures and colors of the final samples from both dryers were quite comparable. The dried courgette slices had a uniform texture. The dried courgette slices showed a vivid green color that was suggestive of quality that had been conserved, and their colors were quite similar in both dryers. The consistency of the two solar dryers' textures and colors demonstrates how equally good they are in maintaining the desired characteristics of the courgette throughout the drying process.

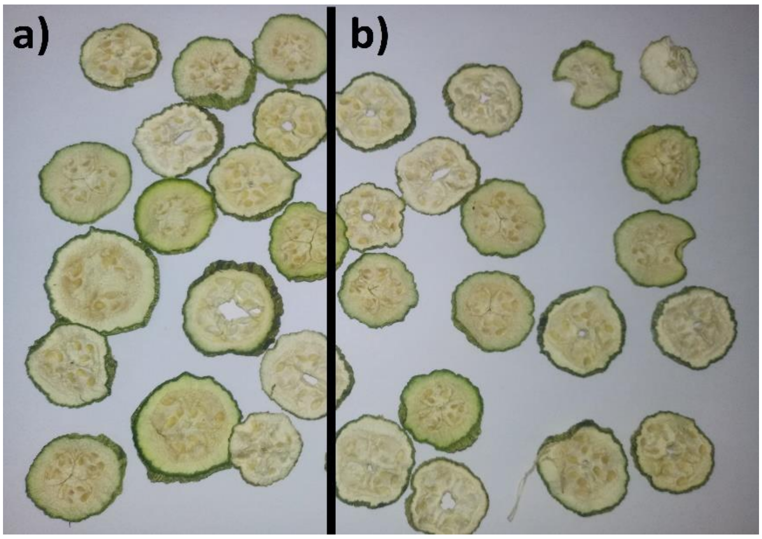

Figure IV. 6. Dried courgette samples. a) With OSF fins b) Without fins

IV.2.1.4. Economic analysis

The different solar dryer economic factors are given in Table IV. 3. The anticipated construction expenses for the ITSD and modified ITSD were 284.45 and 357.39$, respectively. The dryers' annualized cost was computed by deducting 10% of their salvage and maintenance expenses from their respective capital costs and annualized capital costs. The drying time in hours for the number of drying days, 320 days, and the Algerian unit price of one kWh, 0.030 $/kWh, were used to compute the cost of energy. Depending on the dryer and the amount of drying time, the M_{year} varied from 960 to 1280 kg. Real and short-term interest rates at Algerian banks are consistently maintained at 5% and 3%, respectively.

The economic analysis results of the ITSD are provided in detail, together with information on the payback duration, savings, and viability of annualized costs.

Table IV. 3. Economic and cost factors of indirect solar dryers for Courgette

Variable	ITSD with flat collector	ITSD with OSF collector
Capital cost of the dryer, C_{cd} ($)	284.45	357.39
Annualized cost of dryers, AC ()	26.52	32.85
Annualized capital cost, C_{ac} ($)	23.83	29.94
Annualized maintenance cost 10% of C_{ac}, C_m ($)	2.38	2.99
Annualized salvage value, S_a ($)	1.53	1.92
Running electricity cost of fans in the dryer, C_{el} ($)	1.84	1.84
Salvage value 10% of C_{cd}, S ($)	28.45	35.74
Cost of dried product, C_{dry} ($/kg)	11.31	11.31
Cost of fresh product, C_{fre} ($/kg)	0.58	0.58
Savings per kg in comparison to branded product for solar dryer, B_{kg} ($/kg)	23.67	23.67
The selling price of branded dried product, C_{bdp} ($)	35	35

Savings per day for domestic solar dryer in the jth year, B_d ($)	0.91	1.21
Lifespan, n (year)	15	15
Payback period, Pb (year)	1.00	0.95

Due to their comparatively modest initial investment and little electricity costs, both dryers rely entirely on solar power. Fresh courgette costs $0.58 per kilogram, whereas dried courgette costs $35. This significant price difference results in a shorter payback period—which is predicted to be one year for traditional indirect solar dryers and 0.95 years for dryers with OSF.

Annual savings during the life of the developed systems are displayed in Figure IV. 7. Over time, a very modest yearly savings of 578.36 was noted in the traditional solar dryer. However, adding OSF to the solar dryer raised the savings to $769.28 annually. This result indicates that adding OSF to an indirect solar dryer enhances efficiency and financial results.

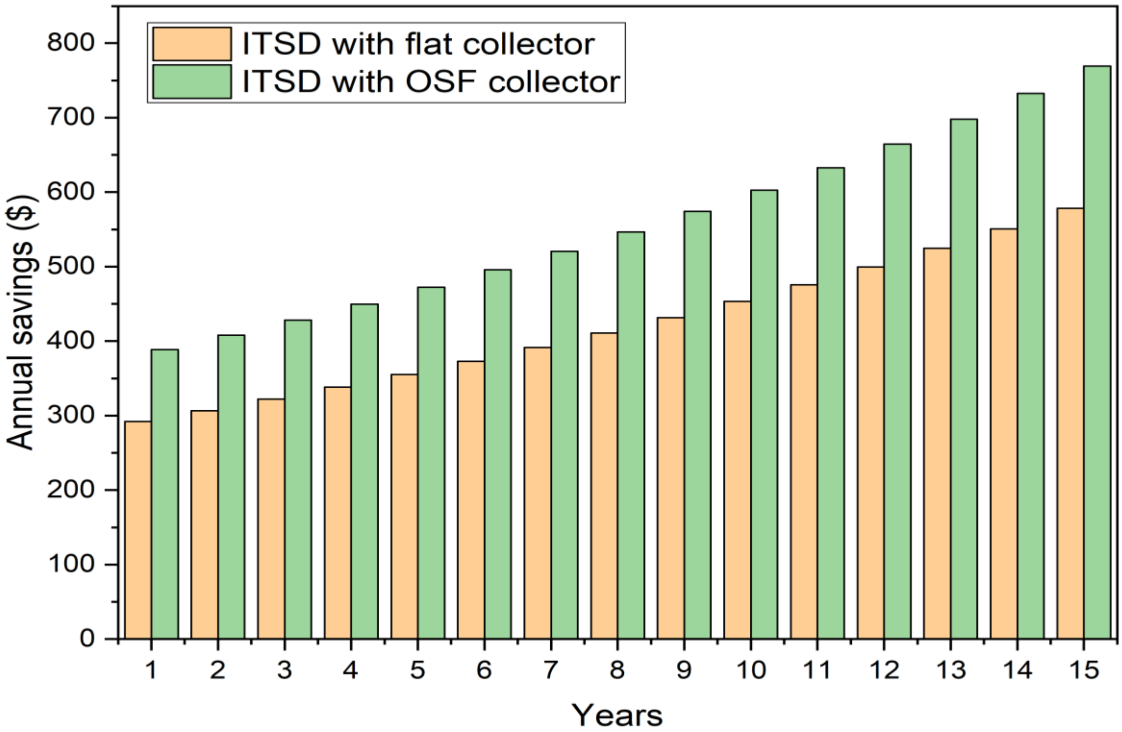

Figure IV. 7. Annual savings of indirect solar dryers with and without obstacles

IV.2.1.5. Environmental analysis

The embodied energy of the different materials used to construct the two solar dryers is listed in Table IV. 4.

The total weight of the ITSD, which is composed of several materials, is 78.4 kg without OSF and 74.08 kg with it.

For the solar dryer without OSF and with OSF, the total embodied energy for the designed systems is 1099.69 and 1338.46 kWh, respectively. Aluminum (43.42 and 53.52%) and foam (24 and 19.71%) share the total embodied energy for the systems with and without OSF, respectively. Furthermore, compared to other building materials, aluminum has a larger embodied energy.

Table IV. 4. Embodied energy of indirect solar dryers with and without obstacles

Materials	Energy density (kWh/kg) [106]	Mass of component (kg)		Embodied energy, Ee (kWh)	
		ITSD	ITSD with OSF	ITSD	ITSD with OSF
Glass	7.27	25	25	181.75	181.75
Aluminum	55.27	8.64	12.96	477.53	716.3
Galvanized iron	9.64	12	12	115.68	115.68
Glass wool	4.037	4	4	16.15	16.15
Wood	0.66	8	8	5.28	5.28
Plastic	19.44	0.5	0.5	9.72	9.72
Steel	8.89	3	3	26.67	26.67
Foam	20.55	12.84	12.84	263.86	263.86
Rubber	30.50	0.1	0.1	3.05	3.05
Total		74.08	78.4	**1099.69**	**1338.46**

The evaporative capacity of the dryers is 3.6 kg per day on average. In solar dryers without OSF and with OSF, the energy payback times are found to be 1.67 and 2.03 years, respectively. The lifetime of the produced solar dryers is far longer than this duration. The computation of the annual CO2 emissions for a life span of 5–15 years is presented in Table IV. 5.

Table IV. 5. CO_2 emissions for various lifespans of indirect solar dryers with and without obstacles

Life span (years)	5		10		15	
	ITSD	ITSD with OSF	ITSD	ITSD with OSF	ITSD	ITSD with OSF
CO_2 emission (Kg/year)	215.54	262.34	107.77	131.17	71.85	87.45

The CO_2 mitigation and carbon credit acquired by both systems throughout the course of their respective lifetimes are displayed in Table IV. 6. If the price per ton of CO_2 emissions is between \$5 and \$20 [104].

Table IV. 6. CO_2 mitigation and carbon credits earned for various lifespans of indirect solar dryers with and without obstacles

Life span (years)	5		10		15	
	ITSD	ITSD with OSF	ITSD	ITSD with OSF	ITSD	ITSD with OSF
CO_2 mitigation (Tons)	4.485	3.997	11.215	10.728	17.945	17.458
Carbon credit earned (\$)	22.42 to 89.7	19.99 to 79.94	56.08 to 224.3	53.64 to 214.56	89.73 to 358.9	87.29 to 349.16

IV.2.2. Effect of sensible energy storage material integration

The temporal variations in solar radiation and temperature during the course of the experiment are shown in Figure IV. 8. During the test days, average solar radiation exceeded 600 W/m², while the highest recorded solar radiation reached a maximum value of 1208.77 W/m². In addition, it was found that the experiment's average ambient temperature was 30.09 °C.

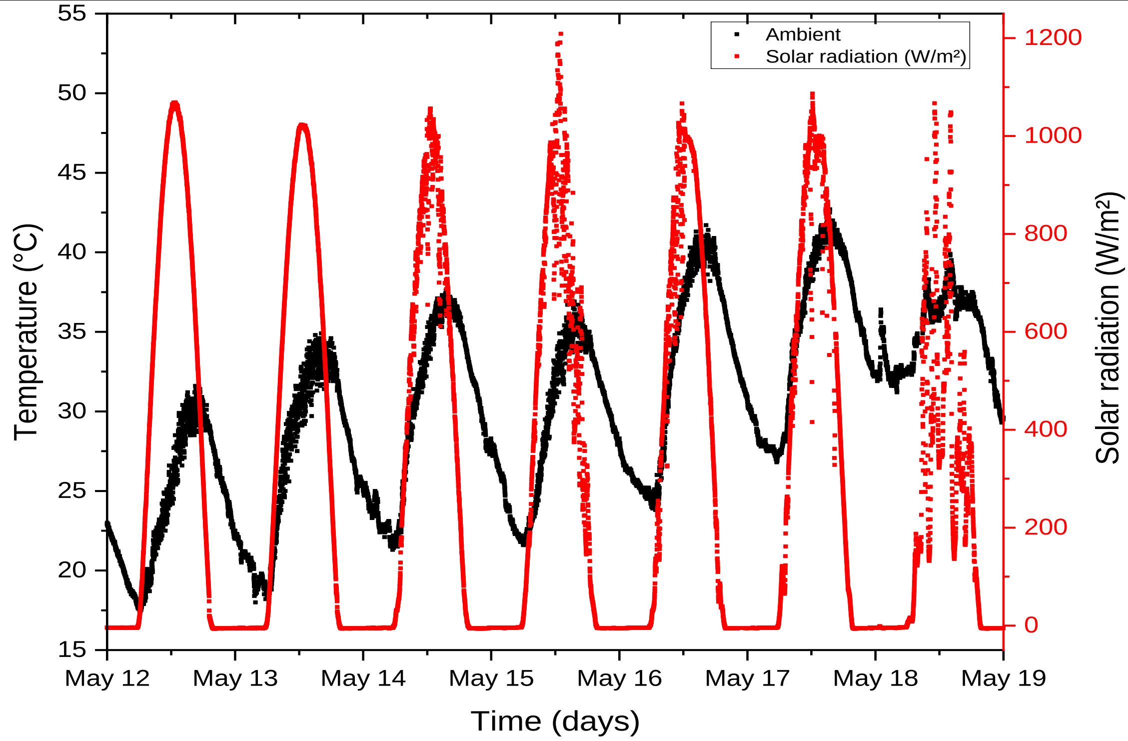

a)

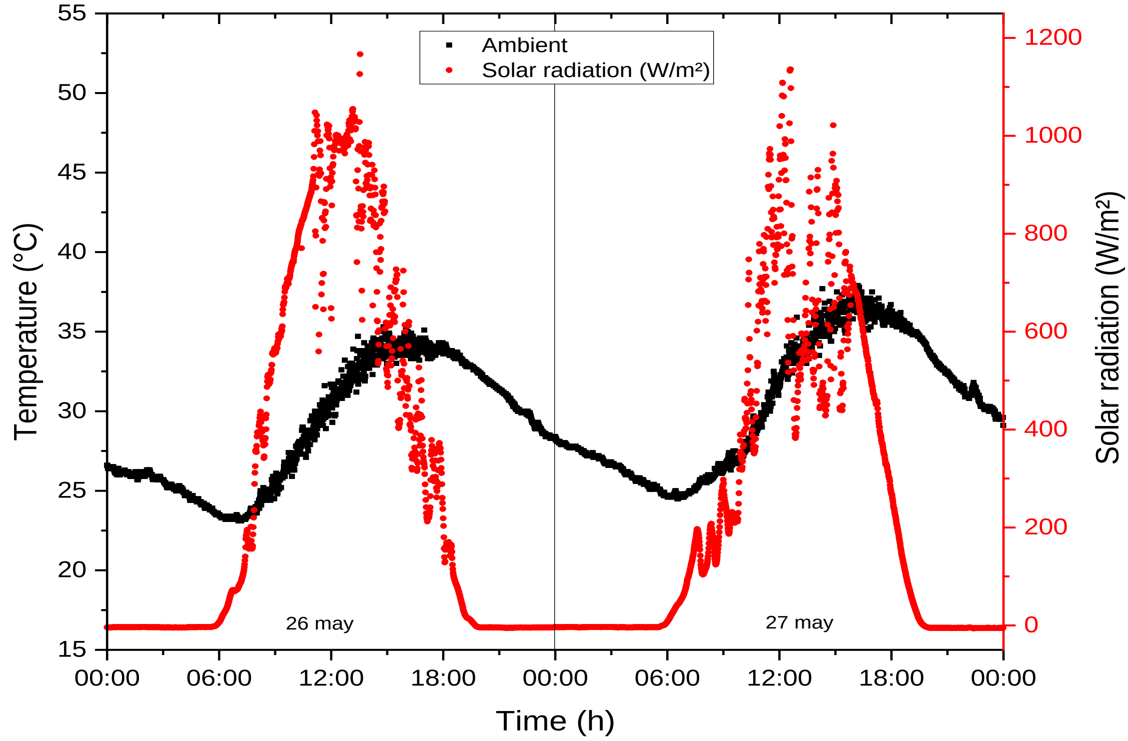

b)

Figure IV. 8. Variations of ambient temperature and solar radiation with time for the 2nd experiment

The temperature change at the outflow of a solar collector with fins and rocks is shown in Figures IV. 9 and 10, respectively. The two different mass flow rates used in the trials were 0.00063 and 0.0767 kg/s. The pebbles and fins act as external surfaces to raise the collector's internal temperature. The collector with fins and the rock collector had maximum temperatures of 76.8 °C and 70.2 °C, respectively. This suggests a significant variation of 6.6 °C at the peak of radiation, favoring the finned collector. The materials utilized to make the fins are responsible for the variations in temperature rise. Higher temperatures are attained when fins composed of materials with high thermal conductivity efficiently transmit heat. By comparison, the rock collector showed a temperature differential of up to 13.6 °C at low sun radiation levels. The rocks serve as both exterior surfaces and a sensible type of energy storage. This demonstrates how rocks have the capacity to sustain high temperatures even when solar radiation is low.

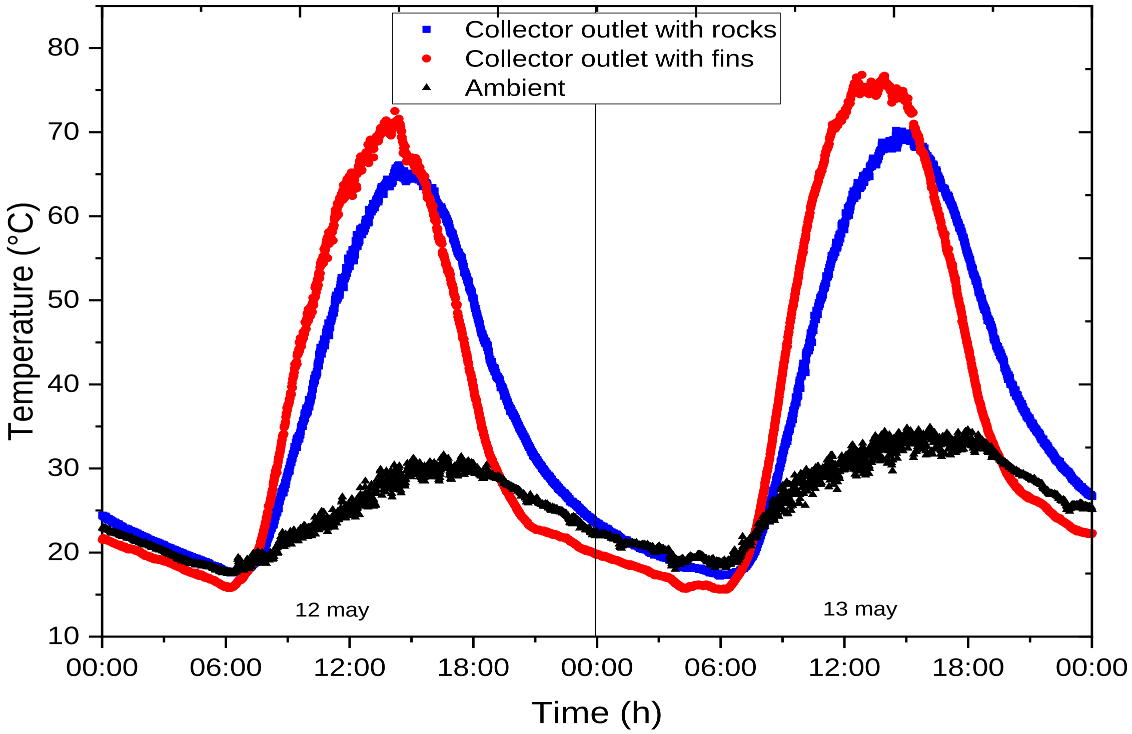

Figure IV. 9. Temperature variation at outlet of collector with fins and with rocks at m=0.00063 kg/s

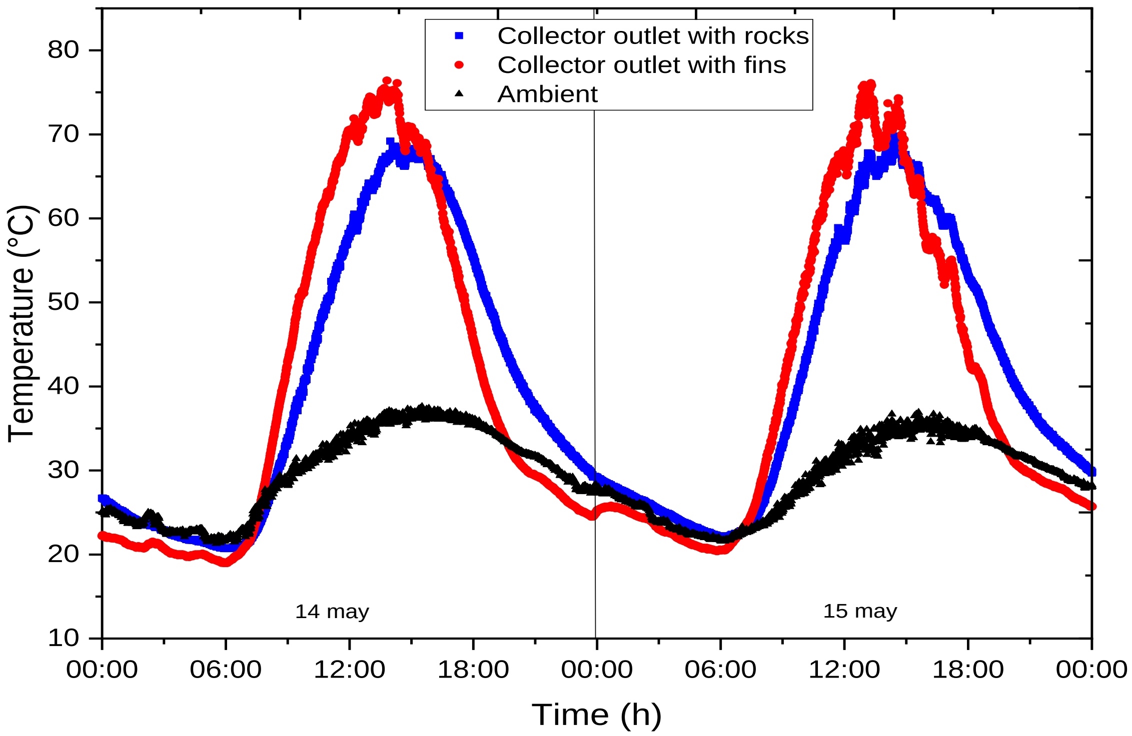

Figure IV. 10. Temperature variation at outlet of collector with fins and with rocks at m=0.0767 kg/s

IV.2.2.1. Drying characteristics

Drying curves

Figure IV.11, which presents experimental data, illustrates how the moisture content of coriander varies while it dries in sun dryers fitted with rocks and fins. During the first phase, which lasted the entire day, both dryers were successful in lowering the moisture content of coriander. The dryer with fins produced values of 34.9% while the dryer with pebbles produced values of 66.2% (kg water/kg wet base). The midnight hours when no bulk data were gathered are represented by the gap in the figure.

The dryer containing rocks showed even more decrease in moisture content over the next night, with a value of 31.7% (kg water/kg wet basis). This is because rocks release heat that has been stored inside of them throughout their discharge phase, which aids in the continuous drying process and encourages more moisture to evaporate from the coriander.

After more drying, the sun drier with fins took 24 hours and 12 minutes to reach a final moisture content of 6% (kg water/kg wet base), and the solar dryer with pebbles took 28 hours and 42 minutes.

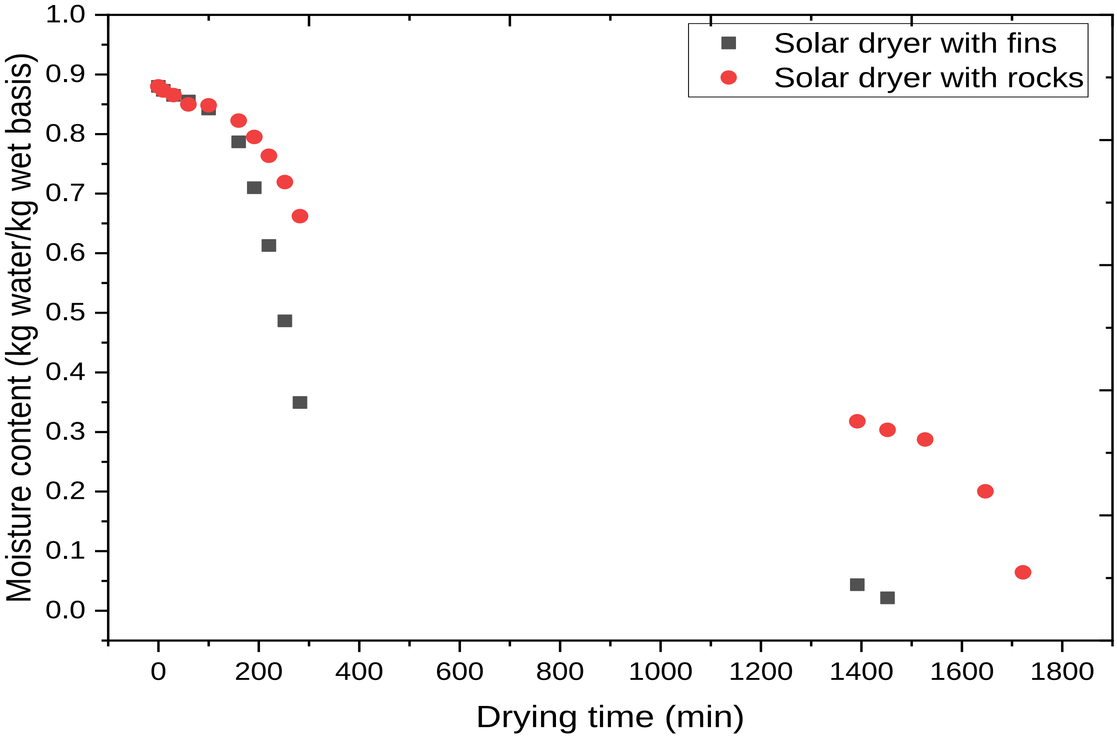

Figure IV. 11. Moisture content change of coriander with time

The drying rate changes in the solar drier fitted with fins and rocks are displayed in Figure IV. 12 in proportion to the moisture content level of coriander. There are two separate times for the drying process. The drying rate shows an increasing trend in the first phase, which is marked by a high moisture content. For the solar drier that uses fins, the values are 0.0000914 and 0.000039 (kg water/kg dry basis s), respectively. Then, when the water starts to evaporate from the coriander, the rate of drying decreases until it reaches a reduced rate. Because fins are made of a more conductive substance and allow moisture to evaporate more quickly, the first dryer's high drying rate is explained by their presence.

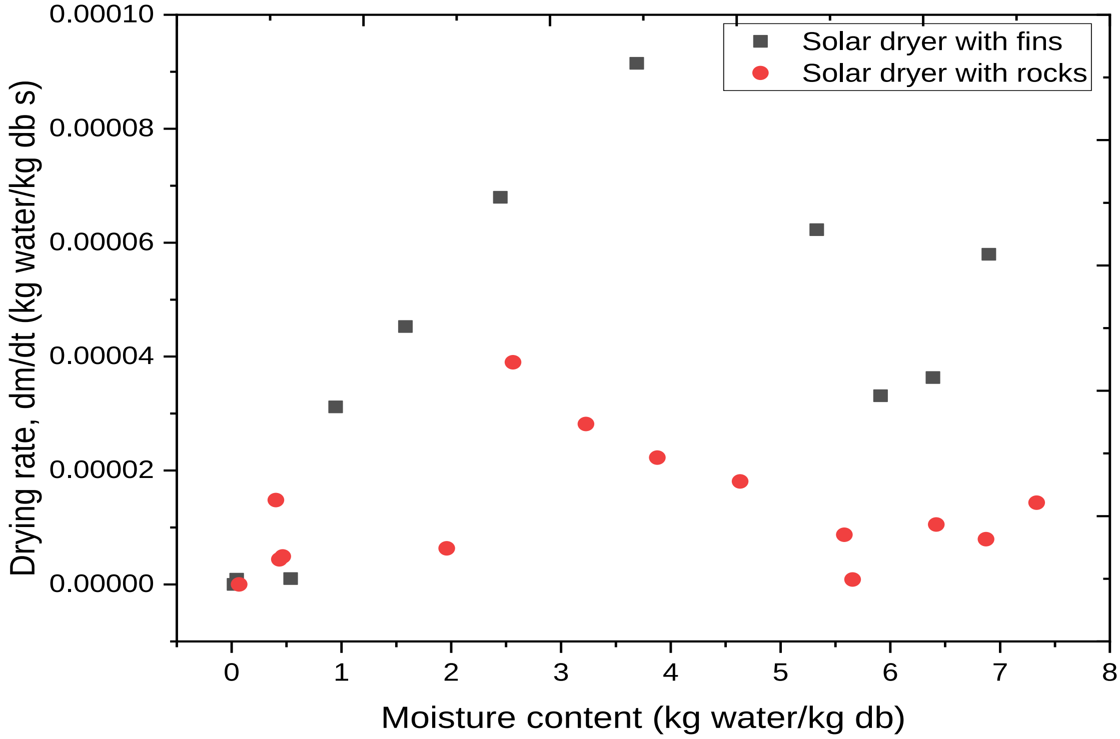

Figure IV. 12. Drying rate change with moisture content of coriander

IV.2.2.2. Empirical models of thin layer drying process

As indicated in Table II.2, seven distinct thin-layer drying models were used to fit the collected experimental data. The moisture content ratio as a function of drying time was calculated using these models. Table IV. 7 presents the findings of the statistical analysis, including the root mean square error (RMSE), reduced chi-square (χ^2), and coefficient of determination (R^2). The best appropriate model is the one with the highest R^2 value, lowest χ^2 value, and lowest RMSE value. In Table IV. 7, the matching values for the models that fit the data the best are indicated in bold. Furthermore, Figures IV. 13 show the best-fit models for coriander in the fin and rock solar dryer designs, respectively. The Midilli-Kucuk model, out of all the models that were assessed, showed the best agreement between the predicted and experimental moisture ratios for coriander in both configurations.

Table IV. 7. Statistical results from various drying models for coriander

Model	System	Constants	R^2	χ^2	RMSE
Newton	With fins	k = 0.00565	0.9513	0.0073	0.0853
	With rocks	k = 9.54887E-4	0.9663	0.004	0.0656
Page	With fins	k = 1.4499E-4; n = 1.70669	0.9868	0.0022	0.0466
	With rocks	k = 3.07367E-4; n = 1.16308	0.9729	0.0037	0.0609
Modified Page	With fins	k = 0.00562; n = 1.75718	0.9869	0.0022	0.0464

	With rocks	k = 9.55001E-4; n = 1.16789	0.9729	0.0037	0.0609
Henderson and Pabis	With fins	k = 0.00599; a = 1.05105	0.9554	0.0073	0.0856
	With rocks	k = 0.00101; a = 1.03306	0.9700	0.0041	0.0642
Logarithmic	With fins	k = 3.64356E-7; a = 1458.95733; b = -1458.30769	0.4944	0.0756	0.2748
	With rocks	k = 3.64356E-7; a = 1458.95733; b = -1457.95954	0.9766	0.003	0.0546
Midilli-Kucuk	**With fins**	**k = 1.30595E-5; n = 2.14885; a = 0.93455; b = -6.83036E-7**	**0.9929**	**0.0015**	**0.0380**
	With rocks	**k = -1.3338E-5; n = 1.23005; a = 0.98579; b = -5.82517E-4**	**0.9796**	**0.0033**	**0.0576**
Approximation of Diffusion	With fins	k = 0.00103; a = 1; b = -2627.84588	0.6197	0.057	0.2384
	With rocks	k = 0.00103; a = 1; b = -2627.84588	0.9684	0.004	0.0635

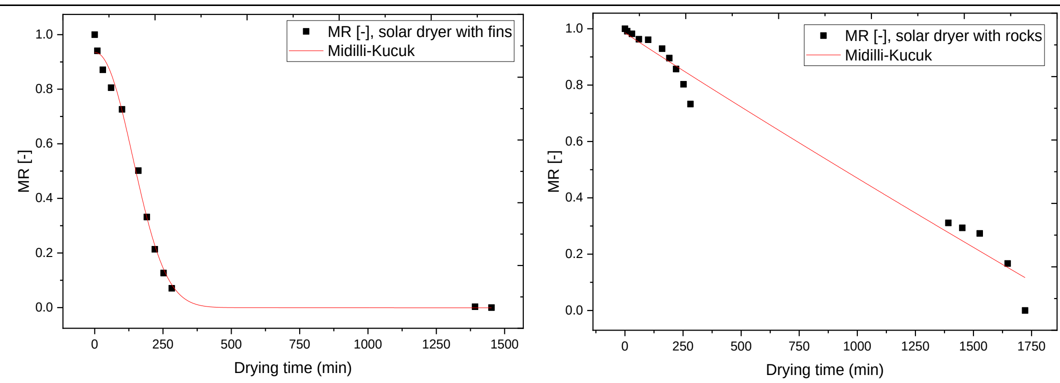

a) b)

Figure IV. 13. Variation of moisture ratio of coriander with drying time, modeled by the most appropriate empirical models, a) Solar dryer with fins; b) Solar dryer with rocks

IV.2.2.3. Determination of the effective moisture diffusivity

We calculated the effective diffusivity using Crank's [97] analytical solution of Fick's second equation in order to evaluate the drying kinetics. The effective moisture diffusivity values, root mean square error (RMSE), reduced chi-square (X^2), and coefficient of determination (R^2) are shown in Table IV. 8. For the plant, the indirect sun drier with fins showed greater effective diffusivity values. Under the sun dryer with fins and rocks, the effective diffusivity values of coriander were 6.39485E-10 and 1.33512E-10 m²/s, respectively. These results are consistent with the research conducted by Jayasuriya et al. [107] and Silva et al. [108].

Table IV. 8. Effective moisture diffusivity of coriander and with their statistical analysis

	Average D_{eff} (m²/s)	R^2	RMSE	X^2
Dryer with fins	6.39485E-10	0.9838	0.2476	0.0613

Dryer with rocks	1.33512E-10	0.9957	0.0347	0.0012

IV.3. Experiment 2: Material consideration

Figure IV. 14 showcases the variation of temperature, relative humidity, and solar radiation over a four-day period, with the first two days representing the drying phase while products are loaded, followed by two days without any load.

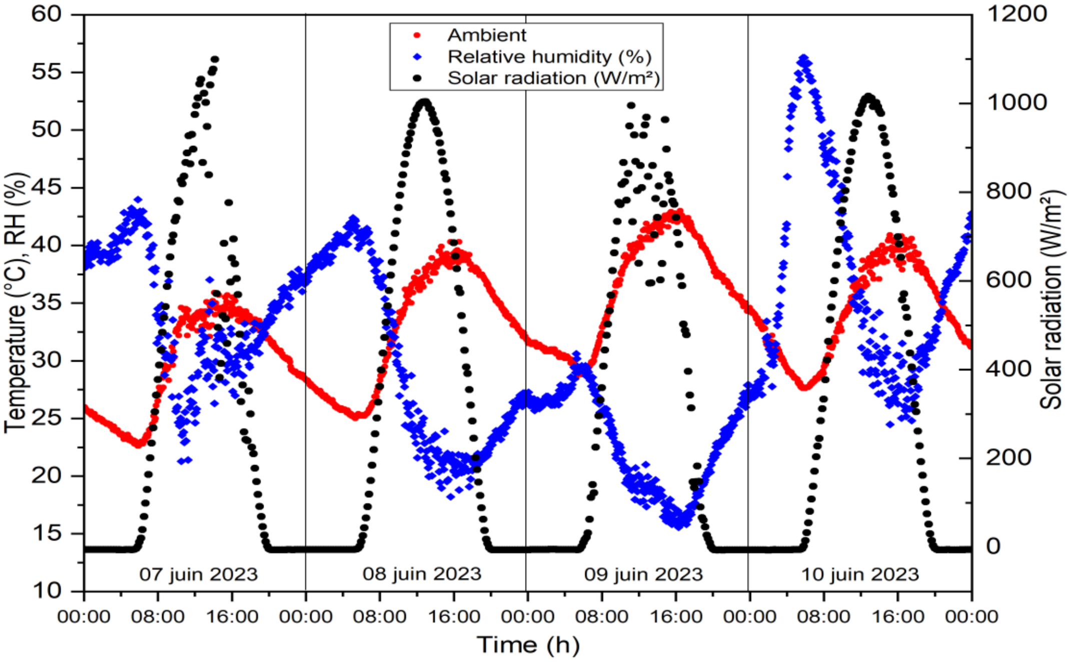

Figure IV. 14. Temporal variations in ambient temperature, relative humidity, and solar radiation for material-based experiments

IV.3.1. Direct solar dryer

The drying process of plants is greatly influenced by the air temperature. The temperature variation over time within the direct dryer in relation to the surrounding air is depicted in Figure IV. 15. The dryer's maximum drying temperature over the trial period was 49.6 °C, with a peak difference of 12 °C. Interestingly, the temperature inside the dryer reached 49.6 °C on the third day, even though the outside temperature only reached 43 °C. The dryer's efficient insulation and clever design, which uses solar radiation to enhance the temperature, are to blame for the noticeable temperature difference. Furthermore, the dryer's forced ventilation system keeps the temperature below 50 °C, which creates the ideal environment for plant drying, according to Müller et al. [109].

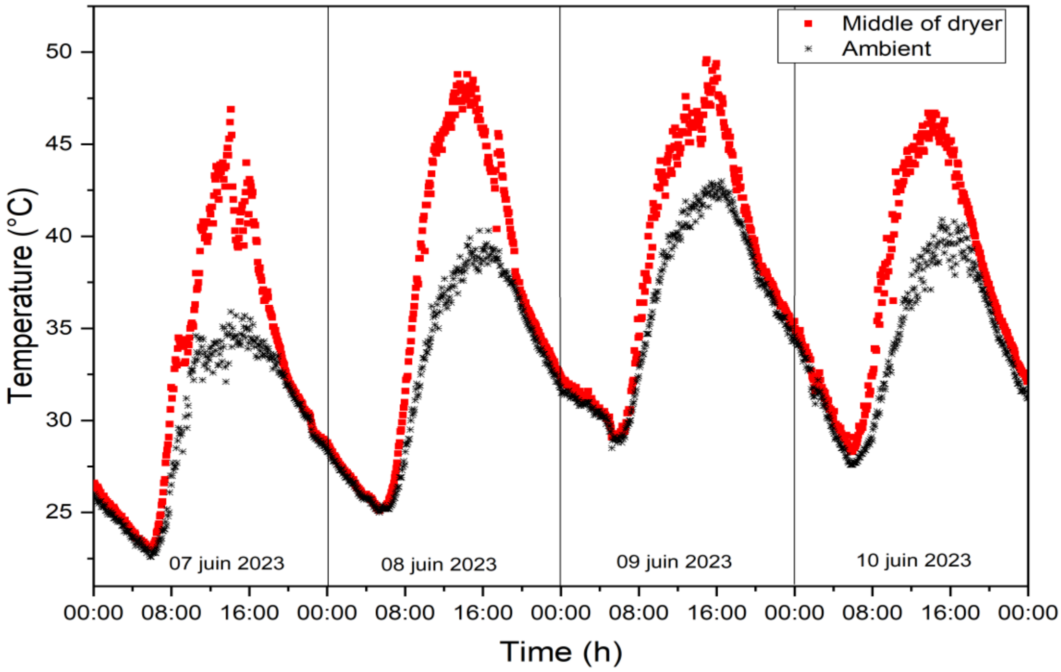

Figure IV. 15. Drying temperature variation in the clay based direct solar dryer

IV.3.2. Indirect solar dryer performance

For the indirect solar dryer, Figure IV. 16 shows the temperature variation at the outlet of the solar collector and in the middle of the drying chamber, the experimental results reveal that the maximum temperatures recorded were 48 °C at the outlet of the solar air collector and 47.8 °C in the center of the chamber. The observed temperature changes exhibit a noticeable resemblance. This alignment suggests a strong correlation between the two locations, emphasizing a consistent thermal behavior throughout the drying process. The similarity in temperature trends supports the effectiveness of heat transfer mechanisms and the overall efficiency of the drying system, indicating successful thermal integration between the collector and the drying chamber. The recorded fluctuations in temperature indicate an optimal drying environment. This temperature range ensures the preservation of plant quality and characteristics during the drying process.

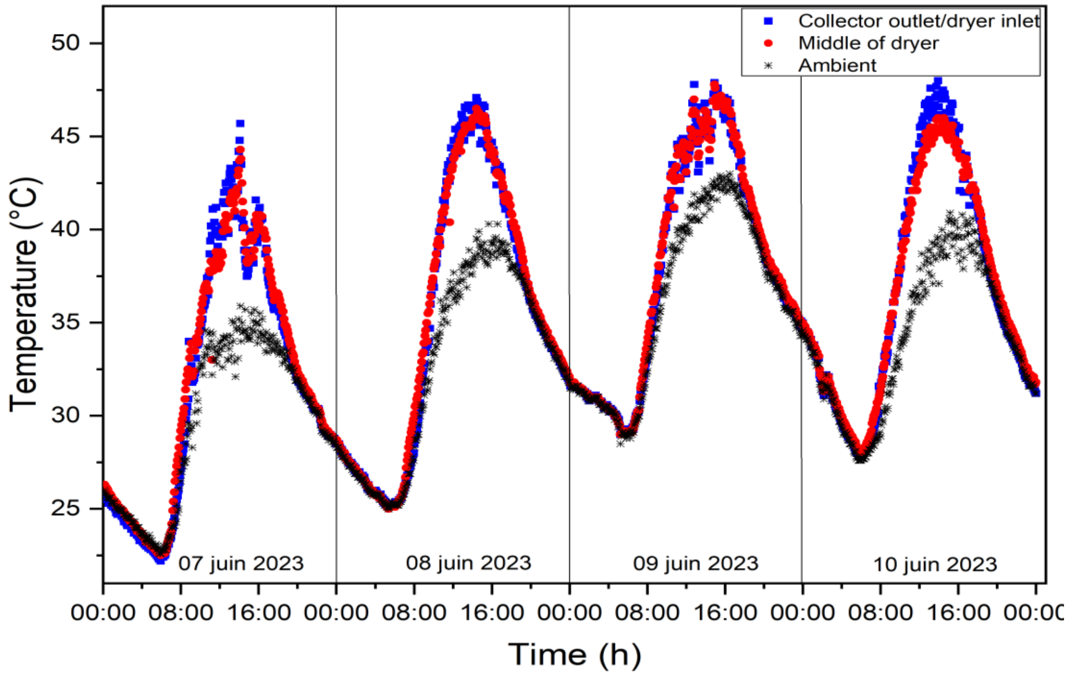

Figure IV. 16. Variation in temperature within the clay based indirect solar dryer and at the solar collector's outlet

Figure IV. 17 compares the drying temperature with time in the middle of the chamber, for direct and indirect dryers. It is observed that they exhibit a relatively similar trend, with a slight advantage favoring the direct solar dryer. This marginal advantage is attributed to the direct solar dryer's increased sunlight exposure, which results in a higher intensity of heat absorption by the drying chamber. As a result, the direct solar dryer tends to have slightly elevated temperatures compared to the indirect dryer.

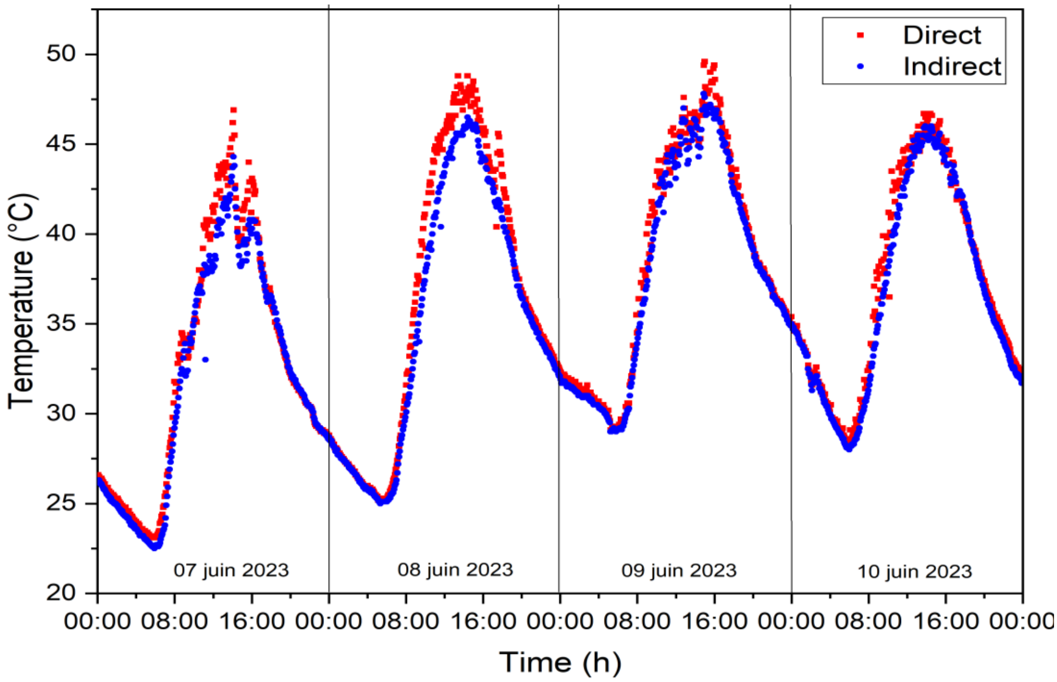

Figure IV. 17. Drying temperature variation in the clay based direct and indirect solar dryers

IV.3.3. Drying characteristics

Drying curves

Moisture content values obtained from the experimental tests are displayed in Figure IV. 18 for both moringa and mint. For the moringa, to reach a moisture content below 10% it took 320 and 1860 min in the direct and indirect solar dryers, respectively. For the mint, to reach a moisture content of 10%, it took 520 and 2495 min in the direct and indirect solar dryers, respectively, the interruptions in the line represent the nighttime. Direct exposure to sunlight in the direct solar dryer provides a higher heat input, leading to faster evaporation of moisture from the product and, consequently, shorter drying time.

The indirect solar dryer demonstrated a distinct advantage over the direct solar dryer in terms of preserving the color quality and aroma of the dried plants, providing a gentle drying environment. Retaining the volatile compounds responsible for the characteristic aroma of the herbs.

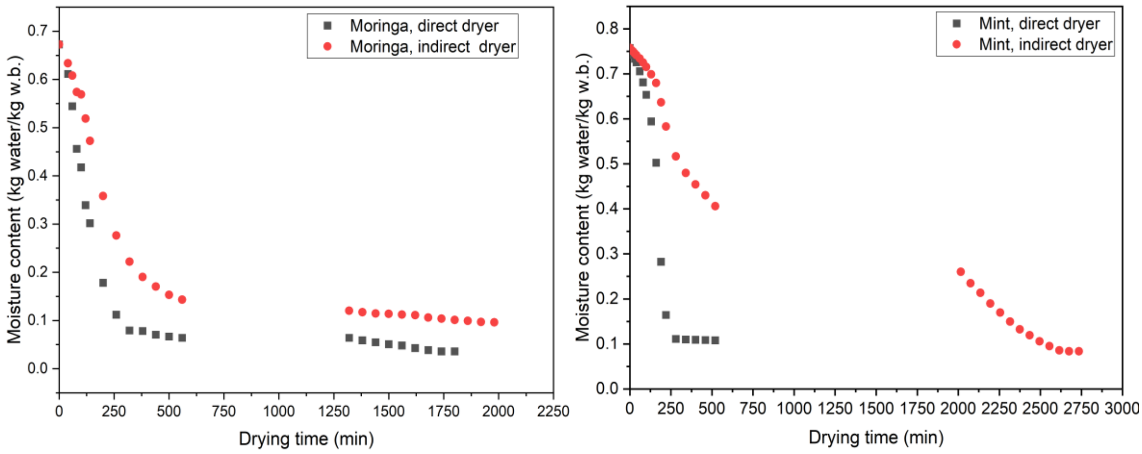

Figure IV. 18. Moisture content variation of moringa and mint with time

Figure IV. 19 shows the drying process of mint in the direct and indirect solar dryers.

Figure IV. 19. Mint samples during the drying process in direct and indirect solar dryers

IV.3.4. Thermal efficiency

The efficiency of both the solar air collector and the drying chambers gauges the energy used for heating the air necessary for drying purposes. This energy efficiency can be influenced by factors including the design of the drying chamber, the velocity of drying air, the moisture content in the drying product, and ambient environmental conditions. Equation (II.17) has been utilized to calculate the collector efficiency (η_c), as demonstrated in Table IV. 9. The average and maximum η_c values are 19.19% and 74.21%, respectively.

Drying efficiency (η_d) was assessed, with η_d being contingent upon input energy and the quantity of moisture eliminated. It exhibited an increasing trend over time until reaching its peak at noon, coinciding with the maximum recorded solar radiation. Subsequently, its value gradually decreased over time. This decline can be attributed to the substantial removal of moisture from the outer surface of the sample during the initial drying phase. The overall η_d of both setups were computed, reaching a maximum and average value of 29.18% and 6.4% in the direct solar dryer, and 7.97% and 1.45% in the indirect solar dryer, respectively.

Table IV. 9. Average and maximum efficiency of the clay based solar dryers

	Average efficiency (%)	Maximum efficiency (%)
Solar air collector	19.19	74.21
Direct solar dryer	6.4	29.18
Indirect solar dryer	1.45	7.97

IV.3.5. Economic analysis

The detailed components and material cost of the direct and ISD is shown in Table IV. 10 and it is estimated to be $898 and $1031, respectively.

Table IV. 10. Components & material specification price of the clay based solar dryers

Material	Price (DZD)	
	Direct dryer	Indirect dryer
Polycarbonate cover (3.44 m²)	4300	4300
Clay wall (4.78 m²)	71700	71700
Polycarbonate U connector (4.4 m)	1026	1026
Sandwich panel (3.55 m²)	/	9940
Trays (108 m)	30000	30000
Wood plank (1.83 m²)	2000	2000
Aluminum sheet (2.64 m²)	/	7920
Rubber sheet (2.2 m²)	2200	2200
Fan	2500	2500
Painting box (1.5 kg)	760	760
Support (15.8 m)	6200	6200
Total	120686 DZD	138546 DZD

1 DZD ≈ 0.0074 $

Results of the dryer's economic study are detailed in Table IV .11.

Table IV. 11. Cost and economic parameters of the clay based direct and indirect dryers for drying mint

Variable	Direct dryer	Indirect dryer
The capital cost of the dryer, C_{cd} ($)	898	1031
Annualized cost of dryers, AC ($)	59.03	66.21
Annualized capital cost, C_{ac} ($)	45.82	52.60
Power price of fans, C_{ele} ($)	10.52	10.52
Price of dried plants, C_{dry} ($/kg)	22.33	22.33

Price of fresh plants, C_{fre} ($/kg)	0.74	0.74
Selling cost of brand-name dried plants, C_{bdp} ($)	26	26
Life cycle, n (year)	30	30
Payback time, Pb (year)	0.52	1.18

IV.4. Experiment 3: Direct solar dryer enhancement

IV.4.1. Validity test

To ensure the reliability of our experimental setup, a validity test was conducted on the two developed solar dryers before introducing any modifications. This test aimed to confirm that both dryers, being identical in design and construction, produced the same output under identical environmental conditions. Temperature changes inside the dryers were monitored over several days. As shown in Figure IV. 19, both dryers achieved consistent alignment and output, validating the uniformity of their initial performance. This confirmation was crucial to ensure that any subsequent changes in performance could be attributed solely to the modifications introduced.

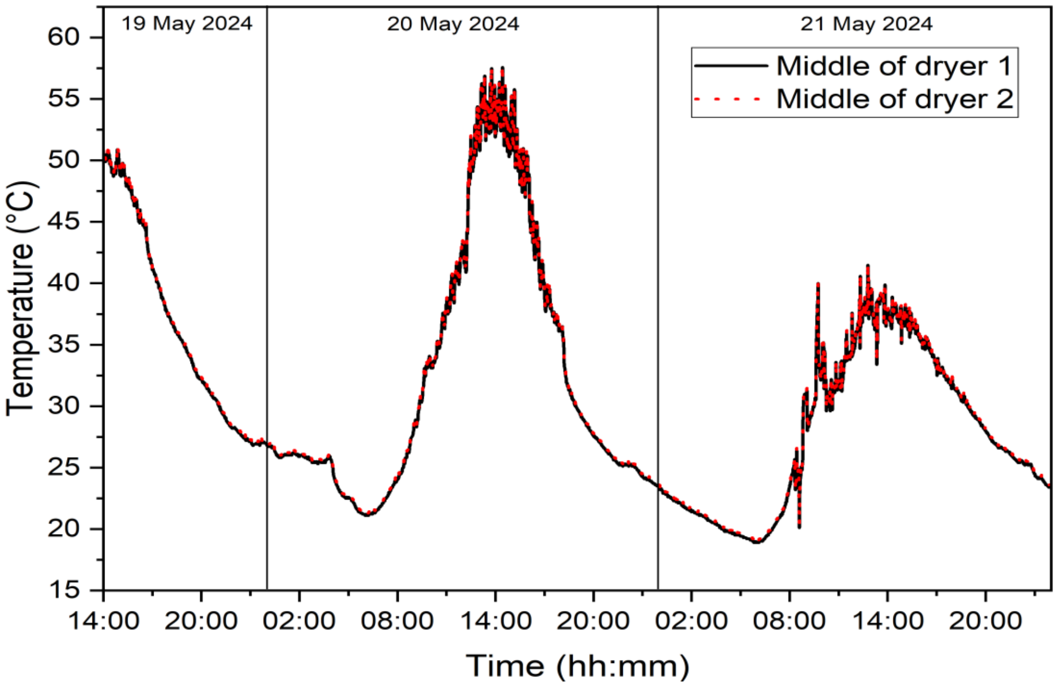

Figure IV. 20. Comparison of temperature inside the solar dryers before adding obstacles

Figure IV. 20 shows the variation of ambient temperature and global solar radiation with time during the test days of 22 – 23 and 27 May 2024

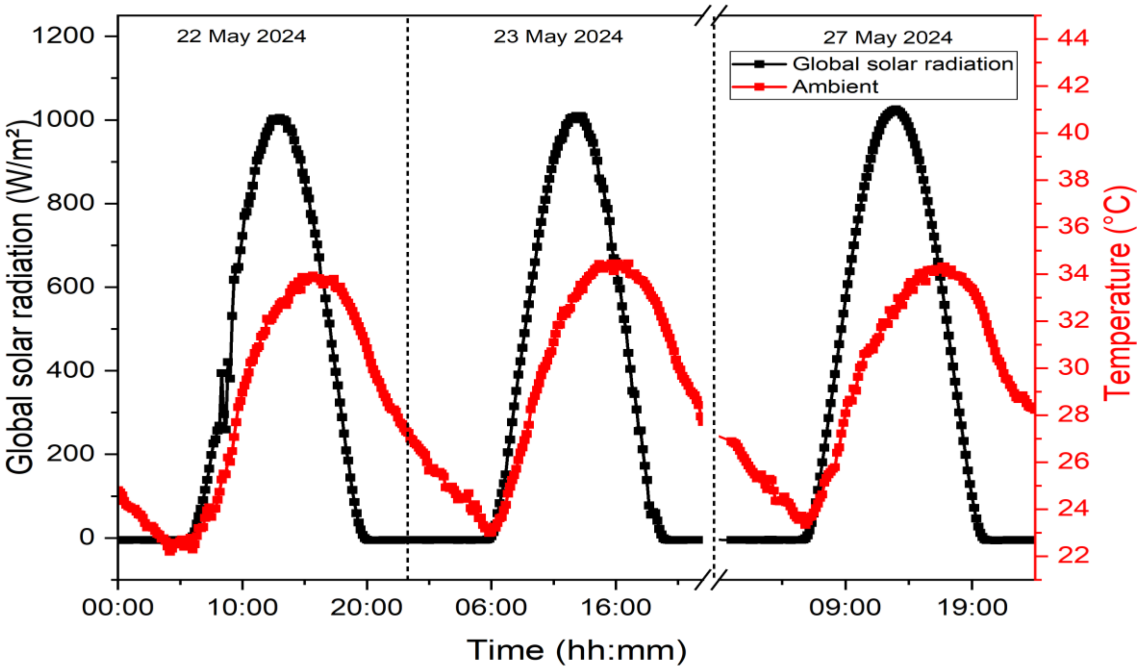

Figure IV. 21. Changes in ambient temperature and solar radiation as a function of time during test days of the 3rd experiment

IV.4.2. Performance of solar dryers

Air temperature plays a crucial role in the drying process of products. Figure IV. 21 shows the temperature change at the outlet of the direct solar dryer with and without obstacles compared to the ambient temperature. During the experimental period, the direct solar dryer with obstacles reached a maximum drying temperature of 48.1°C, achieving an increase of up to 14.1°C compared to a 10°C increase in the conventional dryer. This improvement is attributed to enhanced heat transfer and airflow dynamics introduced by the obstacles. The obstacles induce turbulence, which increases heat transfer and ensures more even air distribution, preventing hot and cold spots. This leads to better contact between the air and heated surfaces. Additionally, the obstacles slow down the airflow, extending the air's residence time within the drying chamber, allowing it to absorb more heat.

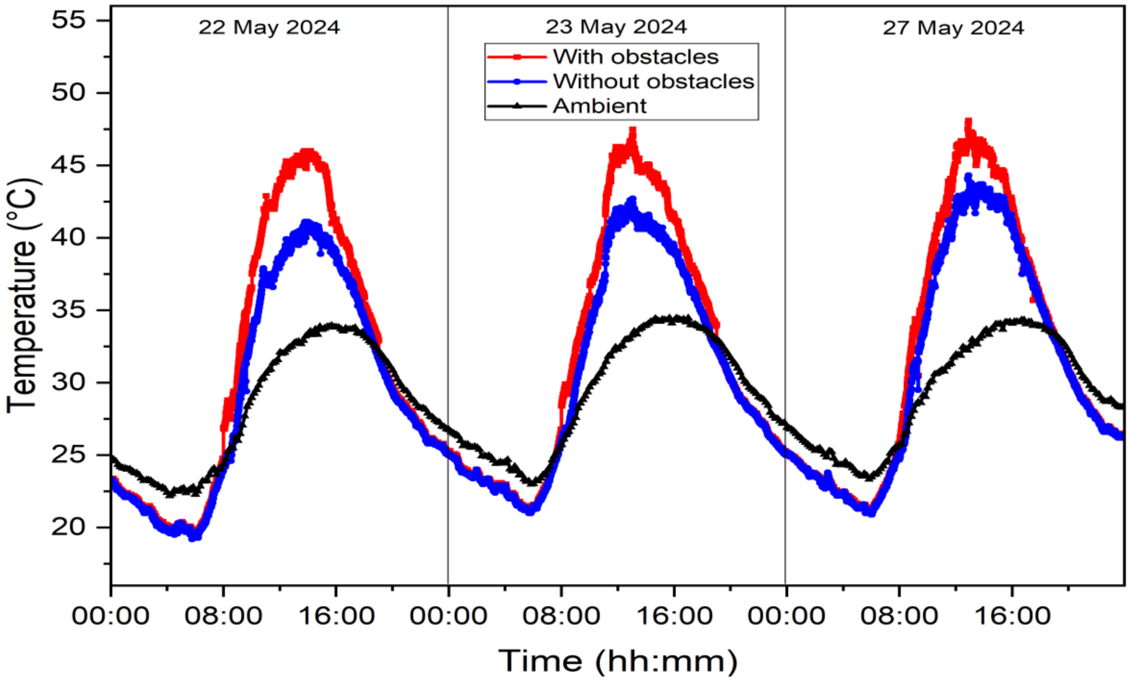

Figure IV. 22. Temperature change at the outlet of the direct solar dryer with and without obstacles

IV.4.3. Numerical results

In this section, the effects of obstacles on the air flow and temperature distribution inside the direct solar dryer are examined using the CFD approach. The input parameters in all of the simulations were taken from the data obtained on 27 May 2024.

IV.4.3.1. Grid independence test

A grid independence test is performed by progressively increasing the number of elements in the computational domain to produce different grid sizes in order to acquire CFD results that are independent of grid resolution. Figure IV. 22 displays the temperature and velocity variation at the direct solar dryer's outlet for various mesh sizes: 0.115, 0.171, 0.233, 0.29, 0.367, 0.42, and 0.5 million elements. It is evident from the chart that the temperature and velocity at the dryer's exit vary very little. Therefore, a mesh size of 0.42 million elements with an average skewness of 0.22 and a maximum skewness of 0.79 is employed in this work to save computational time.

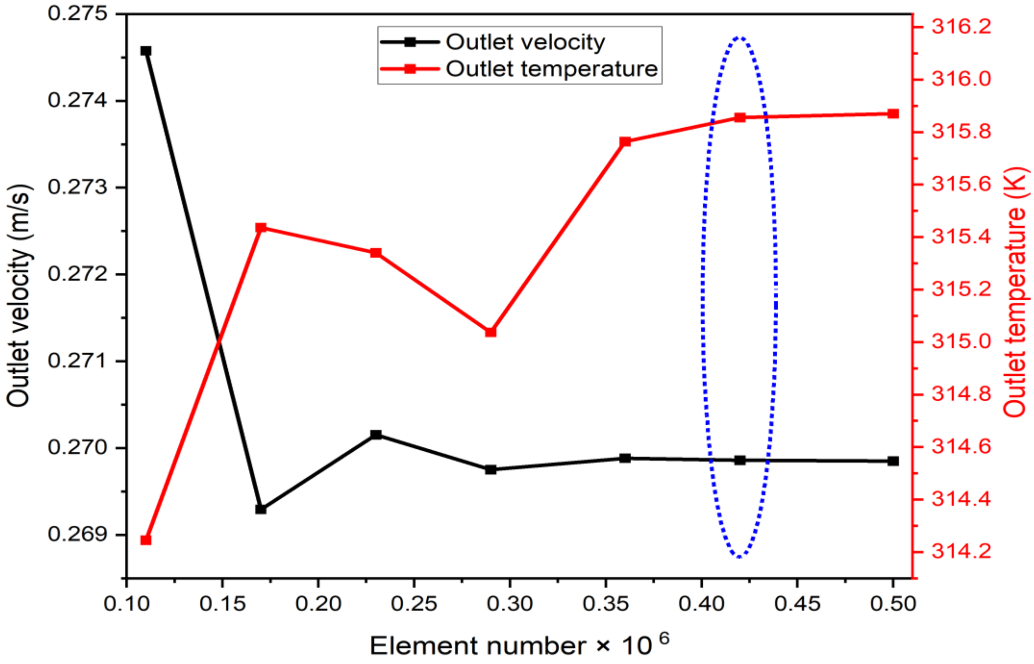

Figure IV. 23. Mesh independency test

IV.4.3.2. Experimental validation

The experimental data from the experiments is used to validate the numerical results. Figure IV. 23 shows the comparison of temperature values obtained at the solar dryer's outlet at various times of the day with the experimental data. The addition of obstacles increased the temperature in comparison to the setup without obstacles because the longer air residence time improved heat transfer. For the solar dryer without obstructions, the average discrepancy between numerical and experimental temperature data is 2.03%, whereas for the solar dryer with obstructions, it is 2.26%. Variations in the surrounding environment, inaccurate measurements, and the inherent simplifications in the numerical model are some of the reasons for this small divergence. The results show that the current numerical approach shows good agreement with the experimental data despite these small differences.

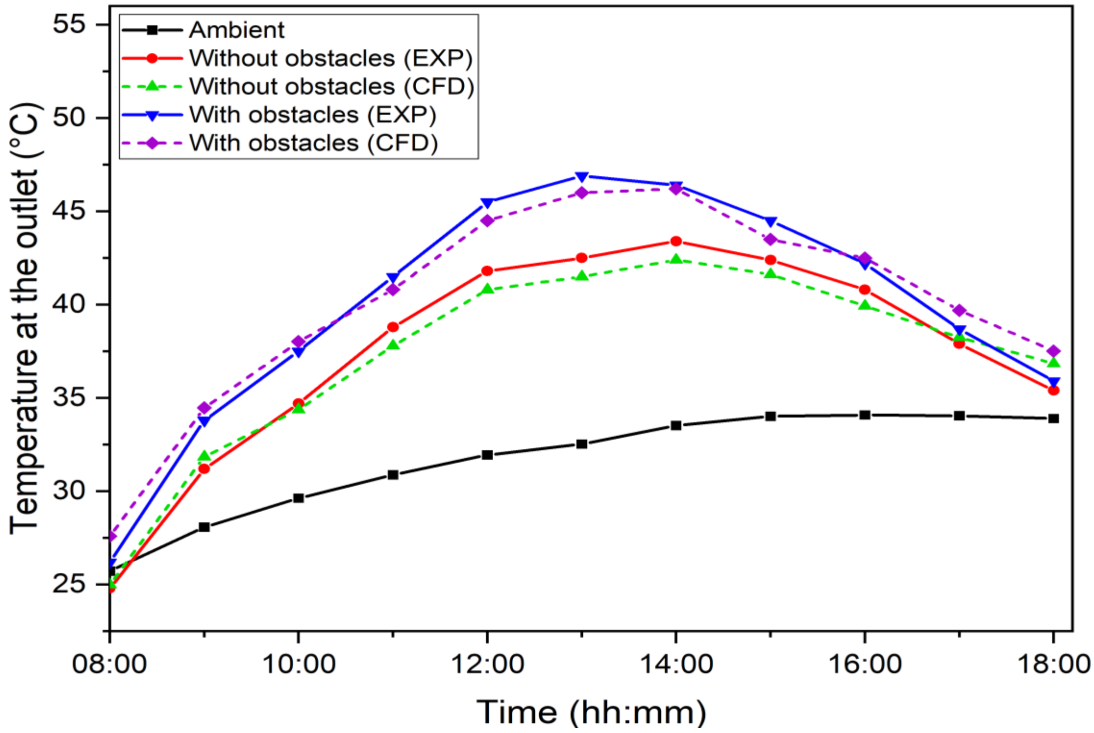

Figure IV. 24. Numerical validation of experimentally obtained data for both setups

Figure IV. 24 shows the velocity volume rendering of the direct solar dryers to illustrate the air flow field and velocity distribution in the air domain with and without obstacles. The figure shows that air does not reach certain zones in the system. Poor air circulation lead to uneven heat distribution, which affect drying efficiency. Adding obstacles increases air distribution inside the chamber, creating turbulence. This results in areas of high velocity near the obstacles, promoting better and more uniform air circulation. This turbulence ensures that all areas of the dryer receive adequate air flow and, consequently, improves drying efficiency.

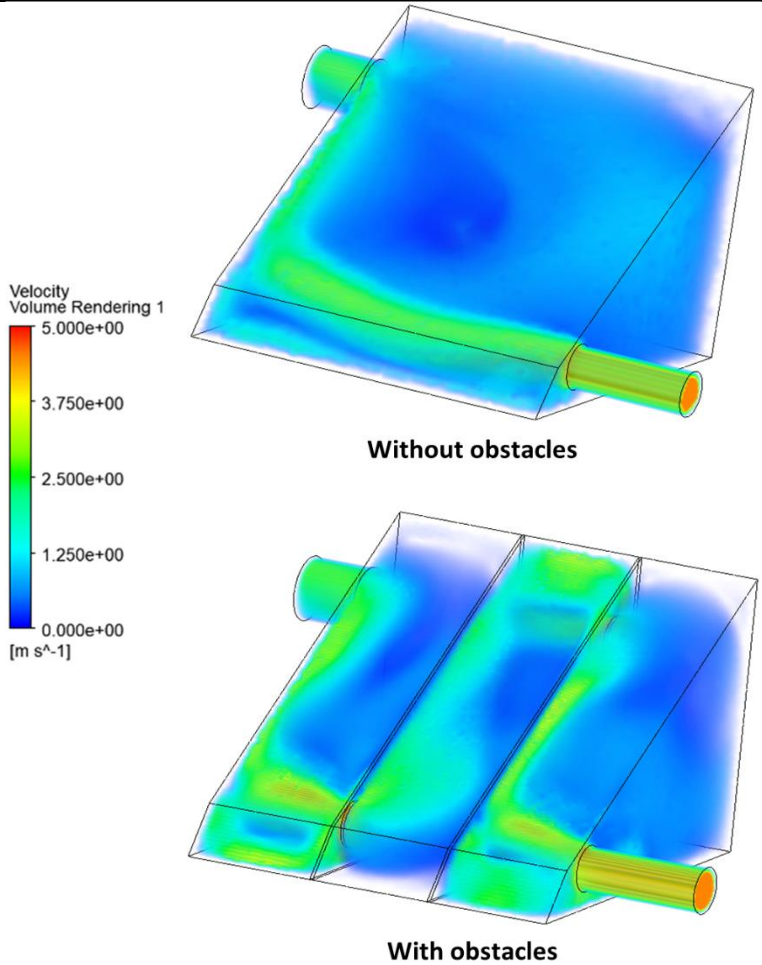

Figure IV. 25. Velocity volume rendering images of direct solar dryers with and without obstacles

Figure IV. 25 shows velocity contours of a plane cut near the outlet for the solar dryer with and without obstacles, for the dryer without obstacles, the velocity remains low throughout the chamber, only increasing near the outlet. This indicates that the airflow is relatively stagnant in most parts of the chamber, leading to inefficient heat transfer and prolonged drying times. In contrast, the dryer with obstacles shows higher velocity regions near the walls and around the obstacles, the increased velocity around the obstacles contributes to faster evaporation and more efficient drying, as the turbulent flow promotes better heat distribution and moisture removal from the product.

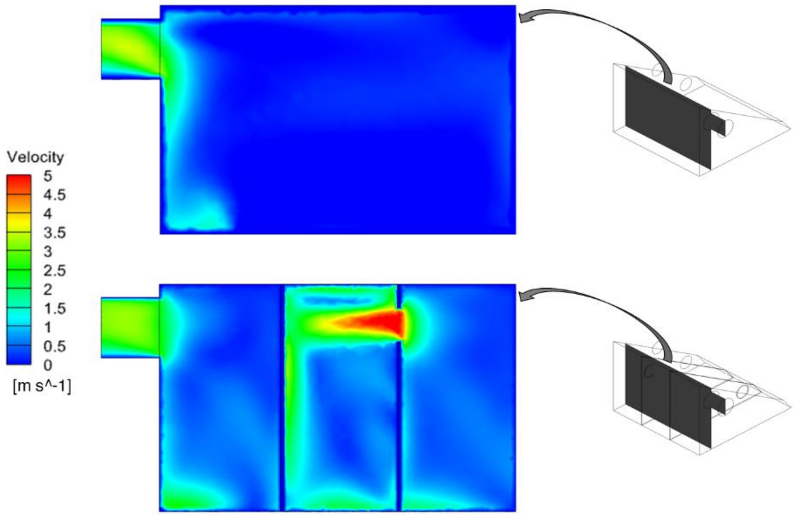

Figure IV. 26. Velocity contours of direct solar dryers with and without obstacles

Figure IV. 26 shows temperature contours of a plane cut near the outlet for the solar dryer with and without obstacles. The temperature contours near the outlet provide critical insights into the thermal distribution within the drying chambers of the solar dryers. In the dryer without obstacles, the temperature is relatively uniform across all regions. This uniformity suggests that the heat distribution is not optimal, as the hot air does not circulate effectively throughout the chamber. However, the dryer with obstacles shows higher temperatures in the second and third zones. This difference is attributed to the strategic placement of obstacles, which were added to improve heat transfer within the chamber, and as a result, more heat is transferred to these specific zones, leading to higher temperatures.

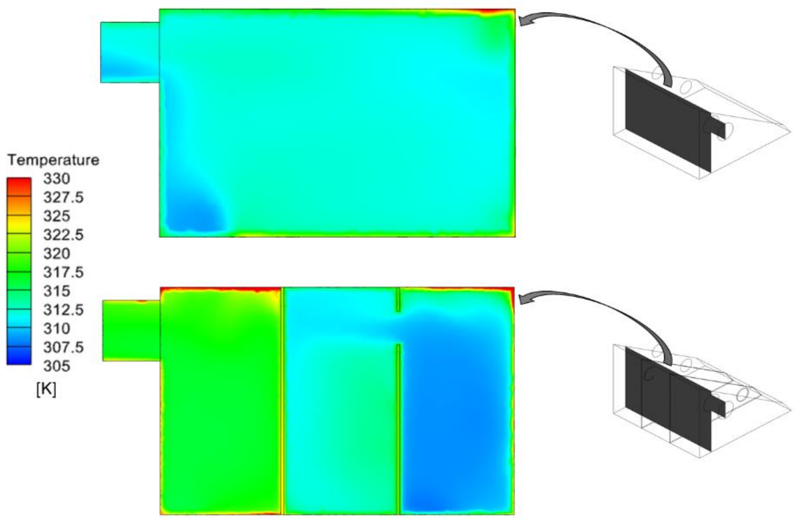

Figure IV. 27. Temperature contours of direct solar dryers with and without obstacles

IV.4.4. Drying proprieties

Figure IV. 27 illustrates the drying chamber divided into three distinct zones for monitoring the weight of the sweet pepper samples: Zone 1 is near the inlet, Zone 2 is in the middle, and Zone 3 is near the outlet. The arrangement of baskets is identical in both the dryer with obstacles and the dryer without obstacles, ensuring a direct comparison of each zone between the two configurations.

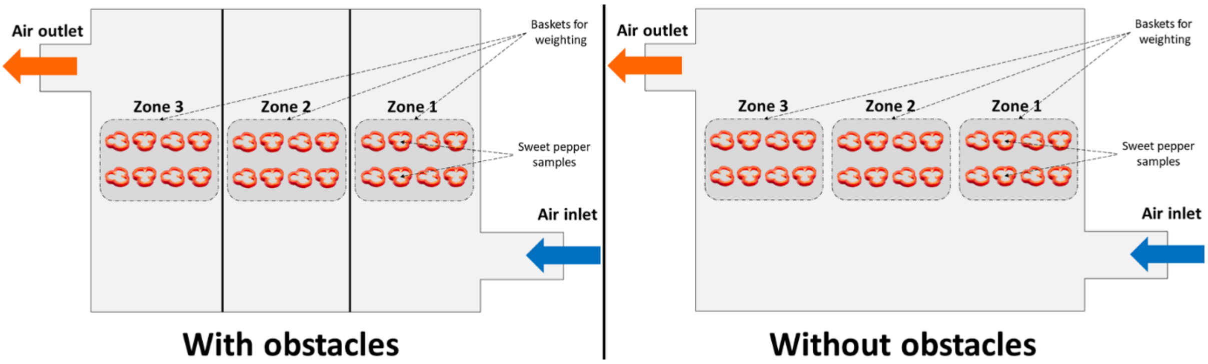

Figure IV. 28. Zones distribution inside the direct solar dryers

Figure IV. 28 shows the variation of moisture ratio with time. The figure clearly illustrates that adding obstacles to the direct solar dryer significantly improved its performance, resulting in a decreased drying time. For the direct solar dryer without obstacles, the recorded drying times were 745 minutes for zone 1, 475 minutes for zone 2, and 425 minutes for zone 3. The addition of obstacles led to a reduction in drying time by 4.5 hours (36.24%), 1.58 hours (20%), and 1.25 hours (17.64%) for zones 1, 2, and 3, respectively, compared to the dryer without obstacles.

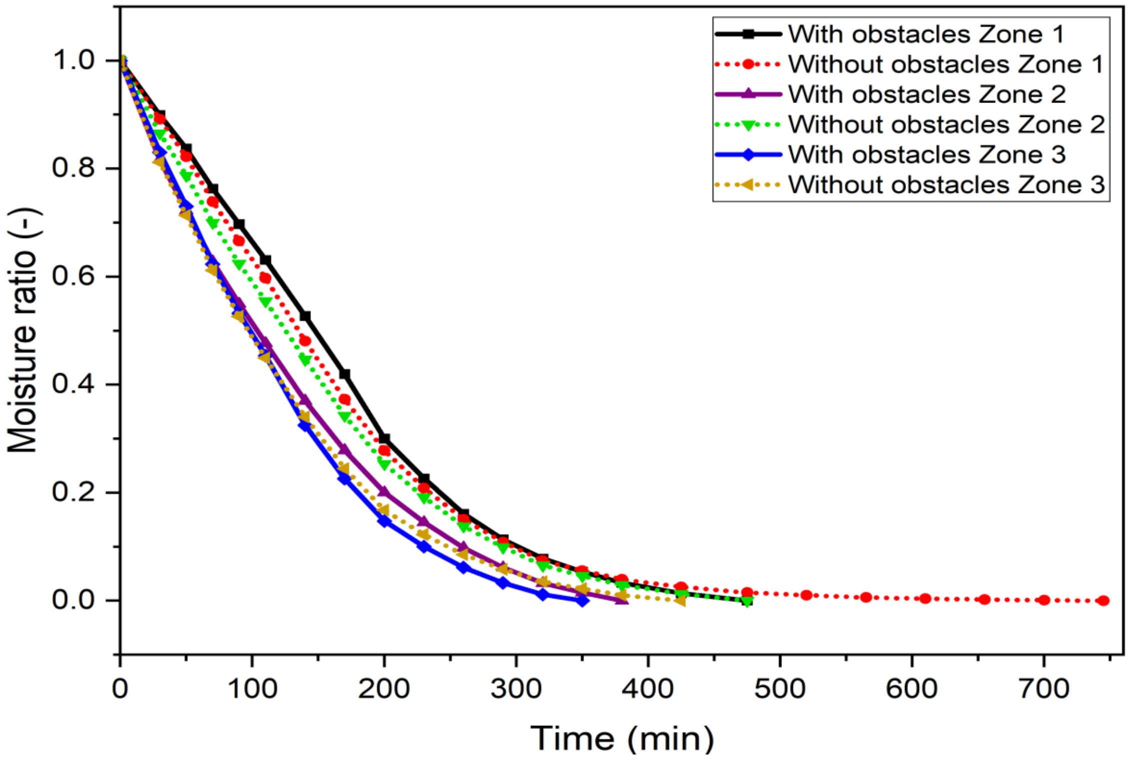

Figure IV. 29. Moisture ratio change with time for different zones inside the direct solar dryers

Figure IV. 29 illustrates the change in drying rate with moisture content variation. It is evident from the figure that the drying rate was highest during the initial phase of drying, corresponding to the period when the moisture content was at its peak. During this phase, the drying rate ranged between 0.0031 and 0.0061 (kg water/ kg dry basis min). As the drying process progressed into the second phase and the moisture content began to decrease, the drying rate also declined. This trend reflects the typical drying behavior where the rate is initially high due to the abundance of free moisture and gradually decreases as the moisture content diminishes and the drying process becomes more challenging.

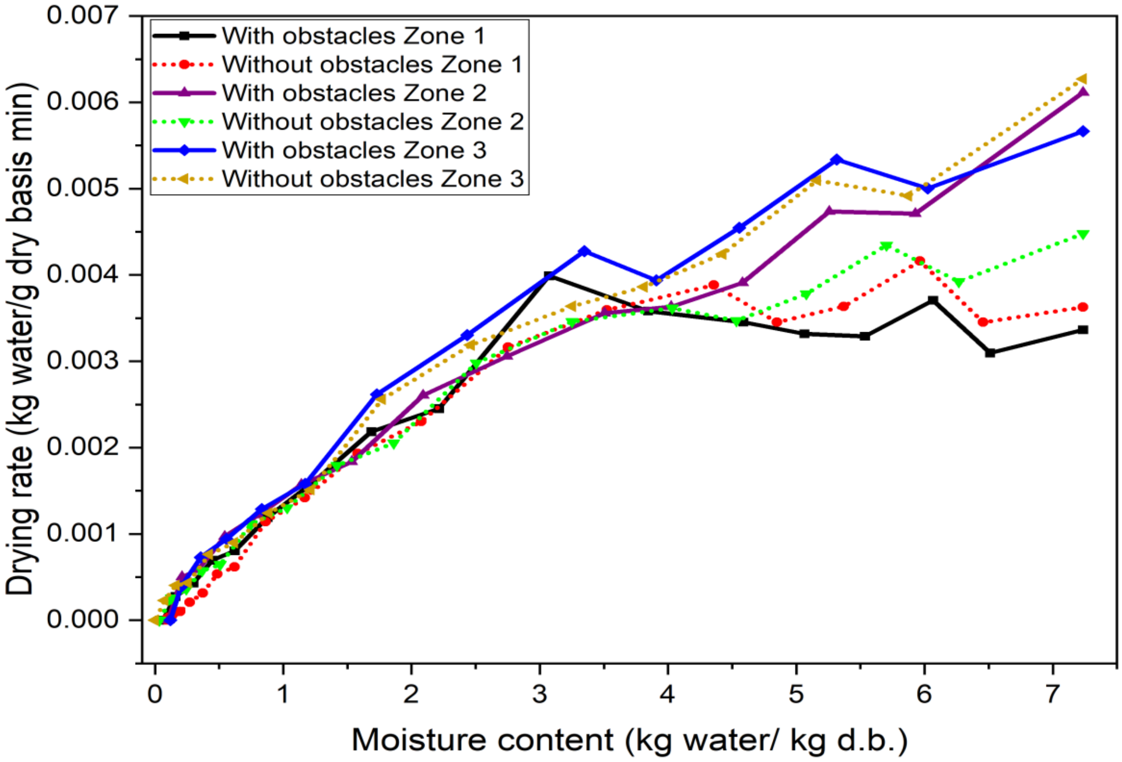

Figure IV. 30. Drying rate change with moisture content for different zones inside the direct solar dryers

IV.4.5. Thermal efficiency

The efficiency of the drying chambers measures the energy used to heat the air required for drying. This energy efficiency can be affected by factors such as the design of the drying chamber, the velocity of the drying air, and ambient environmental conditions. Thermal efficiency (ηc) is calculated using Equation (II.17).

Figure IV. 30 presents the variation in thermal efficiency over time during the test days. The data clearly demonstrate that the solar dryer integrated with obstacles significantly outperformed the conventional dryer. The dryer with obstacles achieved a maximum thermal efficiency of 69.39%, with an average efficiency of 44.67%. In contrast, the conventional dryer without obstacles reached a peak efficiency of 45.65%, with an average efficiency of 27.89%. This substantial improvement highlights the effectiveness of incorporating obstacles in enhancing the heat transfer and overall performance of the solar drying system.

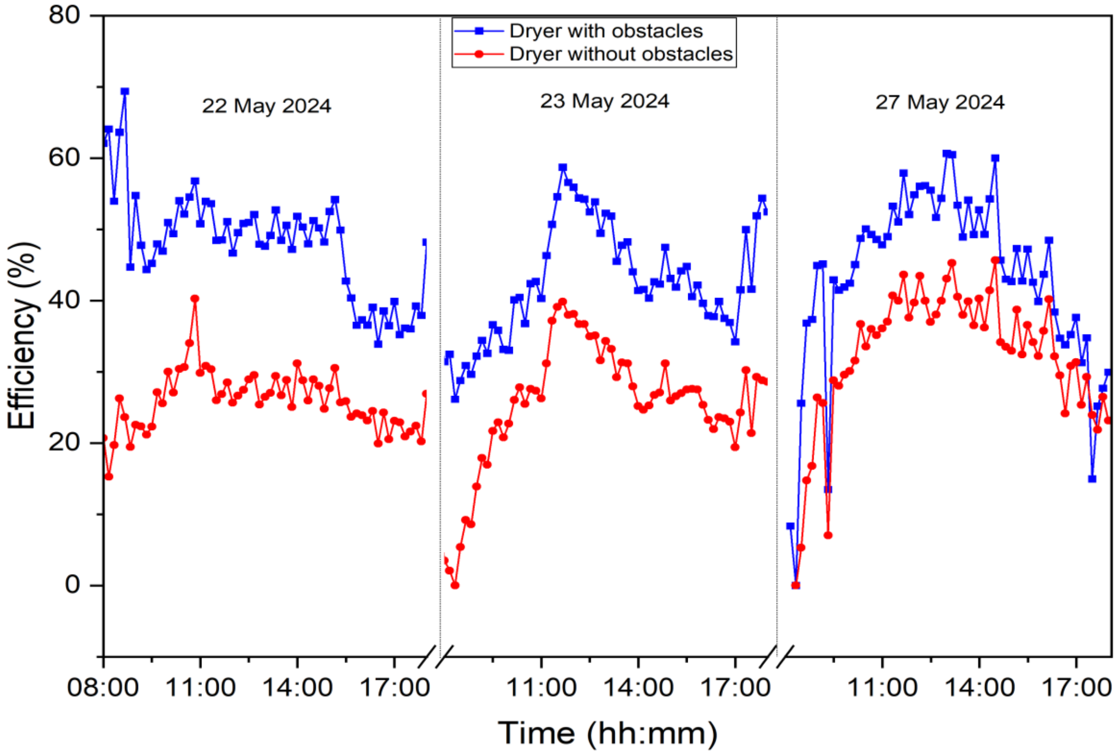

Figure IV. 31. Thermal efficiency variation for the direct solar dryer with and without obstacles

IV.5. Experiment 4: Indirect solar dryer enhancement

IV.5.1. Validity test of the indirect solar dryer

Figure IV. 31 illustrates the temperature stability of a solar air collector heated with an electric heater during the test period. The data reveal that the temperature was maintained at a mean value of 61.44 °C with a standard deviation of 0.9096 °C. This low standard deviation indicates minimal fluctuation around the mean temperature, proving that the system is exceptionally well controlled. Temperature consistency is essential to the efficiency of the drying process, as it ensures uniform drying conditions and improves the quality of the dried products. Electric heating is therefore a reliable and stable source of heat for the solar dryer.

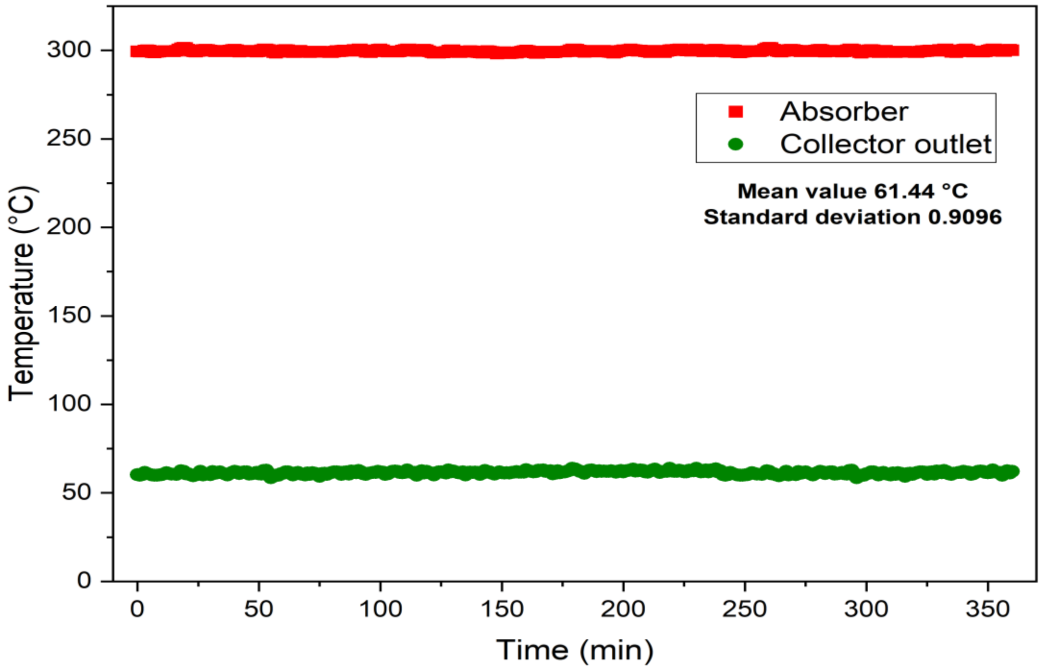

Figure IV. 32. Stability test of the solar air collector system for the indirect solar dryer

IV.5.2. Drying proprieties

Figure IV. 32 illustrates the variation in moisture content over time inside the indirect solar dryer at a drying temperature of 60 °C. The experiments consisted of two tests: one comparing the upper and lower areas of the drying chamber without integrated ribs, and the second with ribs integrated into the chamber. For sweet pepper samples, the initial moisture content of 7.23 (kg water/kg d.b.) was reduced to below 0.05 (kg water/kg d.b.) in 440 minutes without ribs. However, after integrating ribs, this reduction was achieved in just 365 minutes. In the case of cucumber samples, the initial moisture content of 19.88 (kg water/kg d.b.) decreased to below 0.05 (kg water/kg d.b.) in 605 minutes without ribs. With the integration of ribs, this reduction occurred in 380 minutes in the lower area and 455 minutes in the upper area of the chamber.

This improvement is due to the enhanced turbulence and more uniform heat distribution caused by the ribs, which promote faster moisture removal, the integration of ribs proved to enhance the drying process by improving heat transfer and reducing drying time, particularly for the lower area of the chamber where airflow dynamics were positively impacted.

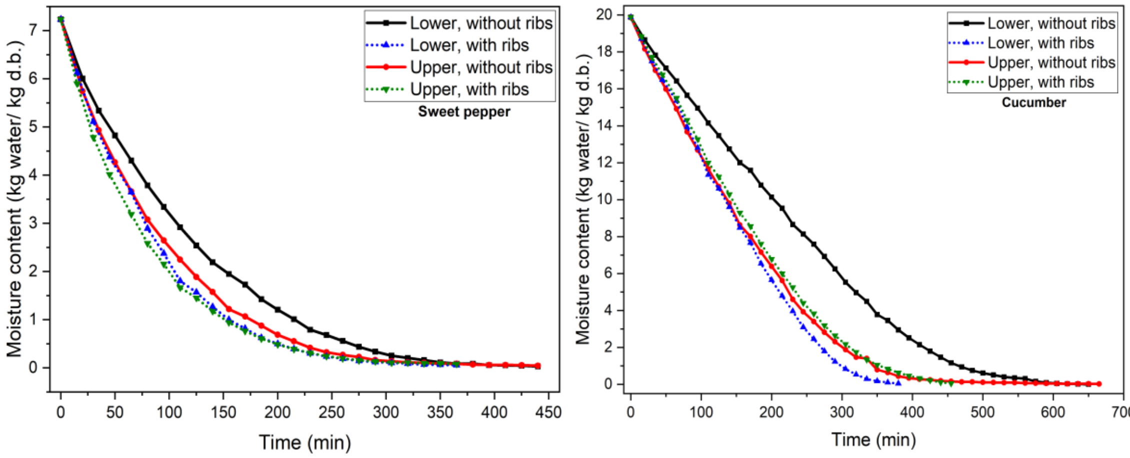

Figure IV. 33. Moisture content variation of sweet pepper and cucumber with time

Figure IV. 33 illustrates the drying rate as a function of moisture content for sweet pepper and cucumber samples. The figure clearly shows that the drying rate was highest during the initial phase, particularly in the configuration with ribs, which corresponds to the period when the moisture content was at its maximum. As the drying process progressed into the second phase and moisture content began to decrease, a corresponding decline in the drying rate was observed. This trend is characteristic of the drying process, where the rate is initially high due to the abundance of free moisture. As the moisture content diminishes, the drying rate gradually slows, reflecting the increasing difficulty of removing the remaining bound moisture.

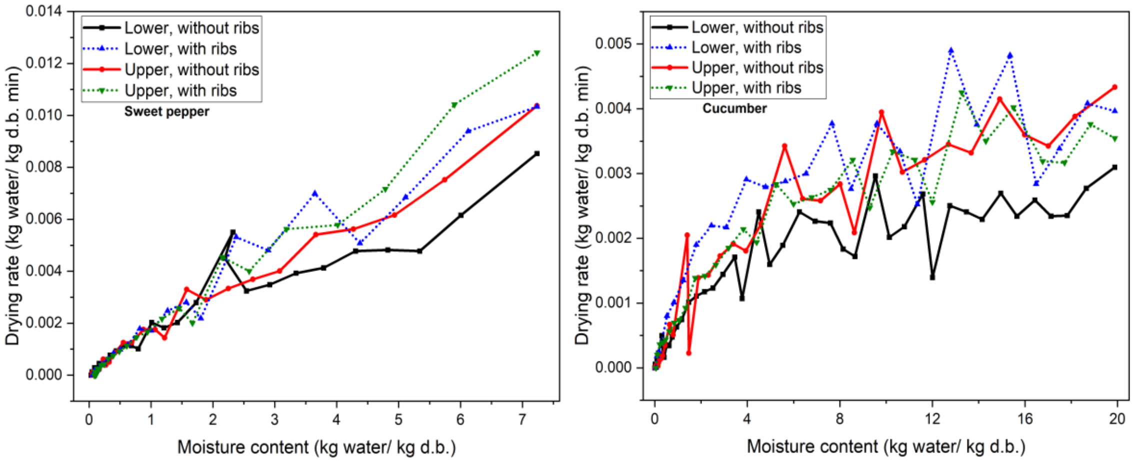

Figure IV. 34. Drying rate change with moisture content for sweet pepper and cucumber

Figure IV. 34 shows samples of dried cucumber and pepper in the developed system.

Figure IV. 35. Dried samples of cucumber and pepper

IV.6. Conclusion

In conclusion, this chapter provides a comprehensive analysis and discussion of the results from the experimental and numerical studies on solar drying systems. The chapter evaluates the impact of various enhancements, including improvements to the solar collector, optimizations of the drying chamber, and the integration of obstacles and ribs, on system efficiency and effectiveness. By comparing experimental data with numerical simulations, the accuracy and practical relevance of the models were assessed. The chapter offers valuable insights into how different configurations affect drying performance and energy efficiency, demonstrating the effectiveness of the proposed enhancements. These findings lay the groundwork for future research and development, highlighting potential areas for further investigation and improvement in solar drying technologies.

General conclusion

This thesis presents a comprehensive investigation into enhancing solar drying technologies through both experimental and numerical approaches. The research aimed at optimizing various aspects of solar dryers, including collector performance, material use, airflow dynamics, and drying efficiency. By integrating innovative design elements such as fins, rocks, and ribs, and employing both direct and indirect drying configurations, this research highlights significant advancements in the field. The combination of experimental validation and numerical simulation using ANSYS Fluent has provided valuable insights into developing more efficient and cost-effective solar drying solutions. The findings emphasize the potential for improved performance and economic benefits across different solar drying systems. The main key outcomes and findings derived from the present research work can be summarized as follows:

Collector performance

- The offset strip fin collector displayed higher output temperatures, as opposed the collector without fins, demonstrating the benefit of adding fins.
- Regarding temperature performance, at low and intermediate flow rates, the collector with pebbles as sensible energy storage medium demonstrated a maximum outlet temperature of 70.2 °C, whereas the collector with fins reached 76.8 °C. A 13.6 °C temperature increase over the night benefits the rock collector.
- The two dryers took varied amounts of time to reach a final moisture content of 6%: the solar dryer with fins took 24 hours and 12 minutes, while the solar dryer with pebbles took 28 hours and 42 minutes.
- The expected payback period for the OSF indirect solar dryer is 0.95 years. The dryer with OSF saves a substantial amount of money over the course of the system's lifespans—an average of 769.28$ compared to 578.36$ for the dryer without OSF. This means that economic efficiency has increased by 33%.
- By constructing the designed systems with locally sourced and reclaimed materials, CO_2 emissions are reduced to 71.85 and 87.45 kg/year, respectively, resulting in a net CO_2 reduction of 17.945 and 17.458 tons over the systems' lifetime. Because they release less greenhouse gases into the atmosphere, both solar dryers are regarded as environmentally beneficial.

Clay-based solar dryers

- The use of clay as a primary material in the solar dryers contributed to efficient insulation, allowing the dryers to maintain optimal drying temperatures below 50 °C even in high ambient temperatures.

- Efficient ventilation systems were implemented, further enhancing the performance of the clay-based solar dryers.
- The direct solar dryer proved more efficient in the drying process for moringa and mint, exhibiting shorter drying times compared to the indirect dryer.
- The payback period for the direct solar dryer is estimated to be 6 months, while the payback period for the indirect solar dryer is 14 months. The direct solar dryer saves a large amount of money over the lifespans of the systems, averaging $7398.62 annually, compared to $3697.46 for the indirect solar dryer. This corresponds to a 100% rise in the direct solar dryer's economic efficiency compared to the indirect.

Integration of obstacles

- The integration of obstacles resulted in a temperature increase of 14.1 °C, compared to 10 °C without obstacles, demonstrating enhanced heat transfer.
- Numerical results indicated that obstacles improved air distribution inside the chamber, creating areas of high velocity near the obstacles and promoting better overall air circulation.
- The introduction of obstacles reduced drying time by up to 4.5 hours, showcasing improved efficiency in moisture removal.
- The direct solar dryer with obstacles achieved a maximum thermal efficiency of 69.39%, significantly higher than the 45.65% observed in the dryer without obstacles, underscoring the effectiveness of obstacle integration in enhancing dryer performance.

Rib integration in the indirect solar dryer

- The solar air collector, heated with an electric heater, maintained a consistent average temperature of 61.44 °C with a minimal standard deviation of 0.9096 °C, demonstrating excellent temperature control and stability, which is crucial for effective drying.
- For sweet pepper samples, integrating ribs into the drying chamber reduced the drying time from 440 minutes to 365 minutes compared to a chamber without ribs, indicating a significant improvement in drying efficiency. For cucumber, the drying time in the indirect dryer without ribs was 605 minutes. With ribs integrated, the drying time was reduced to 380 minutes in the lower area and 455 minutes in the upper area of the chamber.
- The drying rate was highest during the initial stage of drying, particularly with ribs integrated into the chamber, where moisture content was at its peak. As the drying process progressed and moisture content decreased, the drying rate gradually slowed, reflecting the typical behavior of the drying process.

References

1. Kherrafi, M.A., et al., *Advancements in solar drying technologies: Design variations, hybrid systems, storage materials and numerical analysis: A review.* Solar Energy, 2024. **270**: p. 112383.
2. Bilgen, S., *Structure and environmental impact of global energy consumption.* Renewable and Sustainable Energy Reviews, 2014. **38**: p. 890-902.
3. Hassan, Q., et al., *The renewable energy role in the global energy Transformations.* Renewable Energy Focus, 2024. **48**: p. 100545.
4. Ortiz-Rodríguez, N.M., et al., *Solar drying Technologies: A review and future research directions with a focus on agroindustrial applications in medium and large scale.* Applied Thermal Engineering, 2022. **215**: p. 118993.
5. Amit, S.K., et al., *A review on mechanisms and commercial aspects of food preservation and processing.* Agriculture & Food Security, 2017. **6**: p. 1-22.
6. Kherrafi, M.A., et al., *Experimental and numerical study of performance enhancement in a direct solar dryer integrated with obstacles.* Applied Thermal Engineering, 2025. **259**: p. 124942.
7. Kherrafi, M.A., et al., *Experimental investigation and economic analysis of a novel clay-based solar dryers for drying medicinal and aromatic plants under semi-arid climate.* Energy Sources, Part A: Recovery, Utilization, and Environmental Effects, 2024. **46**(1): p. 11658-11672.
8. Kamarulzaman, A., M. Hasanuzzaman, and N.A. Rahim, *Global advancement of solar drying technologies and its future prospects: A review.* Solar Energy, 2021. **221**: p. 559-582.
9. Tedesco, F.C., A.J. Bühler, and S. Wortmann, *Design, Construction, and Analysis of a Passive Indirect Solar Dryer With Chimney.* Journal of Solar Energy Engineering, 2018. **141**(3).
10. Gilago, M.C., V. Reddy Mugi, and C. V.P, *Energy-exergy and environ-economic (4E) analysis while drying ivy gourd in a passive indirect solar dryer without and with energy storage system and results comparison.* Solar Energy, 2022. **240**: p. 69-83.
11. Kalogirou, S.A., *Chapter 7 - Industrial Process Heat, Chemistry Applications, and Solar Dryers*, in *Solar Energy Engineering (Second Edition)*, S.A. Kalogirou, Editor. 2014, Academic Press: Boston. p. 397-429.
12. Castillo Téllez, M., et al., *Solar drying of Stevia (Rebaudiana Bertoni) leaves using direct and indirect technologies.* Solar Energy, 2018. **159**: p. 898-907.
13. Singh, S., et al., *A novel active-mode indirect solar dryer for agricultural products: Experimental evaluation and economic feasibility.* Energy, 2021. **222**: p. 119956.
14. El-Sebaii, A.A. and S.M. Shalaby, *Experimental investigation of an indirect-mode forced convection solar dryer for drying thymus and mint.* Energy Conversion and Management, 2013. **74**: p. 109-116.
15. Bennamoun, L. and A. Belhamri, *Using solar thermal energy for drying of fresh food products in Algeria*. 2010.
16. Lakshmi, D.V.N., et al., *Performance analyses of mixed mode forced convection solar dryer for drying of stevia leaves.* Solar Energy, 2019. **188**: p. 507-518.
17. Sileshi, S.T., A.A. Hassen, and K.D. Adem, *Simulation of mixed-mode solar dryer with vertical air distribution channel.* Heliyon, 2022. **8**(11).
18. Parhizi, Z., et al. *Modeling and Optimization of Energy and Exergy Parameters of a Hybrid-Solar Dryer for Basil Leaf Drying Using RSM*. Sustainability, 2022. **14**, DOI: 10.3390/su14148839.
19. Khanlari, A., et al., *Experimental and numerical study of the effect of integrating plus-shaped perforated baffles to solar air collector in drying application.* Renewable Energy, 2020. **145**: p. 1677-1692.

20. Gong, X., et al., *Heat transfer enhancement analysis of tube receiver for parabolic trough solar collector with pin fin arrays inserting.* Solar Energy, 2017. **144**: p. 185-202.
21. Rajendran, V., et al., *Performance analysis of domestic solar air heating system using V-shaped baffles – An experimental study.* 2021. **235**(5): p. 1705-1717.
22. Rani, P. and P.P. Tripathy, *Experimental investigation on heat transfer performance of solar collector with baffles and semicircular loops fins under varied air mass flow rates.* International Journal of Thermal Sciences, 2022. **178**: p. 107597.
23. Tian, M., et al., *A review on the recent research progress in the compound parabolic concentrator (CPC) for solar energy applications.* Renewable and Sustainable Energy Reviews, 2018. **82**: p. 1272-1296.
24. Li, X., et al., *Performance investigation on a novel single-pass evacuated tube with a symmetrical compound parabolic concentrator.* Solar Energy, 2013. **98**: p. 275-289.
25. Bellos, E. and C. Tzivanidis, *A review of concentrating solar thermal collectors with and without nanofluids.* Journal of Thermal Analysis and Calorimetry, 2019. **135**(1): p. 763-786.
26. Zhu, T., et al., *Performance evaluation of a novel flat-plate solar air collector with micro-heat pipe arrays (MHPA).* Applied Thermal Engineering, 2017. **118**: p. 1-16.
27. O'Keeffe, G.J., *Mathematical modelling of nanofluid-based direct absorption solar collectors.* 2018.
28. Pandey, K.M. and R. Chaurasiya, *A review on analysis and development of solar flat plate collector.* Renewable and Sustainable Energy Reviews, 2017. **67**: p. 641-650.
29. Bhowmik, H. and R. Amin, *Efficiency improvement of flat plate solar collector using reflector.* Energy Reports, 2017. **3**: p. 119-123.
30. Rezaei, M., et al., *Investigating performance of a new design of forced convection solar dryer.* Sustainable Energy Technologies and Assessments, 2022. **50**: p. 101863.
31. Kumar, A., R.P. Saini, and J.S. Saini, *A review of thermohydraulic performance of artificially roughened solar air heaters.* Renewable and Sustainable Energy Reviews, 2014. **37**: p. 100-122.
32. Kumar, A., A.P. Singh, and O.P. Singh, *Investigations for efficient design of a new counter flow double-pass curved solar air heater.* Renewable Energy, 2022. **185**: p. 759-770.
33. Kumar, B., et al., *Effect of V cut in perforated twisted tape insert on heat transfer and fluid flow behavior of tube flow: An experimental study.* Experimental Heat Transfer, 2019. **32**(6): p. 524-544.
34. Pandey, R., M. Kumar, and J.S. Saini, *Experimental study of parametric influence on heat transfer and friction in a rectangular duct having V-down baffle blocks with staggered racetrack-shaped openings.* Experimental Heat Transfer, 2022. **35**(6): p. 818-847.
35. Sharma, A., et al., *Heat transfer and friction characteristics of double pass solar air heater having V-shaped roughness on the absorber plate.* Journal of Renewable and Sustainable Energy, 2013. **5**(2): p. 023109.
36. Jia, B., F. Liu, and D. Wang, *Experimental study on the performance of spiral solar air heater.* Solar Energy, 2019. **182**: p. 16-21.
37. Hassan, H., S. Abo-Elfadl, and M.F. El-Dosoky, *An experimental investigation of the performance of new design of solar air heater (tubular).* Renewable Energy, 2020. **151**: p. 1055-1066.
38. Dong, Z., et al., *A study on heat transfer enhancement for solar air heaters with ripple surface.* Renewable Energy, 2021. **172**: p. 477-487.
39. Wang, D., et al., *Evaluation of the performance of an improved solar air heater with "S" shaped ribs with gap.* Solar Energy, 2020. **195**: p. 89-101.
40. Chabane, F., N. Moummi, and S. Benramache, *Experimental study of heat transfer and thermal performance with longitudinal fins of solar air heater.* Journal of Advanced Research, 2014. **5**(2): p. 183-192.

41. Vaziri, R., M. Ilkan, and F. Egelioglu, *Experimental performance of perforated glazed solar air heaters and unglazed transpired solar air heater.* Solar Energy, 2015. **119**: p. 251-260.
42. Heydari, A. and M. Mesgarpour, *Experimental analysis and numerical modeling of solar air heater with helical flow path.* Solar Energy, 2018. **162**: p. 278-288.
43. Singh, A.P., et al., *Efficient design of curved solar air heater integrated with semi-down turbulators.* International Journal of Thermal Sciences, 2020. **152**: p. 106304.
44. Singh, S., et al., *Utilizing circular jet impingement to enhance thermal performance of solar air heater.* Renewable Energy, 2020. **154**: p. 1327-1345.
45. Gawande, V.B., et al., *Experimental and CFD investigation of convection heat transfer in solar air heater with reverse L-shaped ribs.* Solar Energy, 2016. **131**: p. 275-295.
46. Priyam, A. and P. Chand, *Thermal and thermohydraulic performance of wavy finned absorber solar air heater.* Solar Energy, 2016. **130**: p. 250-259.
47. Karwa, R. and G. Chitoshiya, *Performance study of solar air heater having v-down discrete ribs on absorber plate.* Energy, 2013. **55**: p. 939-955.
48. Bayrak, F., H.F. Oztop, and A. Hepbasli, *Energy and exergy analyses of porous baffles inserted solar air heaters for building applications.* Energy and Buildings, 2013. **57**: p. 338-345.
49. Gabhane, M.G. and A.B. Kanase-Patil, *Experimental analysis of double flow solar air heater with multiple C shape roughness.* Solar Energy, 2017. **155**: p. 1411-1416.
50. Abuşka, M., *Energy and exergy analysis of solar air heater having new design absorber plate with conical surface.* Applied Thermal Engineering, 2018. **131**: p. 115-124.
51. Pandey, N.K., V.K. Bajpai, and Varun, *Experimental investigation of heat transfer augmentation using multiple arcs with gap on absorber plate of solar air heater.* Solar Energy, 2016. **134**: p. 314-326.
52. Kherrafi, M.A., et al., *Performance enhancement of indirect solar dryer with offset strip fins: Experimental investigation and comparative analysis.* Solar Energy, 2023. **266**: p. 112158.
53. Tuncer, A.D., et al., *Testing of a novel convex-type solar absorber drying chamber in dehumidification process of municipal sewage sludge.* Journal of Cleaner Production, 2020. **272**: p. 122862.
54. Krabch, H., et al., *Indirect solar dryer with a single compartment for food drying. Application to the drying of the pear.* Solar Energy, 2022. **240**: p. 131-139.
55. John, M.K., R. Bandaru, and C. Muraleedharan, *Experimental analysis of wavy mesh assisted solar drying system with a survey of common drying technologies employed by farmers.* Sustainable Energy Technologies and Assessments, 2023. **56**: p. 103049.
56. Singh Parihar, J., et al., *Development of novel cabinet solar dryer using UV sheet and its performance evaluation: An experimental study.* Solar Energy, 2022. **239**: p. 1-9.
57. Bennamoun, L., *Improving Solar Dryers' Performances Using Design and Thermal Heat Storage.* Food Engineering Reviews, 2013. **5**(4): p. 230-248.
58. Camci, M., *Thermodynamic analysis of a novel integration of a spray dryer and solar collectors: A case study of a milk powder drying system.* Drying Technology, 2020. **38**(3): p. 350-360.
59. Singh, P., B.K. Pandey, and M.K. Gaur, *Performance evaluation of evacuated solar collector assisted hybrid greenhouse solar dryer under active and passive mode.* Materials Today: Proceedings, 2022. **57**: p. 2002-2008.
60. Jain, R., et al., *Enhancement in thermal performance of solar dryer through conduction mode for drying of agricultural produces.* Energy Nexus, 2023. **9**: p. 100182.
61. Kansara, R., M. Pathak, and V.K. Patel, *Performance assessment of flat-plate solar collector with internal fins and porous media through an integrated approach of CFD and experimentation.* International Journal of Thermal Sciences, 2021. **165**: p. 106932.
62. Verma, G., et al., *Experimental investigation of mixed mode ultraviolet tent house solar dryer under natural convection regime.* Solar Energy, 2023. **251**: p. 51-67.

63. Pardhi, C.B. and J.L. Bhagoria, *Development and performance evaluation of mixed-mode solar dryer with forced convection.* International Journal of Energy and Environmental Engineering, 2013. **4**(1): p. 23.
64. Goud, M., et al., *A novel indirect solar dryer with inlet fans powered by solar PV panels: Drying kinetics of Capsicum Annum and Abelmoschus esculentus with dryer performance.* Solar Energy, 2019. **194**: p. 871-885.
65. Khanlari, A., et al., *Energy-exergy and sustainability analysis of a PV-driven quadruple-flow solar drying system.* Renewable Energy, 2021. **175**: p. 1151-1166.
66. Nabnean, S., et al., *Experimental performance of a new design of solar dryer for drying osmotically dehydrated cherry tomatoes.* Renewable Energy, 2016. **94**: p. 147-156.
67. Shalaby, S.M. and M.A. Bek, *Experimental investigation of a novel indirect solar dryer implementing PCM as energy storage medium.* Energy Conversion and Management, 2014. **83**: p. 1-8.
68. Joshi, S., H. Thakkar, and A. Jani, *A Novel Design Approach of Small Scale Conical Solar Dryer.* International Journal of Applied Quality Management, 2014. **III**.
69. Fterich, M., et al., *Numerical and Experimental Study of Solar Dryer Equipped with PV/T.* Tehnički vjesnik, 2022. **29**(3): p. 896-906.
70. Gürel, A.E., et al., *A detailed investigation of the temperature-controlled fluidized bed solar dryer: A numerical, experimental, and modeling study.* Sustainable Energy Technologies and Assessments, 2022. **49**: p. 101703.
71. Sadri, S.A., et al., *Configuration optimization of the honeycomb core in the latent heat thermal energy storage of a solar air heater: Experimental and numerical study.* 2022. **46**(5): p. 5924-5954.
72. Afshari, F., et al., *Experimental and numerical analysis of a compact indirect solar dehumidification system.* Solar Energy, 2021. **226**: p. 72-84.
73. Prajapati, S., N. Naik, and C. V.P, *Numerical solution of solar air heater with triangular corrugations for indirect solar dryer: Influence of pitch and an optimized pitch of corrugation for enhanced performance.* Solar Energy, 2022. **243**: p. 1-12.
74. Tuncer, A.D., et al., *Experimental and numerical analysis of a grooved hybrid photovoltaic-thermal solar drying system.* Applied Thermal Engineering, 2023. **218**: p. 119288.
75. Ananno, A.A., et al., *Design and numerical analysis of a hybrid geothermal PCM flat plate solar collector dryer for developing countries.* Solar Energy, 2020. **196**: p. 270-286.
76. Abhay, L., V.P. Chandramohan, and V.R.K. Raju, *Numerical analysis on solar air collector provided with artificial square shaped roughness for indirect type solar dryer.* Journal of Cleaner Production, 2018. **190**: p. 353-367.
77. Motahayyer, M., A. Arabhosseini, and H. Samimi-Akhijahani, *Numerical analysis of thermal performance of a solar dryer and validated with experimental and thermo-graphical data.* Solar Energy, 2019. **193**: p. 692-705.
78. Alic, E., M. Das, and E.K. Akpinar, *Design, manufacturing, numerical analysis and environmental effects of single-pass forced convection solar air collector.* Journal of Cleaner Production, 2021. **311**: p. 127518.
79. Al-Kayiem, H.H., K.V. Sreejaya, and A.O. Chikere, *Experimental and numerical analysis of the influence of inlet configuration on the performance of a roof top solar chimney.* Energy and Buildings, 2018. **159**: p. 89-98.
80. Sözen, A., et al., *Thermal performance improvement of an indirect solar dryer with tube-type absorber packed with aluminum wool.* Solar Energy, 2021. **217**: p. 328-341.
81. da Silva, G.M., et al., *Thermodynamic analysis of a sustainable hybrid dryer.* Solar Energy, 2020. **208**: p. 388-398.
82. Hassan, A., et al., *Experimental and thermodynamic analysis of solar air dryer equipped with V-groove double pass collector: Techno-economic and exergetic measures.* Energy Conversion and Management: X, 2022. **16**: p. 100296.

83. Hatami, S., G. Payganeh, and A. Mehrpanahi, *Energy and exergy analysis of an indirect solar dryer based on a dynamic model.* Journal of Cleaner Production, 2020. **244**: p. 118809.
84. Djebli, A., et al., *A new approach to the thermodynamics study of drying tomatoes in mixed solar dryer.* Solar Energy, 2019. **193**: p. 164-174.
85. Lingayat, A., V.P. Chandramohan, and V.R.K. Raju, *Energy and exergy analysis on drying of banana using indirect type natural convection solar dryer.* Heat Transfer Engineering, 2019.
86. Kherrafi, M.A., et al., *Performance evaluation of innovative sensible energy storage material integration as an obstacle in solar collectors for drying applications.* Journal of Energy Storage, 2023. **74**: p. 109317.
87. Lewis, W.K., *The rate of drying of solid materials.* Industrial Engineering Chemistry, 1921. **13**(5): p. 427-432.
88. Xanthopoulos, G., G. Lambrinos, and H. Manolopoulou, *Evaluation of Thin-Layer Models for Mushroom (Agaricus bisporus) Drying.* Drying Technology, 2007. **25**(9): p. 1471-1481.
89. Midilli, A., H. Kucuk, and Z. Yapar, *A new model for single-layer drying.* Drying Technology, 2002. **20**(7): p. 1503-1513.
90. Zhang, Q. and J.B. Litchfield, *AN OPTIMIZATION OF INTERMITTENT CORN DRYING IN A LABORATORY SCALE THIN LAYER DRYER.* Drying Technology, 1991. **9**(2): p. 383-395.
91. Yaldýz, O. and C. Ertekýn, *Thin layer solar drying of some vegetables.* Drying Technology, 2001. **19**(3-4): p. 583-597.
92. Yaldiz, O., C. Ertekin, and H.I. Uzun, *Mathematical modeling of thin layer solar drying of sultana grapes.* Energy, 2001. **26**(5): p. 457-465.
93. Verma, L.R., et al., *Effects of drying air parameters on rice drying models.* Transactions of the ASAE, 1985. **28**(1): p. 296-0301.
94. Dandamrongrak, R., G. Young, and R. Mason, *Evaluation of various pre-treatments for the dehydration of banana and selection of suitable drying models.* Journal of Food Engineering, 2002. **55**(2): p. 139-146.
95. Ertekin, C. and O. Yaldiz, *Drying of eggplant and selection of a suitable thin layer drying model.* Journal of food engineering, 2004. **63**(3): p. 349-359.
96. Benseddik, A., et al., *Mathematical empirical models of thin-layer airflow drying kinetics of pumpkin slice.* Engineering in Agriculture, Environment and Food, 2018. **11**(4): p. 220-231.
97. Crank, J., *The Mathematics of Diffusion. 2nd Edition*. 1975: Oxford University Press, London.
98. Prakash, O. and A. Kumar, *Historical review and recent trends in solar drying systems.* International journal of green energy, 2013. **10**(7): p. 690-738.
99. Zare, D., et al., *Computer simulation of rough rice drying in a batch dryer.* Energy Conversion and Management, 2006. **47**(18-19): p. 3241-3254.
100. Selvanayaki, S. and K. Sampathkumar, *Techno-economic analysis of solar dryers.* Solar Drying Technology: Concept, Design, Testing, Modeling, Economics, and Environment, 2017: p. 463-493.
101. Alwan, Z. and P. Jones, *The importance of embodied energy in carbon footprint assessment.* Structural Survey, 2014. **32**(1): p. 49-60.
102. Kesavan, S., T.V. Arjunan, and S. Vijayan, *Thermodynamic analysis of a triple-pass solar dryer for drying potato slices.* Journal of Thermal Analysis and Calorimetry, 2019. **136**(1): p. 159-171.
103. Chauhan, P.S., A. Kumar, and C. Nuntadusit, *Thermo-environomical and drying kinetics of bitter gourd flakes drying under north wall insulated greenhouse dryer.* Solar Energy, 2018. **162**: p. 205-216.

104. Tiwari, S. and G.N. Tiwari, *Exergoeconomic analysis of photovoltaic-thermal (PVT) mixed mode greenhouse solar dryer.* Energy, 2016. **114**: p. 155-164.

105. Youcef-Ali, S., *Study and optimization of the thermal performances of the offset rectangular plate fin absorber plates, with various glazing.* Renewable Energy, 2005. **30**(2): p. 271-280.

106. Gilago, M.C., V.R. Mugi, and V.P. Chandramohan, *Investigation of exergy-energy and environ-economic performance parameters of active indirect solar dryer for pineapple drying without and with energy storage unit.* Sustainable Energy Technologies and Assessments, 2022. **53**: p. 102701.

107. Jayasuriya, H., et al. *Drying Kinetics and Quality Analysis of Coriander Leaves Dried in an Indirect, Stand-Alone Solar Dryer*. Processes, 2023. **11**, DOI: 10.3390/pr11061596.

108. Silva, A.S., et al., *Drying kinetics of coriander (Coriandrum sativum) leaf and stem cinéticas de secado de hoja y tallo de cilantro (Coriandrum sativum).* Ciencia y Tecnologia Alimentaria, 2008. **6**(1): p. 13-19.

109. Müller, J. and A. Heindl, *Drying of medicinal plants.* Frontis, 2006: p. 237-252.